



UNIVERSITÀ
DEGLI STUDI
DI PADOVA

UNIVERSITÀ DEGLI STUDI DI PADOVA

Dipartimento di Ingegneria Industriale DII

Corso di Laurea Magistrale in Ingegneria dell'Energia Elettrica

**ANALYSIS OF THE INTERNAL SHORT-CIRCUIT
CONDITIONS OF THE ACCELERATION GRID
POWER SUPPLY OF THE MITICA EXPERIMENT**

Relatore: Prof. Paolo Bettini
Correlatore: Ing. Loris Zanotto

Laureando: Mattia Dan

Anno Accademico 2015/2016

Contents

Ancronymus	1
Sommario	3
1 Introduction	5
2 Thermonuclear fusion	7
2.1 Physisc and application	7
2.2 Additional heating systems	10
2.2.1 Neutral Beam Injector.....	10
2.3 PRIMA project	12
2.3.1 SPIDER.....	13
2.3.2 MITICA	14
2.4 MITICA power supply systems.....	18
2.4.1 AGPS	21
2.4.2 ISEPS.....	21
2.4.3 GRPS	22
3 The Acceleration Grid Power Supply (AGPS)	23
3.1 Main requirements	23
3.1.1 Current and voltage in nominal operation	23
3.1.2 Dynamic performance requirements	24
3.1.3 Breakdown and Beam Off	25
3.2 General scheme	26
3.2.1 Middle voltage ac distribution grid	28
3.2.2 AGPS-CS scheme.....	28
3.2.3 NPC inverters	30
3.2.4 Electrical requirements at the interface between AGSP-CS and AGPS-DCG	31
3.2.5 AGPS-DCGs scheme.....	32
3.3 Layout of the AGPS-CS.....	33
3.4 Internal faults.....	35
3.4.1 Protections from internal short-circuits of the inverters	36
4 AGPS simulation model for the study of the internal faults	39
4.1 Model of the NPC inverters	39
4.2 Model of dc link	42
4.3 AGPS-DCG and load model	44
4.4 Simplified model	45
4.5 Detailed model.....	47
4.5.1 Step down transformers model.....	47
4.5.2 Impedances between transformers and ac/dc converters.....	48
4.5.3 Ac/dc converter	49
4.5.4 Stray inductances between the ac/dc converter and the dc link	50

4.6	Protection systems	51
4.6.1	Crowbar	51
4.6.2	Fuses	52
5	Simulations	55
5.1	Nominal operation in steady-state	55
5.1.1	Simplified circuit	55
5.1.2	Detailed model	57
5.2	Fault analysis	58
5.3	Fault simulations with the simplified circuit	61
5.3.1	Prospective currents during the fault	61
5.3.2	Prospective current and I^2t at the input of the inverter	70
5.3.3	Selection of the fuse	72
5.3.4	Using the fuses as protection	74
5.3.5	Analysis of trends simulating the fault in different inverters	81
5.3.6	Using the crowbar as protection.....	82
5.4	Fault simulations with the detailed model	85
5.5	Conclusions on the results of the simulations	90
6	Conclusions	91
7	Acknowledgments	93
8	References	95

Acronymus

AGPS	Acceleration grid power supply
AGPS-CS	Acceleration grid power supply-Conversion System
AGPS-DCG	Acceleration grid power supply-DC Generator
EG	Extraction grid
EGPS	Extraction grid Power Supply
EUDA	European Domestic Agency
GRPS	Ground Related Power Supplies
IGCT	Integrated Gate-Commutated Thyristor
ISEPS	Ion Source and Extraction Power Supplies
ITER	International Thermonuclear Experimental Reactor
MITICA	Megavolt ITER Injector & Concept Advancement
NBI	Neutral Beam Injector
NBTF	Neutral Beam Test Facility
PI	Proportional-Integral
PG	Plasma Grid
RFX	Reverse Field eXperiment
rms	Root mean square
RF	Radio Frequency
RFPS	Radio Frequency Power Supply
SPIDER	Source of Production of Ion of Deuterium Extracted from RF plasma

Sommario

La tesi riguarda MITICA, un esperimento in costruzione presso il CNR (Centro Nazionale di Ricerca) di Padova, nell'infrastruttura PRIMA. MITICA, assieme a SPIDER, l'altro esperimento in costruzione nell'infrastruttura PRIMA, sarà fondamentale per lo studio del funzionamento dei sistemi di riscaldamento ausiliari nei futuri reattori a fusione nucleare.

MITICA è infatti un prototipo in scala 1:1 dei sistemi di iniezione di particelle neutre (chiamati NBI, Neutral Beam Injector) che verranno costruiti a Cadarache in Francia per l'esperimento ITER, che sarà la più grande macchina Tokamak al mondo. Servirà per studiare il comportamento del NBI prima dell'installazione in ITER, avendo caratteristiche superiori a tutti gli NBI costruiti finora.

MITICA fornisce in uscita un fascio di particelle neutre con potenza fino a 16.5MW, avente un'energia fino a 1MV. Questa energia è fornita accelerando le particelle in forma di ioni, che vengono successivamente neutralizzati.

L'accelerazione è un'accelerazione elettrostatica, basata sull'applicazione di una differenza di potenziale alle griglie di accelerazione. Per ottenere una buona ottica del fascio è previsto l'uso di 5 stadi di accelerazione, in cui in ogni stadio si applica la differenza di potenziale di 200kV alle griglie.

La tesi riguarda il sistema di alimentazione delle griglie di accelerazione di MITICA (chiamata AGPS, Acceleration Grid Power Supply), il quale deve fornire una potenza nominale di circa 55MW e deve fornire in uscita una tensione totale fino a 1MV. A causa dell'elevatissima potenza i componenti che lo costituiscono devono riuscire a lavorare ad alte tensioni e correnti e per l'elevata tensione (fino a 1MV) i componenti di tale sistema necessitano di requisiti di isolamento molto spinti.

L'AGPS è basata su componenti switching che permettono di avere un controllo della tensione in uscita, per variare l'accelerazione del fascio di ioni. In tale sistema durante il funzionamento nominale è accumulata un'energia capacitiva di 760kJ, dovuta all'elevato livello di tensione e a requisiti sull'oscillazione della tensione. Nel caso di un guasto interno del sistema tale elevata energia può causare la distruzione di parti del sistema.

Nella tesi si è studiato e simulato tramite un software di simulazione circuitale il guasto interno più pericoloso che coinvolge l'energia accumulata nel banco di condensatori, valutando l'efficacia dei diversi sistemi di protezione considerati.

Nel capitolo 1 viene introdotto il sistema studiato e l'analisi effettuata nella tesi.

Nel capitolo 2 viene spiegata brevemente il principio fisico della fusione nucleare e l'applicazione negli attuali reattori sperimentali, approfondendo la descrizione sugli NBI come sistemi di riscaldamento ausiliario. Viene successivamente descritta la struttura PRIMA e i due esperimenti SPIDER e MITICA attualmente in costruzione.

Nel capitolo 3 viene descritta la struttura dell'AGPS di MITICA, con requisiti e modalità operative, concentrandosi sul layout del sistema interessato dal guasto considerato e viene introdotto il tipo di guasto interno più pericoloso, che viene in seguito analizzato. Sono inoltre presentati i sistemi di protezione considerati contro la situazione di guasto interno studiata.

Nel capitolo 4 vengono presentati i modelli circuitali utilizzati per la simulazione del guasto del sistema nelle diverse condizioni studiate.

Nel capitolo 5 sono esposti e commentati i risultati ottenuti dalle simulazioni, effettuando un confronto tra i sistemi di protezione considerati.

Le conclusioni sono riassunte nel capitolo 6.

1 Introduction

ITER (International Thermonuclear Experimental Reactor), which is under construction in Cadarache, will be the largest tokamak machine in the world. It should prove the technological feasibility of fusion as source of energy. It will be the first experimental fusion reactor producing more energy than it spends to start and sustain the fusion reaction and its operation can last for tens of minutes.

To reach the fusion reaction conditions, additional heating systems are required to heat the plasma up to the required temperature, and one of the main methods is the injection of high-energy neutral particles.

In ITER 2 NBIs (Neutral Beam Injector) are foreseen in order to provide to the plasma a power of about 16.5MW each, and a third one may be added optionally. These systems require a high absorption of electrical power, about 60MW each. Moreover, the acceleration of particles up to the nominal energy requires acceleration voltages as high as 1MV dc. The ITER NBI concept is based on the acceleration and neutralization of negative ions to enhance the efficiency.

Such a large NBI facility has never been built and represents a technological challenge from many points of view. To mitigate the risk of unexpected failures in ITER, it has been decided to test the NBI concept in advance of ITER operations. For this reason a full scale prototype of ITER's NBIs is under construction in Padua, at Consorzio RFX premises, and is planned to begin operation in 2018. It is named MITICA (Megavolt ITER Injector & Concept Advancement). MITICA aims at demonstrating the technological feasibility of the challenging ITER NBI requirements, mainly related to the high power, voltage and energy to be delivered by the beam.

In MITICA the negative ions are extracted by means of electrostatic grids. Then they are accelerated up to 1MeV, again using electrostatic grids. The high-energy ion beam is subsequently neutralized using a neutralizer, and finally the neutral beam is obtained. In MITICA, being the plasma not available, the beam is directed to a calorimeter and its energy is dissipated.

The power supply system of MITICA is fed by the 400kV grid. A High Voltage switchgear provides a 22kV distribution voltage to the main power supplies, which are:

- The Acceleration Grid Power Supply (AGPS), a high voltage, high power system supplying the acceleration grids
- The Ion Source Extraction Power Supply (ISEPS), which is devoted to the generation and extraction of the ions
- The Ground Rated Power Supply, which is a power supply at ground potential for auxiliary functions in the NBI.

The subject of the thesis is the AGPS system. The AGPS is a special switching power supply with demanding requirements: high rated power (about 55 MW), extremely high output voltage (-1MV dc), long duration pulses up to 1 hour, flexibility of operation and a peculiar operational scenario, where frequent short-circuits of the acceleration grids have to be tolerable. The procurement of the AGPS is split in two parts: the low voltage conversion system, namely the AGPS-Conversion System (AGPS-CS), being procured by the European domestic agency (Fusion For Energy, F4E), and the high voltage DC Generators (AGPS-DCG), being procured by the Japanese domestic agency (Japanese Atomic Domestic Agency, JADA).

Being the two parts procured by different companies, from different countries, the interface between the systems has been defined and agreed in detail. One of the fundamental parameters of the interface is the output voltage level of the AGPS-CS. In the final design of the AGPS-CS, the voltage level together with other requirements on voltage fluctuations and precision led to, a design based on a special switching power supply where a high capacitive energy is stored, about 760 kJ in nominal operation. This is potentially very dangerous in case of a fault like a short circuit in the inverters connected downstream of the capacitive storage. This particular fault needs to be deeply investigated in order to ensure and design the proper protection and to avoid the risk of catastrophic explosion of components following the fault.

In the thesis, after a general introduction about thermonuclear fusion and neutral beam injection systems, the design of the AGPS-CS will be described. Then, a very detailed simulation model of the AGPS-CS components set up to study the internal short-circuit fault will be presented and discussed. With this model the event of a fault of the active switches composing the Neutral Point Clamped (NPC)

inverter has been simulated in different conditions. This event causes a quick discharge of the capacitor bank on the legs of the inverter modules. If no proper protections are foreseen, the destruction of the inverter module and the fault propagation to other components in the system may occur.

The traditional protections for these systems have been considered and analyzed. It has been shown in the thesis that they are not applicable here due to the too high level of involved energy in respect to common industrial applications. Alternative provisions have been considered: the use of decoupling diodes on the DC bus section or of thyristor crowbars has been discarded and an innovative solution based on fuses at the input of the inverter has been finally selected. Being the use of fuses for such a high energy not common, it has been necessary to evaluate the behaviour of the circuit when the fault occurs in order to properly size the fuses and to verify if the system is actually protected in this way, considering all the range of possible operative conditions.

In this thesis the simulations will be performed using the circuital software simulator PSIM. The failure of one IGCT of a leg of an inverter will be analysed, observing the maximum current and energy that the components of the inverters have to withstand, without being damaged or damaging other modules with explosions.

The simulation will also allow to obtain the value of currents at the input of the healthy inverters, in order to ensure the selectivity of the fuse intervention: only the fuses of the damaged inverter have to intervene.

It has been found that the results are very sensitive to the stray parameters of the simulated circuit, such as the resistance and stray inductance of the busbars and of the active switches. Therefore, the simulation models have been derived following a very accurate calculation of such parameters, starting from the actual design and layout of the system. At the same time some simplifications have been introduced to reduce computational times. Sensitivity analysis have been also carried out to conform the robustness of the fuse selection.

2 Thermonuclear Fusion

2.1 Physic and application

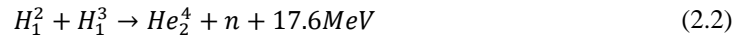
The controlled thermonuclear fusion reaction is a possible technology for the future production of electric energy and it is still in research phase. It is estimated to be available for commercial use in about 50 years.

The fusion reaction develops energy thanks to the mass defect: 2 light atoms merge to produce a heavier atom whose atomic mass is lower than the sum of the mass numbers of the 2 reacting atoms. This mass reduction release energy according to Einstein's relativity law:

$$\Delta E = mc^2 \quad (2.1)$$

With $c=299792.458$ km/s, speed of light in vacuum.

Theoretically every element could be fused, but practically only very light nuclei can be fused. The most energetically fusion reaction is the fusion of two protons and two neutrons to produce a nucleus of He^4 . However this reaction is very difficult to be implemented, while the reaction between Deuterium (H^2) and Tritium (H^3), two isotopes of hydrogen, is the easier to be achieved and the reaction is:



That because the cross section of the particles for this fusion reaction (measured in barn: 1 barn= $10^{28}m^2$) is the highest. The cross section is the area which is proportional to the probability that a nucleus accelerated toward another nucleus causes a fusion reaction. It is the combination of the probability that the Coulomb barrier is overcome (288keV for Deuterium-Tritium reaction) and the probability that the fusion really occurs.

In fact, the cross section for fusion collisions involves nuclear quantum mechanical effects and it is not just a spherical collision: there is a certain probability to have the reaction also with lower energy compared to the Coulomb barrier and the probability decreases for high values of particle energy due to the short time for the interaction. Moreover under certain conditions of relative velocity the combined potential energies of the two colliding nuclei can exhibit a resonance with an enhanced probability of nuclear reaction.

Because of the relatively high probability of the occurring of the nuclear fusion reaction, this is the fusion reaction that will be developed in the first reactors.

The nuclei have positive charge, so they are affected by repulsive Coulomb forces, which cause the Coulomb barrier. For this reason they must have a speed sufficient to overcome these forces to be able to collide. Energy must be provided to them heating the gas mixture Deuterium-Tritium up to about 150 million of degrees Kelvin (using a more common energy measure unit in fusion field, 10keV). At this temperature electrons separate from nuclei and an ionized gas is then created: the plasma.

The plasma must not touch the vacuum chamber wall because it would be cooled down and the fusion conditions would not subsist; moreover impurities would be released in it. Hence magnetic fields are used to confine the plasma, forcing its ions to move along helical trajectories along the magnetic field lines produced in the vacuum chamber, which is toroidal to let ions move continuously in their motion.

Now it is needful to introduce Lawson criterion both for its historical importance and for its significance in defining the condition for a fusion reactor to reach ignition. Ignition is the condition where the heating of the plasma by products of the fusion (the He_2^4 , called alpha particle, which is a charged particle and is confined by the magnetic field) is sufficient to maintain the temperature of the plasma against all losses, without external power input. The Lawson criterion gives a minimum required value for the product of the plasma electron density and the energy confinement time. Later analysis suggested that a more useful figure of merit is the "triple product" of density, confinement time, and plasma temperature.

In order to have that the reaction can sustain itself the following inequality must be verified:

$$\eta \cdot T \cdot \tau_E \geq 1.2 \cdot 10^{21} \text{ KeV} \cdot s \cdot m^3 \quad (2.3)$$

This condition correspond to $Q=3$, where Q , called plasma energy gain, is:

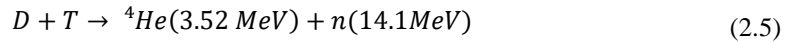
$$Q = \frac{\text{Output Power}}{\text{Input Power}} \quad (2.4)$$

Q must be greater than 1 to produce more power than the input power.

$Q=1$ is told breakeven condition, $Q = \infty$ is the ignition condition.

In current experiments the breakeven condition has never been reached, the maximum value of Q was reached in JET, in England, with $Q \cong 0.65$. In ITER, thanks to scaling laws (much higher ratio between volume and surface of the reaction chamber) this limit will be overcome, and the reaching of $Q=10$ is one of the target.

The first type of fusion reactor would exploit the deuterium-tritium reaction, producing an amount of energy of about 17MeV for reacting couples of atoms. This energy is subdivided on the reaction products, inversely proportional to their masses:



The mass of ${}^4\text{He}$ atom, called α particle, is four time the mass of neutron, so it has an energy four times lower than the one provided to the neutron. This is a positive charged particle, therefore it is confined by magnetic field lines and heats up the plasma through collisions. However, unless the reactor is working in ignition condition, this energy is not enough to sustain the reaction and additional heating methods are necessary; the most studied are the radiofrequency heating and the heating through neutral beam injection.

Instead the produced neutrons are not affected by magnetic fields, so they escape from the confinement and collide against the wall, depositing the heat that will be used to generate steam using a heat exchanger which feeds a conventional thermodynamic cycle to produce electric energy.

The wall of the chamber has more layers and the first must withstand the high temperature produced by neutrons collision. The subsequent layer, called breeding blanket, has the purpose of producing Tritium. In fact, while Deuterium is a stable hydrogen isotope so it is present in small part in seawater (0.0156%) and it is easily and economically extractable, Tritium is a radioactive isotope of hydrogen, with a half time of 12 years. For this reason its presence in atmosphere is very low and it must be produced in some way. The most studied way is by exploiting the reaction with Lithium:



Even if Lithium is composed for 7.3% by ${}^6\text{Li}$ and for 92.7% by ${}^7\text{Li}$, the first reaction is much more probable.

Tritium is thus produced, recovered and fed back in the chamber.

It is estimated that reserves of lithium should allow energy for 20000 years with this type of reaction and with current world energy consumption.

A CAD view of ITER is shown in figure 2-1.

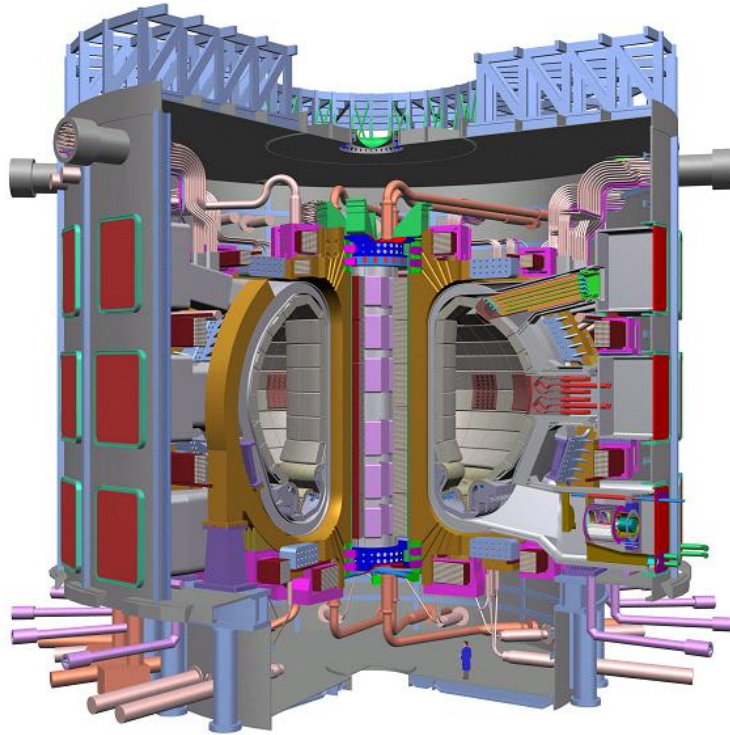


Figure 2-1 ITER's CAD representation

We have spoken about magnetic field used for confinement, but a Tokamak has different components of magnetic field (see fig. 2-2):

B_{ϕ} : it is the toroidal field, which provides the stability. It is created by the toroidal field coils that wrap around the chamber in the poloidal plane. The current flowing into these coils must be very high to create magnetic field of the order of some Tesla, therefore superconductor materials kept to very low temperature (only some Kelvin degrees) are necessary to avoid high ohmic dissipations. The toroidal field in a Tokamak machine must be about one order of magnitude greater than the poloidal field to ensure the stability.

B_{θ} : it is the poloidal field. In this component there is both the magnetic field necessary to initiate and sustain the plasma by induction using the inner poloidal coils and the magnetic field created by the outer poloidal field coils and by the current of plasma for plasma positioning and shaping.

B_v : it is the additional vertical field necessary for equilibrium, avoiding the radial outwardly drift of the plasma, and for shape, making the plasma fill the chamber to not have oversizing. It is created by coils not represented in fig. 2-2, wrapping toroidally the inner poloidal field coils, symmetrically in the two halves of the cross section of the chamber.

B_r : it is the additional radial field, which provides shape and stability. They are created by saddle coils placed over the vacuum vessel (not shown in fig. 2-2).

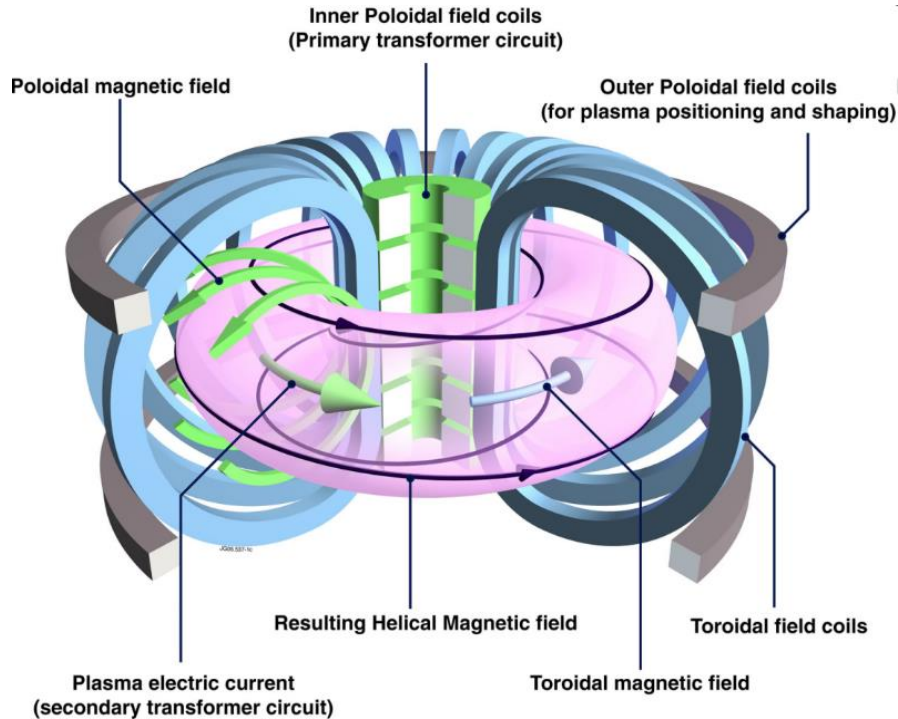


Figure 2-2 Magnetic components and coils producing them

2.2 Additional heating systems

High values of the toroidal magnetic field allow a better confinement of the plasma, because a higher plasma current can be set up. Being the plasma a conductor with a resistance related to its temperature as $T^{-3/2}$, the plasma current provides a contribute in the heating of the plasma through ohmic heating. The problem is the technological limits of the magnitude of the toroidal magnetic field, in ITER will reach 5.3T, which is a limit for the ohmic heating. The initial heating in all Tokamaks comes from the ohmic heating. In large Tokamaks, like ITER, it produces temperatures of few keV. At the temperature required for ignition the ohmic heating is much reduced because the resistivity falls down, leading to the requirement for additional heating. The two main methods that are envisaged for heating to ignition temperatures are:

- the injection of energetic neutral beams
- the resonant absorption of radio frequency electromagnetic waves

The first method heats the plasma by collisions with high kinetic energy particles, the second method uses the resonance excitation of ions or electrons of the plasma using antennas working at the frequencies with whom ions or electrons move around the magnetic field lines, or at an intermediate frequency related to the plasma frequency.

Both of these methods would in principle be capable of providing heating to the required magnitude, and both have been successfully tested at power levels of tens of MW.

The injection of energetic neutral beams is done with a device called NBI. The heating using NBIs is dominant in most large past, present and planned tokamaks.

2.2.1 Neutral Beam Injector

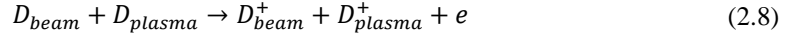
In a NBI ions are generated, electrostatically accelerated and neutralized, producing the neutral particles beam wanted.

NBIs are used for:

- plasma heating
- current drive
- diagnostic

Neutral atoms injected into a plasma by a NBI travel in straight lines, being unaffected by the magnetic field. Since the ions and electrons in the beam have the same velocity, the energy is carried almost entirely by massive ions. The energy of the injected ions is gradually transferred to the plasma electrons and ions through Coulomb collisions. The beam is made up by atoms of the same type of the ones that form the plasma, therefore deuterium atoms, being tritium radioactive. In this way deuterium is added in camera to sustain the reaction.

The basic atomic process leading to beam energy absorption is the ionization by ions, dominant for beam energy higher than 90keV:



Since the radius of the vacuum chamber will be larger than 2m in ITER and in future reactors, high acceleration values are necessary to reach the centre of the plasma and deposit there the heat, to avoid the quick dispersion of the heat in the case of energy transferred only to the edges of the plasma. The acceleration energy of the beam will be 1MeV in ITER.

A NBI can work by accelerating positive or negative ions. It is easier to produce positive ions, yet their neutralization efficiency decreases quickly at the increasing of the beam energy. The neutralization of negative ions has a high efficiency also for high energy, as can be seen from the figure 2-3, experimentally obtained.

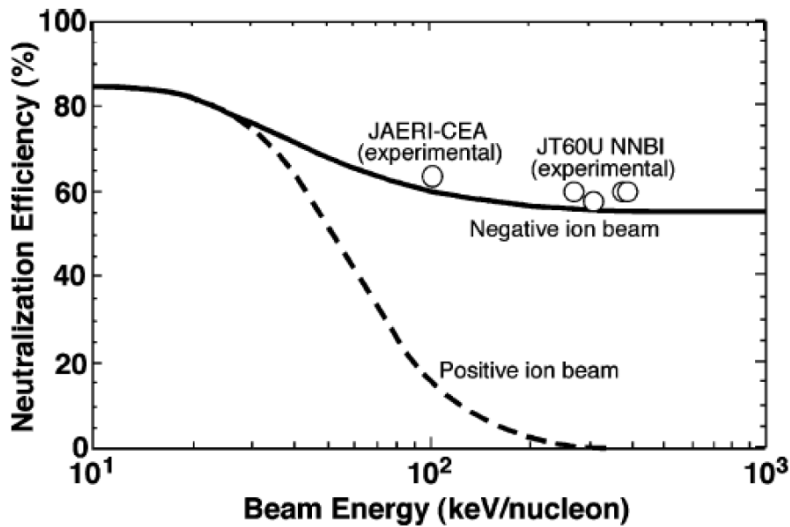


Figure 2-3 Efficiency of the neutralization at the variation of the beam energy

Being necessary accelerations of the order of 1MeV, the NBIs have to work with negative ions, and they have a neutralization efficiency of about 60%.

The ion generation is done using radiofrequency excitation, using windings supplied by RF generators that wraps the vacuum chamber where plasma is generated.

The ions generated are extracted by grids set to a certain potential. It is difficult to produce negative ions, they can easily lose an electron, so Cesium is used to produce a higher number of electrons next to the plasma grid and a magnetic filter is used to reduce the extraction of electrons and the stripping of ions caused by high energy electrons present in the chamber.

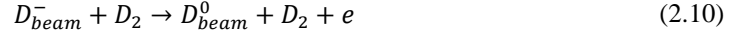
After the plasma grid there is the extraction grid, set to a higher potential than the plasma grid to accelerate the negative ions. The electric field present between these two grids and after the extraction grid create an electrostatic lens that corrects the optical beam: due to the geometry of grids and their distance there is a defocusing of the beam. Moreover, there is a drift that must be correct too, owing to the deflection of the electron from the beam, since they are useless in the creation of the neutral beam.

After that the ion beam is accelerated by a series of grids, set to gradually increasing potentials: the acceleration grids. The presence of these grids modifies the beam optic, because of grids' shape and holes' dimension, and it is optimized if the acceleration voltage and the ion beam follow the perveance law:

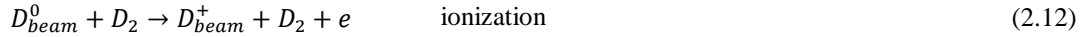
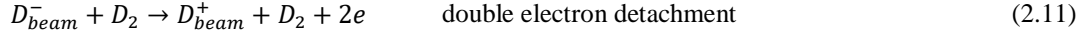
$$I_{beam} = \frac{k}{\sqrt{m}} V_{acc}^{\frac{3}{2}} \quad (2.9)$$

Where I_{beam} is the current of the beam flowing through the grids, V_{acc} is the acceleration voltage, m is the ions mass and k is a constant determined by the geometry of the grids.

Subsequently the ions are neutralized in a chamber where there is the same type of gas of the ion beam. They collide against the atom of the gas and create a beam of neutral atoms with similar energy to the one of the entering ionic beam. The neutralization occurs with single electron detachment:



Nevertheless, other processes can occur and they create positive ions:



Not all ions collide with a gas molecule, therefore part of the beam exits from the neutralizer having still the negative charge.

The exiting beam is therefore composed of neutral atoms for the 60%, and the remaining 40% is composed by positive and negative ions, fairly with the same quantity.

Charged particles with high kinetic energy cannot be injected in the reaction chamber because the magnetic field used for the confinement causes deflections of the beam, with the impossibility of control it and probable damages to the wall. These energetic ions are deflected after the neutralizer using the magnetic or electrostatic deflection, making them collide against the beam dump. Solutions are being studied to recover this energy because the neutralization efficiency should be the easiest to improve in a NBI system.

Overall, a NBI has an efficiency of about 30%. Other loss factors are the loss for electron stripping or for stray particles, i.e. the generation and acceleration of particles different from the wanted ions, in the zone before the neutralizer which cause losses of about 30%. Moreover, there are the ionization after the neutralizer and the beam-plasma coupling which cause losses of about 20%. Since these losses are mainly produced by the presence of the background gas, high pumping requirement are necessary to create a high level of vacuum before and after the neutralizer.

2.3 PRIMA project

In order to develop and test injectors to be installed on ITER, in parallel to the construction of ITER, it has been initiated and is ongoing at the Consorzio RFX, the realization of the new international laboratory for the development of the neutral injectors, the Neutral Beam Test Facility (NBTF)-PRIMA Project. The construction of NBTF began in September 2012.

The scientific goal of the PRIMA project is to get ready a system to obtain a beam of high energy (1MeV) and power (about 16.5MW) atoms, with an operation of the plant almost continuous, to heat the plasma in ITER. These are performance never achieved before. The achievements are now in course and the works already completed enabled the starting of the installation of the first equipment, the supply of which is entrusted to Europe and Japan, with the support of India.

PRIMA includes two experiments: a full size plasma source with low extraction voltage called SPIDER (Source for Production of Ion of Deuterium Extracted from RF plasma) and a full size neutral beam injector at full beam power called MITICA (Megavolt ITER Injector Concept Advancement).

Many information of next paragraphs and of next chapter are taken from [1].

2.3.1 SPIDER

SPIDER [2] is the first experimental device to be built and operated in PRIMA. Its purpose is testing the extraction of a negative ion beam (made of H^- and afterwards D^- ions) from an ITER size ion source. SPIDER is showed in fig.2-4.

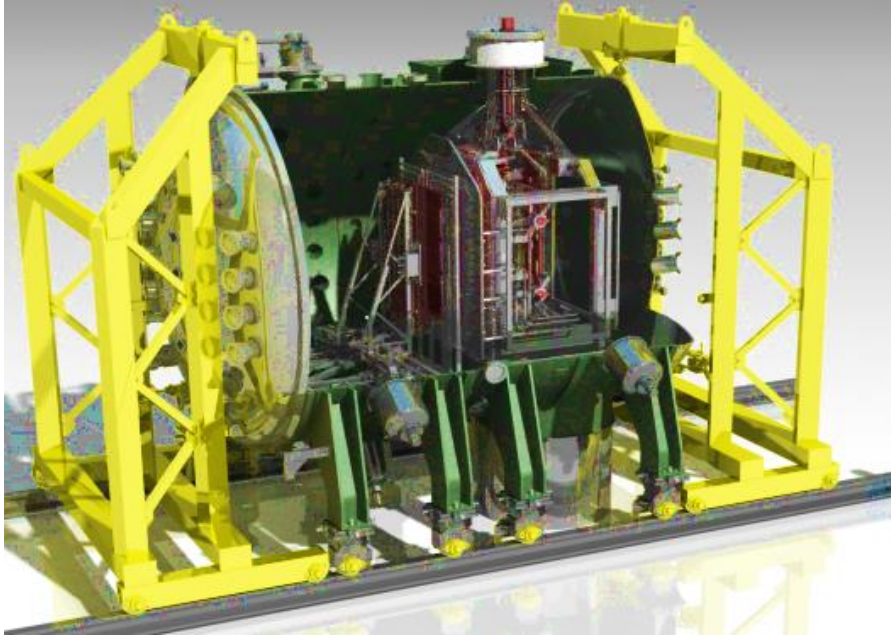


Figure 2-4 CAD representation of SPIDER

The main aim this experiment is to optimize the performance of an ITER-like ion source by maximizing the extracted negative ion current density and its spatial uniformity and by minimizing the ratio of co-extracted electrons, in order to match ITER requirements. Moreover the experiment needs to optimize the low work pressure condition, the steady state operation and the beam modulation.

This should be achieved varying some parameters like RF power, Caesium injection, temperature, current and bias of the plasma grid, and optimizing the magnetic configuration, materials of the plasma grid and its apertures.

The main requirements of this experiment are a H^-/D^- current of approximately 70A/50A and an energy of 100 keV. The pressure of the beam source is 0.3Pa and the pulse can last up to 3600s.

The beam source assembly is a radio frequency ion source, the one that will be used in ITER and in MITICA, with some modifications to adapt it to SPIDER. It is a chamber where there is a main space facing the plasma grid, on whose surface most of negative ions are generated, and eight rear smaller chamber called drivers, where the gas is injected (hydrogen or deuterium). RF coils are wrapped around lateral wall of the drivers and connected to a 1MHz oscillator; they transfer the power to the atoms in the chamber, ionizing the gas and producing a plasma. The addition of Caesium is necessary to increase the number of negative ions generated on the surface of the plasma grid.

Like the beam source, the first two grids (plasma and extraction grids), are the same that will be used in ITER.

Then in SPIDER there is just another acceleration stage of 100 kV to the grounded grid, unlike ITER, where there will be an overall acceleration of 1MeV. For this reason the beam source assembly is kept at -100 kV by electrical power supplies and ceramic insulators.

An internal view of SPIDER, with a zoom on the beam generator system is shown in fig. 2-5.

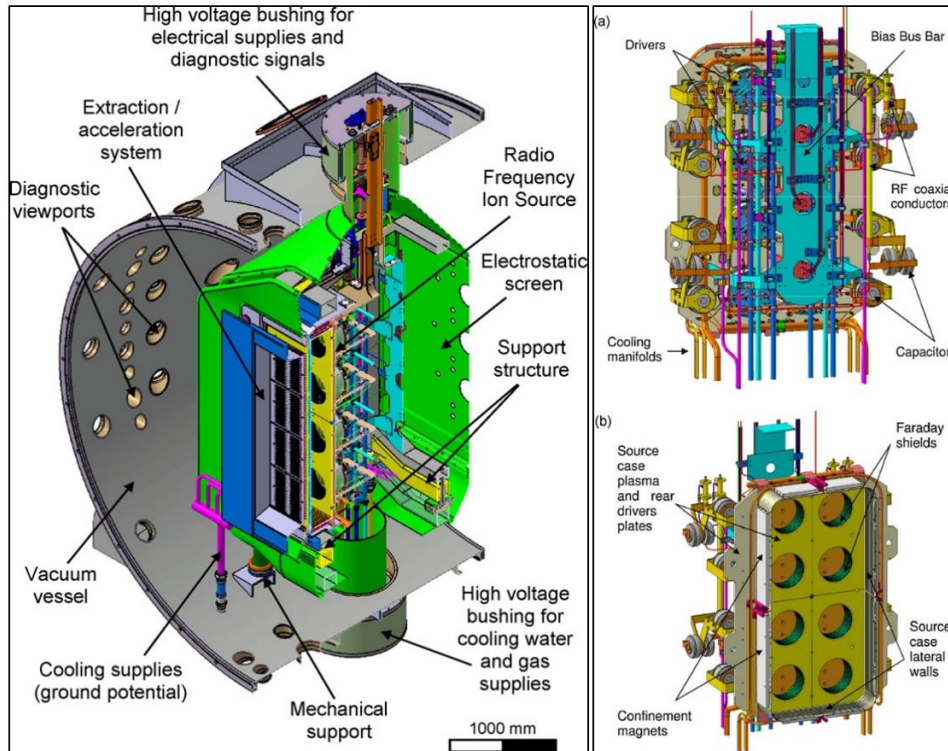


Figure 2-5 SPIDER, internal view and zoom on the beam generation system

2.3.2 MITICA

MITICA is a full scale prototype of ITER's NBIs. It will be very similar to them, with a higher number of diagnostic devices which will allow a deep analysis during the operation. In fact, MITICA is being built to test the devices that in future will be used in ITER.

Unlike SPIDER, MITICA has all the component similar to ITER's NBIs, not only the beam source assembly. It is designed to create a beam of 16.5MW of power that will be entirely dissipated on a calorimeter. Being the beam not injected in the chamber, in that experiment there will not be the effect of the stray magnetic field caused by the inductors around the vacuum vessel of a Tokamak, as it will be in ITER. Therefore, in MITICA the correction coils to shield the ion beam from these disturbs are not necessary, while residual magnetic field coils will be mounted to reproduce the residual magnetic field that will be present inside ITER's NBIs despite the intervention of the correction coils.

The main beam requirements of MITICA are reported in table 2-1 for Hydrogen and Deuterium beams.

Table 2-1 Main requirements of MITICA

Parameter	Hydrogen	Deuterium
Beam energy	870 keV	1000 keV
Beam current	49 A	40 A
Beamlet divergence	<7 mrad	<7 mrad
Extracted ion current density	35 mA/cm ²	29 mA/cm ²
Extraction voltage	12kV	12kV
Pulse length	3600 s	3600 s
Source pressure	0.3 Pa	0.3 Pa
Co-extracted electron fraction	<0.5 e/H	<1 e/D
Uniformity	±10%	±10%

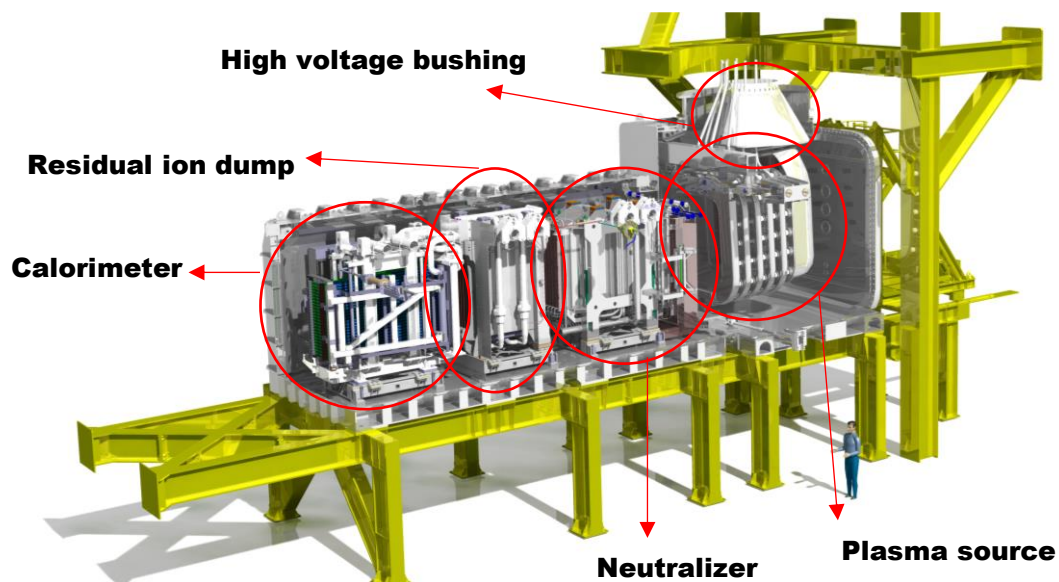


Figure 2-6 CAD view of MITICA

MITICA (shown in fig. 2-6) is made up by a plasma source very similar to the SPIDER's one. It is a radiofrequency negative ion source, with all the characteristics exposed in the previous paragraph.

The electrostatic accelerator (fig 2-7), placed after the extraction grid, provides an acceleration of 1MeV. It is made up by five accelerating grids at increasing potential, from the -1MV of the first grid to the ground potential of the last one, with steps of 200kV. Therefore the beam source potential is set at -1MV, with respect to the vessel of MITICA.

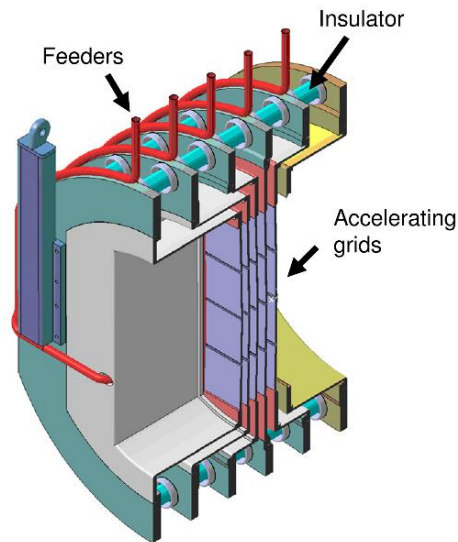


Figure 2-7 Simplified CAD view of MITICA's accelerator grids

The neutralizer (fig 2-8) contains neutral gas at a high pressure, enough to provide a good neutralization efficiency when the beam collides with the molecules of this gas and the charge exchange occurs. The pressure must not be too high, else the gas diffuses out of the neutralizer and there is a higher pressure of background gas in the acceleration stage, causing losses due to ion stripping and stray particles.

Into the neutralizer, the beam flows between 4 vertical channels.

To control the pressure, the neutral gas is continuously injected into the channels and removed by cryo pumps.

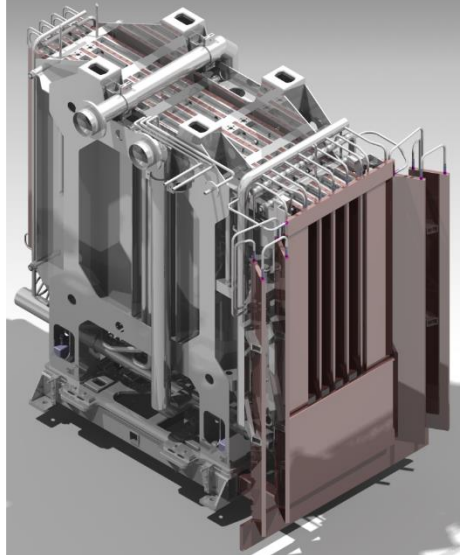


Figure 2-8 CAD view of MITICA's neutralizer

The residual ion dump (fig 2-9) placed after the neutralizer is the device where the high quantity of ions exiting from the neutralizer is deposited, since the neutralization process has an efficiency of about 50%. The charged particles are diverted from the beam by means of magnetic fields and converged into metallic components. Methods to recover the energy of the accelerated residual ions are being studied: this should be the easiest way to increase the overall efficiency of a NBI.

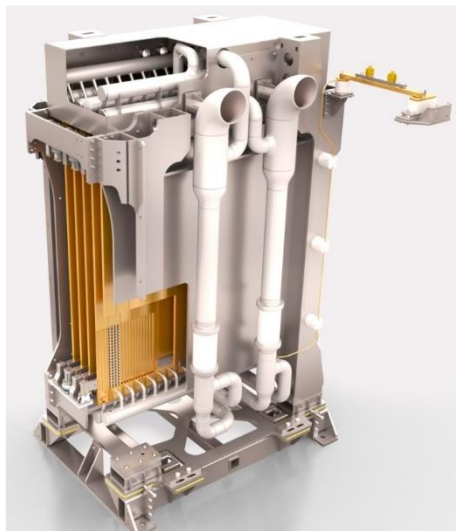


Figure 2-9 CAD view of MITICA's residual ion dump

The calorimeter (fig. 2-10) needs to stop the beam when the valve between the NBI and the reactor chamber is closed, for example in case of commissioning. For this reason, this device must be able to withstand the entire power of the beam (up to 20MW) and for long times, up to 3600s, which is the maximum duration of the beam pulse. In MITICA there will not be the injection of the beam in a reactor chamber, so the beam power will be always dissipated on this device.



Figure 2-10 CAD view of MITICA's calorimeter

All the component where the beam flows are subjected to high heat fluxes, which can reach locally peaks of tens of MWm^2 . This implies high mechanical stresses and the need of removing that heat using water cooling. Therefore, acceleration grids, neutralizer, residual ion dump and calorimeter must be fed of water cooling.

Experiments duty cycle of 1:4 (one hour on, 4 hours stand-by) allows power optimization: for both SPIDER and MITICA the energy is stored in two underground basins (850m^3) and then cooled down by air coolers and cooling towers with a continuous cooling power of 24MW. The heat removal for the two experiments can reach the peak of 70MW.

The high voltage bushing (fig. 2-11), which has the function to separate the transmission line, is insulated with high pressure SF_6 (6 bar) from the high vacuum of the beam vessel. Moreover through the bushing all the electric, water and gas feeders must pass to supply RF ion source, the acceleration grids, water cooling systems and the gas injection of the beam source. Neutralizer, residual ion dump and calorimeter are referred to MITICA's ground reference, so they are fed directly from the beam line vessel.

Being the acceleration grids at 5 different potentials, they must be connected to the respective busbars of the transmission line. The connection are made by tubes, passing through high voltage bushing, where flows also the water for the cooling of that grids.

Inside the bushing high electric fields appears due to the high insulation voltage, so electrostatic shield are necessary to mitigate it. And for the high insulation capability requested, the device is very big: it is 4.7m high and it has big ceramic rings that divide the 5 insulation stages having a diameter of 1.56m.

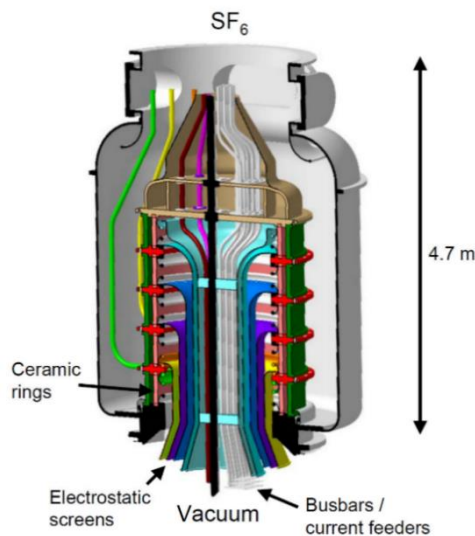


Figure 2-11 CAD view of MITICA's high voltage bushing

2.4 MITICA power supply systems

The power supply system of MITICA is fed by the 400kV grid. A High Voltage switchgear provides a 22kV distribution voltage to the main power supplies, which are:

- The Acceleration Grid Power Supply (AGPS), a high voltage, high power system supplying the acceleration grids
- The Ion Source Extraction Power Supply (ISEPS), which is devoted to the generation and extraction of the ions
- The Ground Related Power Supply, which is a power supply at ground potential for auxiliary functions in the NBI.

MITICA supply systems will be placed in different buildings from the building that will host the two experiments SPIDER and MITICA (fig 2-12). Besides, some parts of the electrical system will be placed outdoor (step-down and step-up transformers and the filter tanks). The power supply systems at high voltage are connected to MITICA through a transmission line insulated in SF₆.

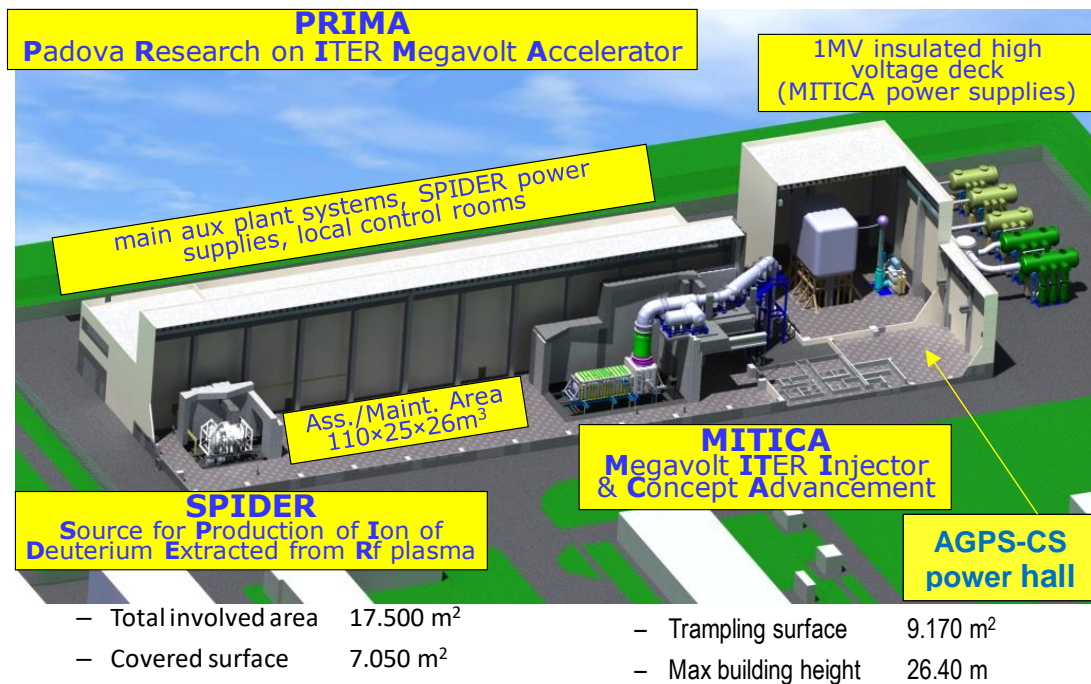


Figure 2-12 PRIMA facility

The overall power supply system of MITICA is represented in a CAD view (fig 2-13), where there are also some components not showed in fig. 2-12, and in the electrical scheme (fig 2-14). The layout of the system and the schemes are based on the conceptual design documents prepared to launch the call for tender for the procurements.

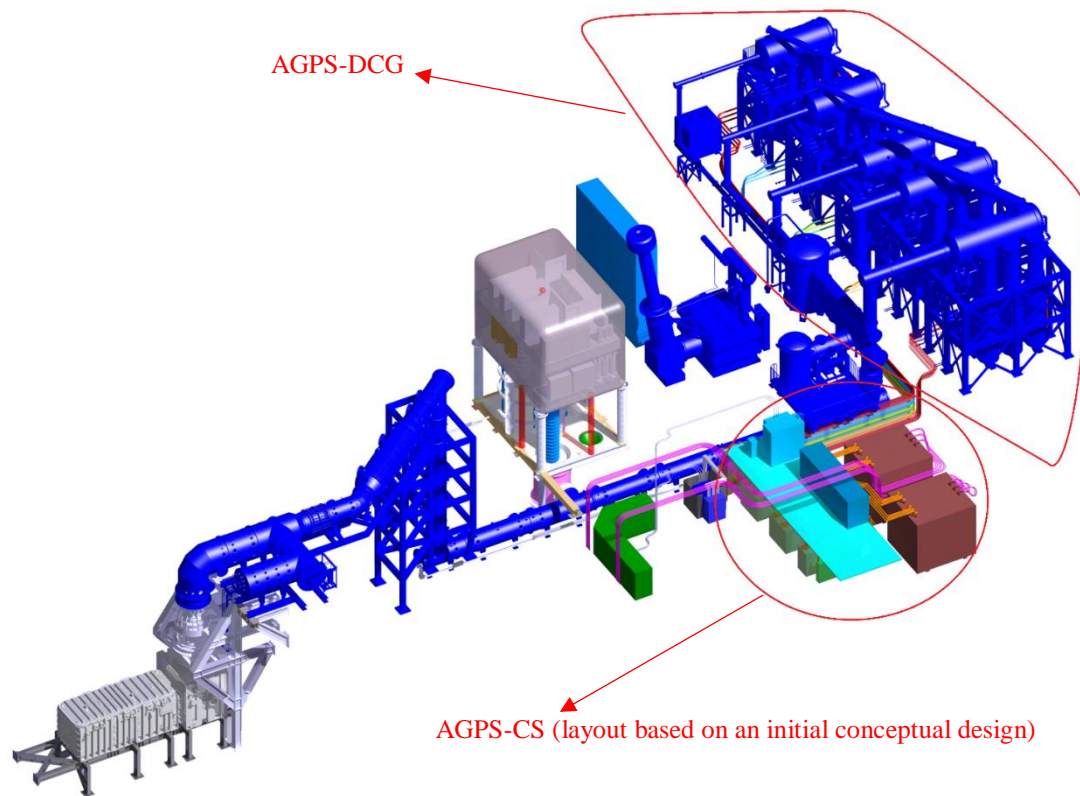


Figure 2-13 CAD view of MITICA power supplies

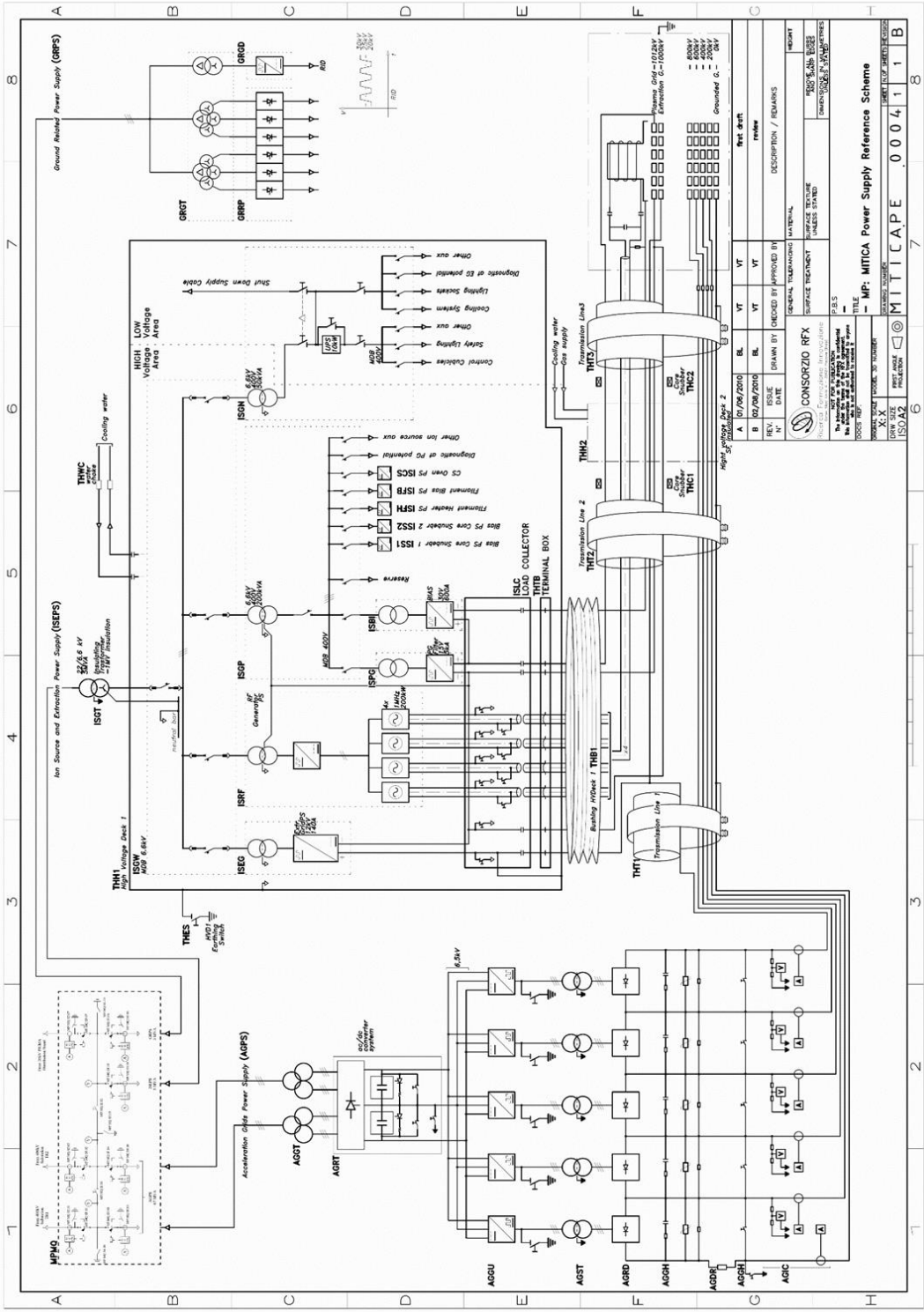


Figure 2-14 Electrical scheme of MITICA power supplies

2.4.1 AGPS

The AGPS (fig.2-15) is a special switching power supply with demanding requirements: high rated power (about 55 MW), extremely high output voltage (-1MV dc), long duration pulses up to 1 hour and a peculiar operational scenario, where frequent short-circuits of the acceleration grids have to be tolerable. The procurement of the AGPS is split in two parts: the low voltage conversion system, namely the AGPS-Conversion System (AGPS-CS,) being procured by the European domestic agency, and the high voltage DC Generators (AGPS-DCG), being procured by the Japanese domestic agency. The AGPS-DCG is presently in the installation phase, the final delivery of the system is foreseen for January 2018.

The AGPS-CS, which is the subject of this thesis, is presently being procured. The contract for the procurement has been awarded to NIDEC-ASI, a company based in Milan [3] specialized in the design and manufacturing of medium voltage drives, motors and power supplies for industrial automation, Energy, Marine, Metals, Oil and Gas and General Industry applications. The AGPS-CS is presently in the detailed design stage, construction, delivery and commissioning are foreseen in late 2016 and 2017.

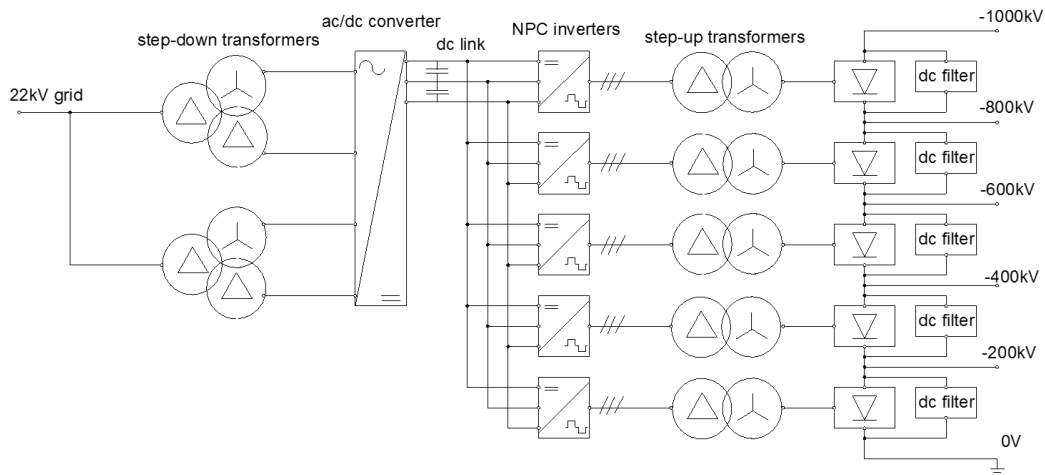


Figure 2-15 AGPS scheme

Conceptually, the AGPS-CS is composed, downstream the step down transformers, by an ac/dc conversion system based on thyristors, rated for 6.5kV and 9kA, supplying five three-phase Neutral Point Clamped (NPC) inverters. The design of the AGPS-CS presents some challenging aspects, in particular concerning the feasibility of the NPC inverter power modules, due to the high power and voltage. Conventional medium voltage inverter drives are not suitable for the required ratings, therefore the design has to be customized on the basis of the requirements. More details on the AGPS-CS requirements are given in the following chapter.

Each inverter is connected to a DC Generator (DCG). A DCG is composed by a step-up transformer feeding a diode rectifier; the five rectifiers are connected in series at the output side to obtain the nominal acceleration voltage of -1 MV, with availability of the intermediate potentials in steps of 200kV.

To accelerate negative ions the grids are set at negative potential, and the first grid is set at -1MeV with respect to the local ground potential. Therefore the components of the AGPS-DCG supplying the first grid need higher insulation capability. The diode bridges and the transmission lines are connected to the grids are all insulated using SF₆ because of the high voltages in all the 5 stages, with the first one having higher requirements, and the step-up transformers are insulated in oil.

2.4.2 ISEPS

ISEPS includes all the power supplies devoted to the creation and extraction of ions. In this system there are:

- the Radio Frequency Power Supply, which feeds the RF drivers. It is made up of an ac/dc conversion system, 4 RF generators (one feeding a couple of drivers) rated for 200kW on a 50Ω matched load and 4 coaxial lines. The RF generator can modulate in feedback the power from 10% to 100% with an accuracy of 1%, with a frequency variable in real time from 0.9MHz to 1.1MHz and an accuracy of 1kHz, which allows the continuity of the matching conditions of the load;

- the Extraction Grid Power Supply, rated for 12kV and 140A, which is connected to the Plasma Grid and the Extraction Grid (through a dedicated insulated cable), polarizing positively the Extraction Grid with respect to the Plasma Grid. The voltage can be regulated continuously in feedback from 0% to 100% with a resolution of 100V and an accuracy of 2%. The rise time from 10% to 90% can be settled in the range 500 μ s-100ms;
- the Plasma Grid Filter Power Supply that generates the current flowing into the plasma grid in order to generate the magnetic field to not extract electrons. It is rated for 5kA and 15V and it is connected to the vertical extremities of the plasma grid. The current is tunable in real time and in the full range;
- the Bias Power Supply, which produces the bias voltage of the Plasma Grid with respect to the source body. Thanks to that voltage the negative ion yield is increased, decreasing the quantity of extracted electrons. It is rated for 600A and 30V, with current and voltage adjustable in real time and in feedback;
- the Bias Plate Power Supply, which provides a positive biasing of a bias plate with respect to the source body. This bias plate is an additional experimental tool to enhance the negative ion yield and reduce the electrons extraction. It is rated for 30V and 150A;
- minor power supplies, which are: Caesium ovens, the starter filaments and the bias power supply for the two core snubber of the transmission line

All these power supplies are referred to -1MV with respect to the ground. Therefore, it is necessary to insulate them and they are placed inside a high voltage deck (HVD1), insulated for 1MV, which acts as an air insulated Faraday cage. The high insulation requirement necessitates a distance of at least 5m between the HVD1 and building walls. Moreover all ISEPS devices will be fed by an insulating transformer, which has to insulate 1MV too.

2.4.3 GRPS

GRPS is a power supply at ground potential and it includes:

- the Residual Ion Dump Power Supply, which generate a 25kV dc bias voltage to polarize the residual ion dump plates, with a superimposed alternating voltage of ± 5 kV at 50Hz. These voltages are controlled in real time, in feedback. The rated current is 60A;
- the Residual Magnetic Field Power Supply, which supplies the residual magnetic field coils, creating the residual magnetic field that is foreseen in ITER due to the external magnetic fields

3 The Acceleration Grid Power Supply (AGPS)

3.1 Main requirements

The AGPS shall operate to provide a maximum beam pulse of 1 hour. The supply system has to withstand at least 50000 pulses, not all having the maximum pulse length: the overall beam on time specific is 5500 hours. If the pulses are short (less than 150s), they can be triggered with 10 minutes of pause. Longer pulses must be triggered with a pause time that is 25% of the pulse duration.

During system's operation, breakdowns between grids will occur and they are not considered a fault condition; but there is a maximum number of breakdowns foreseen (see table 3-1).

During the operational life of the AGPS, which is foreseen 20 years, the maximum number of energization and de-energization of the dc link (explained in paragraph 3.1.2) is 10000.

All these AGPS requirements are reported in table 3-1.

Table 3-1 AGPS operational requirements

Parameter	Value
Maximum pulse length	3600s
Total number of pulses	50000 (not all at full pulse length)
Total beam on time	1.98×10^7 s
Total number of breakdowns	4.5×10^5
Duty cycle	1 shot/10 minutes for $t < 150$ s 25% for $150s < t < 3600$ s
Maximum number of energization/ de-energization in the life	10000
Operational lifetime	20 years

These were the operational requirements of the AGPS, in next paragraphs its electrical requirements will be presented, related mainly both to the output of the AGPS (therefore before the transmission line connecting it to the grids) and to the dc link, which is important for the interface between AGPS-CS and AGPS-DCG.

3.1.1 Current and voltage in nominal operation

The purpose of the AGPS is to supply the acceleration grids, which are the loads of the system. There are five acceleration grids; in nominal operation they are supplied in steps of -200kV down to -1MV dc for Deuterium operation.

The loads of the acceleration grids are equivalent from the point of view of the power supply to current generators connected between the grids. The current of each generator corresponds to the ion beam current. The current of the first stage, therefore between the grids at -1MeV and -800kV, is the maximum current, then it decreases in the following stages. The cause is that part of the ions of the beam impinges on the previous grids and that corresponds to a loss of load current.

As it is shown in figure 3-1, where the nominal current and voltage of each acceleration stage are represented for Deuterium operation, the beam is generated in the ion source and then accelerated with the voltage of 12kV between the plasma grid and the extraction grid; notice that this part is supplied by the ISEPS. Between these two grids a current of almost 120A is generated, but here also electrons contribution is considered, while these useless particles are deflected out of the beam before the first acceleration grid. Moreover there are losses for the defocusing of the beam and in overall about half of

the current is lost in this stage. The extracted beam current, accelerated by the first stage, is 59.4A and then fractions of it are lost into the grids, where the quantity can be calculated simulating the beam optics. Hence, in the first stage there is the higher power requirement, as can be obtained from the product between the current flowing in the stage and the 200kV of impressed voltage. Summing up the powers provided by the 5 acceleration stages, we obtain that the AGPS must be able of providing about 52MW and at the output it produces a current beam of almost 40A, a beam D⁻ of about 40MW of power.

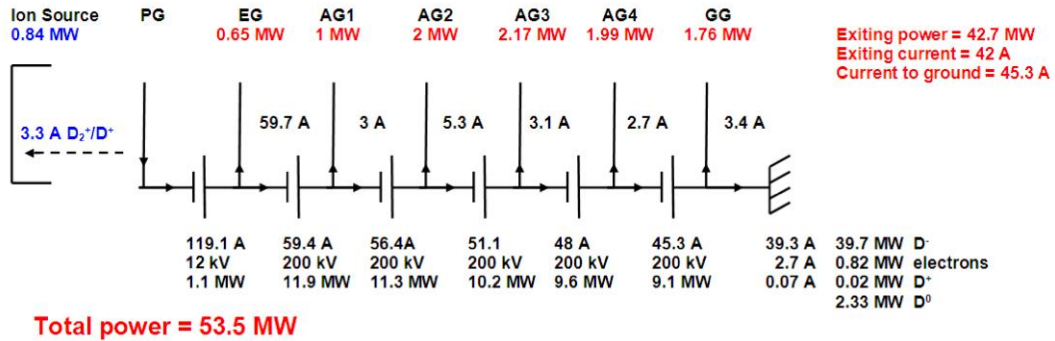


Figure 3-1 Current distribution in the generation and acceleration stages in deuterium operation

The system is foreseen to operate with Hydrogen too. In the operation using Hydrogen the voltage step imposed between the acceleration grids is lower (174kV) than in Deuterium operation, while the output beam current is higher, about 46A of nominal value, to generate about the same beam power at the exit of the accelerator: a beam H⁻ of about 40MW of power.

Actually the system is rated for a higher power: the beam currents represented in figure 3-1 are increased by 5% to consider eventual uncertainties in current estimation and possible developments of the accelerator.

From estimation of current distributions taking into account the beam optic, the result with this increment are shown in table 3-2, where the values for operation with hydrogen are reported too.

Table 3-2 Current and voltage on the different stages

	D-operation		H-operation	
	Voltage	Current	Voltage	Current
Stage 1	200kV	62.4A	174kV	65.9A
Stage 2	200kV	59.2A	174kV	63.4A
Stage 3	200kV	53.7A	174kV	58.9A
Stage 4	200kV	50.4A	174kV	55.7A
Stage 5	200kV	47.6A	174kV	53.5A

As we can see from the table, the system has to operate with a current value up to about 66A, in Hydrogen operation, and a voltage step up to 200kV in Deuterium operation. These two specifics are related to different way of operating the system, therefore they shall not be satisfied together.

3.1.2 Dynamic performance requirements

The acceleration voltage has to be controlled with the perveance law to guarantee the best focalization of the beam. This means that the extracted current and the total acceleration voltage must be linked by eq. 2.9. To start-up the beam, two possible scenarios can be realized:

- Start-up in perveance matching: the RF drivers are controlled to generate the extracted ion current corresponding to 80-90% of the perveance law as the AGPS output voltage ramps up. When the acceleration voltage approaches the set-point, the ion beam current is increased up to 100% of the value of the perveance law
- Start-up at maximum voltage: the AGPS output voltage is ramped up to the operating value without the presence of the beam, which is successively increased to follow the perveance law

For both scenarios, the acceleration voltage is required to reach 90% of the setpoint within 80ms (rise time). Another dynamic requirement for the acceleration voltage ramp up is the settling time (time from 90% to 100% of the setpoint), which must be less than 50ms.

The two modes of operation are shown in figures 3-2.

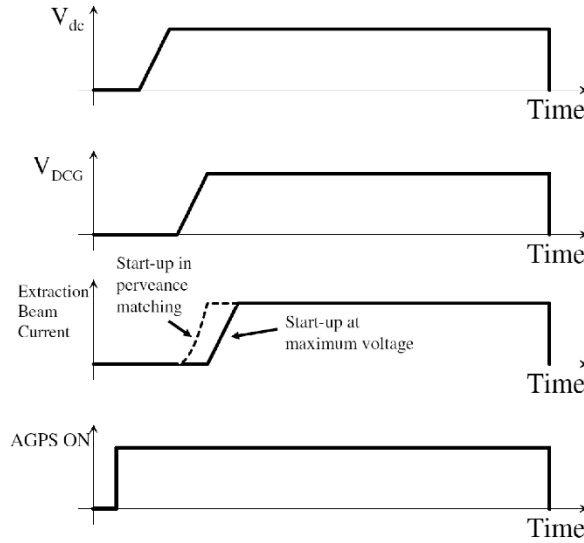


Figure 3-2 Beam initiation and shutdown

The overall dynamic requirements that the AGPS has to fulfil during the operation are reported in table 3-3.

Table 3-3 Main operation requirement for the AGPS output voltage

Parameter	Value
Voltage regulation range	20% - 100%
Voltage resolution	1 kV
Output voltage accuracy for 1 hour operation	$\pm 2\%$ with respect to the full voltage
Maximum voltage fluctuation	$\pm 2.5\%$ at the flat top
Maximum voltage ripple	$\pm 5\%$
Maximum raise time of the output voltage	80ms
Maximum settling time	50ms
Maximum undershoot at beam on	15%

3.1.3 Breakdown and Beam Off

Due to the high voltages between the acceleration grids, very close to the voltage withstanding capability of the insulation, during the operation breakdowns will frequently occur between the grids. Accordingly, the breakdown between the grids must be taken into account in the normal operation, it is not considered a fault. When a breakdown occurs, the load of the AGPS is short circuited and to avoid high values of currents that are supplying the involved grids, the AGPS has to be switched off as quickly as possible; the EGPS and the RFPS have to be switched off too.

The maximum time between the breakdown and the triggering of the AGPS breakdown sequence (detection time) must be not greater than $50\mu s$ and the maximum time between the triggering of the AGPS breakdown sequence and the time when the AGPS is turned off must be not greater than $100\mu s$ (cut-off time).

After a certain time, at least 20ms, the breakdown is extinguished and the AGPS, the EGPS and the RFPS shall be restarted, controlling the DCG voltage equal as in the start-up sequence previously explained in paragraph 3.1.2.

Up to 50 consecutive breakdowns are allowed, above this number the AGPS is stopped permanently and the status is recognized as a fault by the control system of the power supply. The total number of breakdowns admitted in the nominal pulse duration (3600s) is 200.

The operational requirements for the AGPS for the grid breakdown are reported in table 3-4.

The ISEPS is not affected by the breakdown: between plasma and extraction grids only 12kV of voltage are imposed, too low to generate the breakdown.

Table 3-4 Operational requirements for the AGPS for the grid breakdown

Parameter	Value
Maximum detection time	50 μ s
Maximum switch off time	100 μ s
Time to be ready to restart after a grid breakdown	20ms
Maximum number of grid BD in a single pulse	50 consecutive 200 total in the nominal pulse duration

The sequence of operation during the breakdown is shown in figure 3-3.

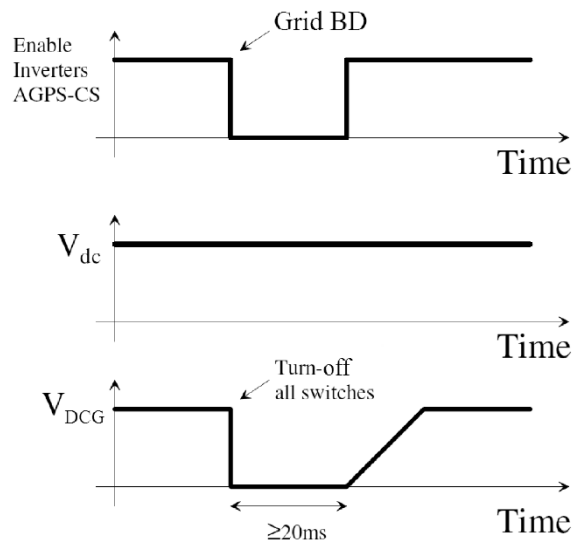


Figure 3-3 Restart operations after a breakdown

Another situation to be considered during operation is the beam off situation, i.e. when an unintentional interruption of the beam occurs.

This situation is equivalent to a sudden loss of load for the AGPS, therefore at the output of the DCGs an overvoltage establishes.

The beam off condition is a fault and a protection must be triggered to avoid electrical stresses on the high voltage components. The AGPS must be therefore switched off in less than 100 μ s.

During the beam off the GRPS is not turned off to supply its loads.

3.2 General scheme

As already said in paragraph 2.4.1, the AGPS (see fig 3-4) is divided in two parts: the AGPS-CS and the DCG, awarded to different procurements.

The AGPS-CS takes electrical power from a high voltage transmission line, more precisely from a middle voltage substation which supplies PRIMA, to provide the power to the five DGCs supplying the relative acceleration stages.

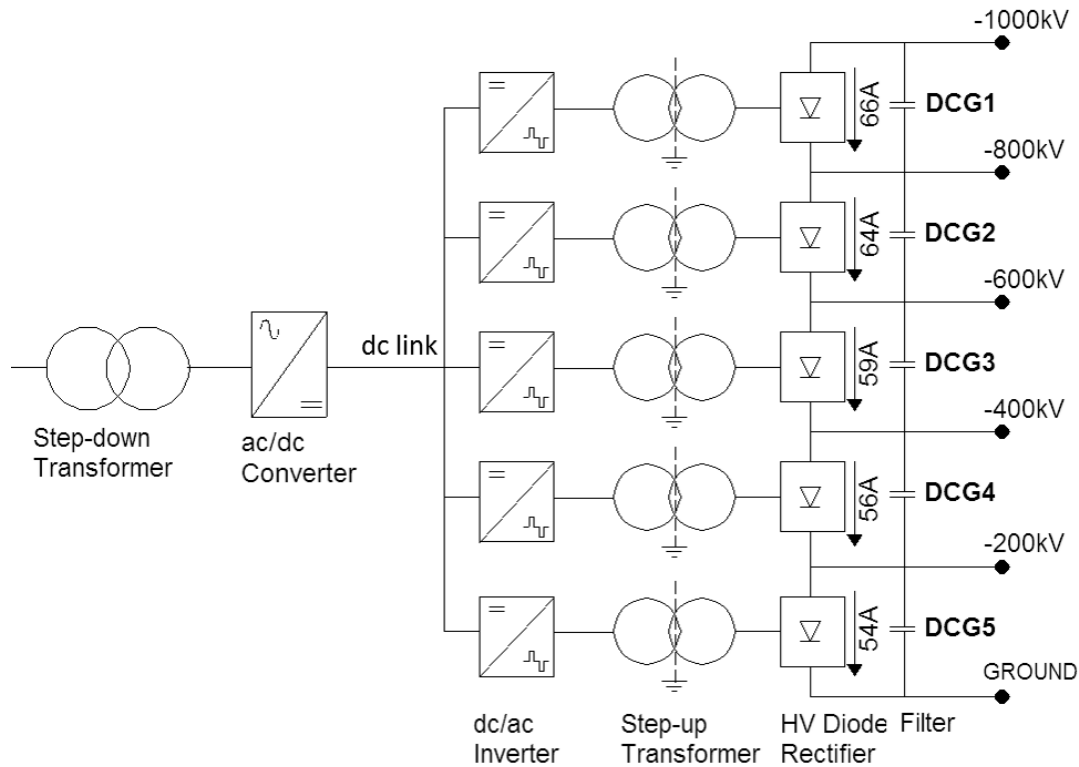


Figure 3-4 AGPS scheme

The conceptual design of the AGPS-CS foresees a system that provides the five alimentations to the 5 DCGs, which have to be supplied by an alternated power, with controllable voltage.

The AGPS-CS is therefore constituted by a transformation stage to lower the voltage, an ac/dc conversion stage, a dc link to reduce voltage oscillations and a dc/ac conversion stage which allows to control the output voltage.

This conceptual design has been developed and now it is quite a definitive design, except for some parts of the system, since the procurement is in progress. The following description is based on this design.

The AGPS-CS transformation stage is composed by two parallel transformers with two secondary windings, set in series, that reduce the middle voltage (22kV) of the substation supplying PRIMA to a lower middle voltage value. This because downstream the transformers there is the ac/dc converter, made up of thyristors. It is necessary to reduce the voltage to a value that is sustainable by the thyristors. The ac/dc converter provide a controllable dc voltage on the dc link, filtered by a capacitor bank in order to fulfil the requirements on the ripple and the overshoot (table 3.3). Ten NPC three levels inverters, two in parallel for each stage, are connected to the dc link and produce the 5 medium voltage ac sources supplying the DCGs.

The DCGs have been already installed, procured by JADA, and the scheme here described is the result of the development of the conceptual design realized by the JADA.

The DCGs are all composed by the same equipment, which is different only in the insulation capabilities, higher for the first two stages. The input alternated medium voltages coming from the output of the AGPS-CS are increased by five step-up transformers in order to have the alternated voltages that allow to reach the wanted 200kV dc voltage for each step using 5 diode bridges downstream the transformers. At the output of these ac/dc converters there are filters to fulfil the requirement of table 3-3 and the outputs are set in series to generate the total nominal voltage of 1MV.

The output of each stage is connected to the relative acceleration grids of MITICA with a high transmission line insulated in SF₆.

3.2.1 Middle voltage ac distribution grid

The supply systems of PRMA are connected to a 400kV transmission line with short circuit capacity between 12GVA and 18GVA, with 50Hz of nominal frequency.

Two main transformers rated for 50MVA and having a 6% short circuit impedance are installed to provide two separated 22kV networks. Since the transmission line voltage can vary up to $\pm 10\%$, a tap changer with 25 regulation steps for each transformer is provided, in order to keep almost constant the 22kV medium voltage grid that supplies MITICA and SPIDER. This grid is distributed with neutral insulated from earth. Whereas RFX-mod is supplied by this grid too, the tolerance of that medium voltage grid is increased to the interval of variation of -16% and +4%.

The 22kV grid has a nominal voltage of 22kV, a short circuit current of 12.5kA and a maximum power available of 5MVA. It can be supplied by the 20kV local utility operator too, in the case of low power operation.

The scheme of MITICA medium voltage distribution system is reported in fig. 3-5, where it can be seen that a circuit breaker is foreseen for every line arriving and departing from the MV busbar and for the connection with the 20kV external supply grid (in normal condition left opened) to provide continuity of service at reduced power.

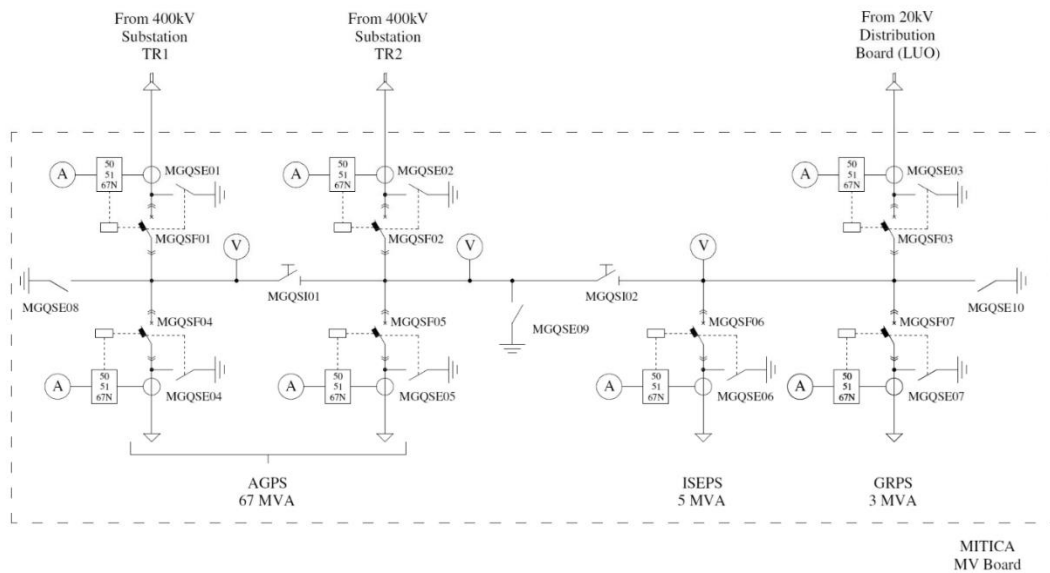


Figure 3-5 MITICA medium voltage distribution grid

3.2.2 AGPS-CS scheme

The AGPS-CS is directly connected to medium voltage distribution grid.

The two step-down transformers, as shown in fig. 3-6, have two uncoupled secondary windings which reduce the 22kV voltage of the middle voltage grid to 1.5kV. Their main parameters are reported in table 3-5.

Table 3-5 Step down transformers parameters

Parameter	Value
Nominal power	38.2MVA (2x19.1MVA)
Primary nominal voltage	22kV
Secondary nominal voltage	1.5kV
Transformer connections	Dy11 and Dd0
Short circuit impedance (respect to 19.1 MVA)	10% (with a tolerance of $\pm 5\%$)
Coupling factor ($X_p/(X_p+X_s)$)	Uncoupled secondaries
Magnetization current	<0.2%
No load losses at 100% primary voltage	≤ 27 kW
Short circuit losses	≤ 250 kW

Notice that the two secondary windings are connected in different ways: one is star connected and the other is delta connected. The voltage on the two secondaries is therefore phase shifted of 30° and each one supply one thyristor bridge.

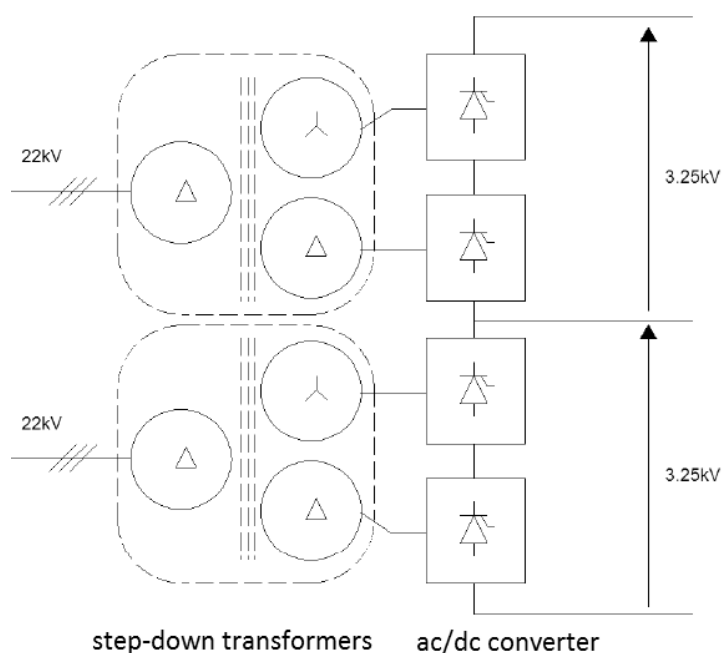


Figure 3-6 Scheme of the connection of step-down transformers to the ac/dc converter

The thyristor bridges are three phase bridges, therefore made up by 6 thyristors, which provide at their output a 6 impulses voltage with a continue component (the medium voltage) and a ripple related to the triggering of thyristors.

The dc link is half supplied by two bridge converters and the other half is supplied by the other two bridge converters. Since these two bridge converters are supplied by two secondary windings whose voltages are phase-shifted of 30° , their output voltage are shifted of 30° too. Setting them in series (see fig. 3-6), the overall voltage has twelve pulses each period. For this reason a group of two thyristor bridges is called a 12 pulse converter and it guarantees a lower harmonic generation both on the downstream voltage and on the upstream current, compared to a 6 pulse converter (a single bridge converter).

Thanks to the use of bridges composed by controllable semiconductor device, the medium voltage at the output of the ac/dc converter can be controlled with a feedback control system measuring the dc link voltage and this is necessary both to reduce the ripple on the dc link and to allow its energization and de-energization.

The dc link has a nominal voltage of 6.5kV and a ripple that must be reduced to comply with the specifications (table 3-3). To reduce the ripple the use a capacitor bank acting as filter is provided.

The overall capacitance of the dc link capacitor bank has been chosen at 36mF to have a proper filtering of the voltage, which allows the restriction of the voltage oscillations around the nominal value of 6.5kV within the $\pm 5\%$ in normal operation and $\pm 9\%$ in transient situations, as from requirements.

This is a very high capacitance and while on the one hand is needed to meet the requirements on the dc link voltage, on the other hand has the drawback of a very high energy stored in the bank during the normal operation.

The three phase NPC inverters are connected to the dc link.

3.2.3 NPC inverters

The scheme of the used NPC inverters is shown in fig. 3-7.

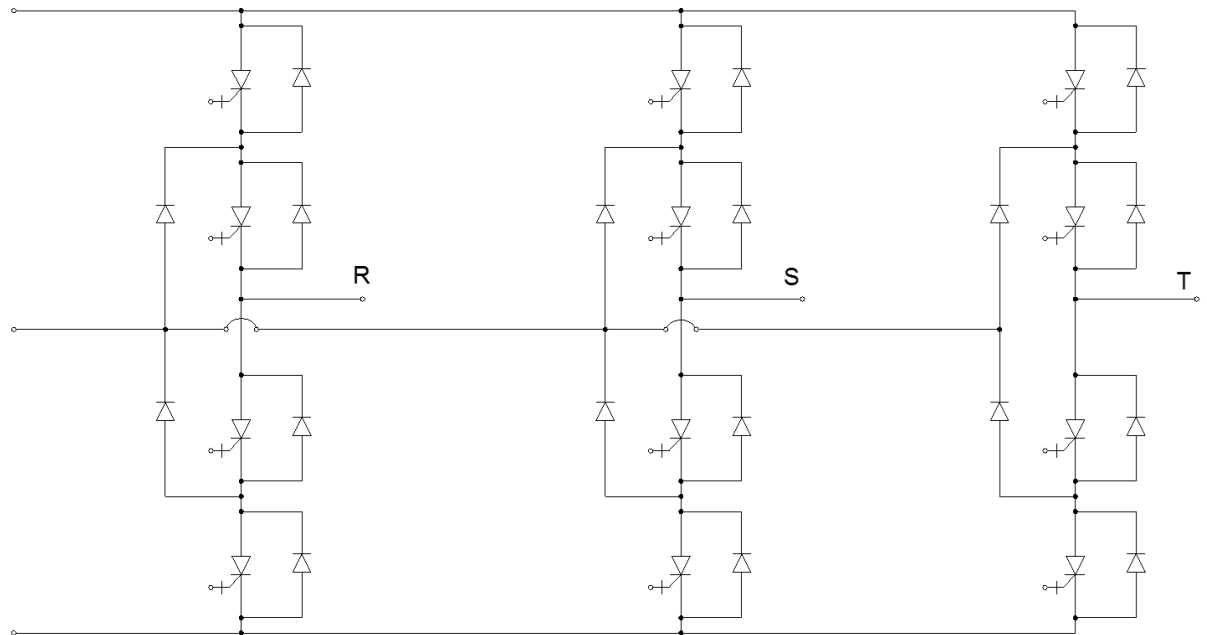


Figure 3-7 Scheme of an inverter

Each inverters' leg is made up by 4 IGBTs, the respective freewheeling diodes and the clamped diodes which allow the connection to the ground potential.

The components chosen are the IGBT 5SHY 42L600 produced by ABB semiconductors [4] and the diodes D1131SH produced by infineon [5]; the datasheets are reported in annexes 1 and 2. The same type of diode is used both for freewheeling and for clamped action. The main parameters of IGBTs and diodes are summarized in tables 3-6 and 3-7.

Table 3-6 IGBT main parameters

V_{DRM}	6500 V
I_{TGM}	3800 A
I_{TSM}	26 x 10³ A
V_(T0)	1.88 V
r_T	0.56 mΩ
V_{DC}	4000 V

Table 3-7 Diode main parameters

V_{RRM}	6500 V
I_{FAVM}	1100 A
I_{FSM}	22 x 10³ A
V_(T0)	2.19 V
r_T	1.364 mΩ

NPC inverters have been chosen to obtain a lower production of harmonics in the output voltage. Due to the high power and voltage required, the inverters are modulated in square wave at 150Hz as from requirements.

Using the middle potential level, the waveform of phase voltage at the output is not a square wave (except for some particular values of the modulation index: $m=2/3$ and $m=1/3$), but assuming the middle

potential value for a certain time during the period the harmonic content is reduced with respect to a square wave.

In figure 3-8 is shown the output phase and line voltages for an ideal NPC inverter at three levels, supplied by a 6.5kV dc voltage, having the three potential level to +3.25kV, 0V, -3.25kV. This waveform at 150Hz is obtained using a unipolar modulation with modulation index of 0.9, which is the nominal value that results to have the nominal operation of the AGPS, and using a triangular carrier at 150Hz. Including the internal stray and clamp inductances and the inductances downstream of the inverter, the waveform is altered.

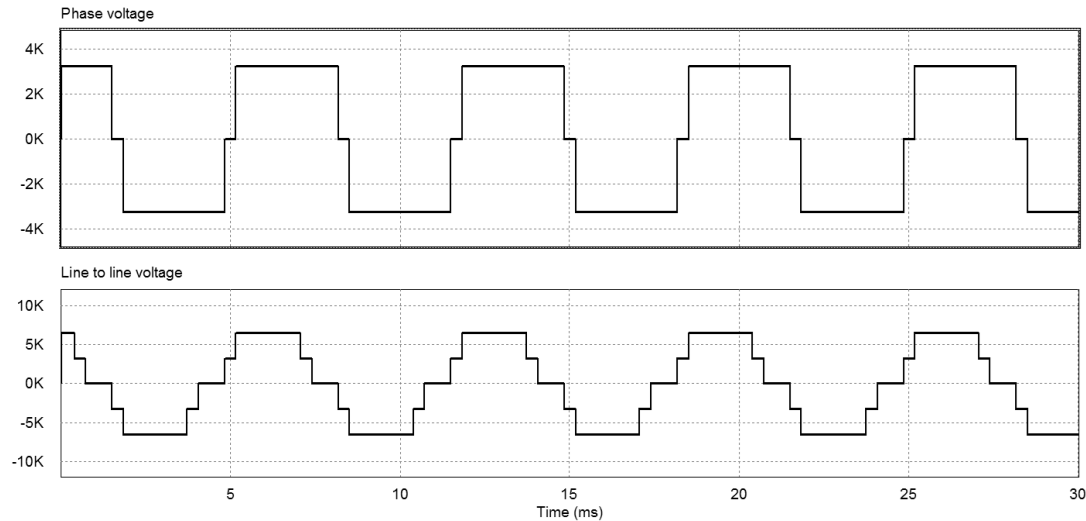


Figure 3-8 Output voltage from an ideal three phase NPC inverter at three levels, supplied by a 6.5kV dc voltage

The high output voltage level is obtained when the upper two IGCTs of the leg are conducting connecting the phase to the high potential of the dc link. When the two central IGCTs are conducting the phase is connected to the ground potential through the clamped diodes, therefore the phase has the null potential. When the two lower IGCTs are conducting the phase is connected to the negative potential of the dc link and so the output voltage has the low potential level. [6]

The freewheeling diodes allow to have current circulating in the opposite direction with respect to the conduction verse of the IGCTs during the time when its relative IGCT is switched on.

The NPC inverters are the components which allow to control the voltage at the output of the AGPS-CS, and consequently at the output of the DCGs. This is done by varying the modulation index with a feedback control (based on a PI controller) having as input the difference between the requested voltage and the voltage at the output of the DCG.

Since the current necessary to supply each stage is too high to be withstood by the IGCTs which make up these inverters, it is necessary to use two inverters in parallel for each stage. Therefore 10 inverters are connected to the dc link.

3.2.4 Electrical requirements at the interface between AGSP-CS and AGPS-DCG

Since the AGPS-CS is procured by the EUDA, while the AGSP-DCG is procured by the JADA, the electrical parameters inherent to the interface between the two subsystems must be well defined, with detailed requirements. It involves the value of the nominal voltage on the dc link and its ripple, the type of inverter used and the voltage waveform that they produce, parameters of the step-up inverters and of the inductances downstream the inverters. They are summarized in table 3-8.

Table 3-8 Electrical requirements at the interface between AGPS-CS and AGPS-DCG

Parameter	Value
Inverter topology	Three-phase Neutral Point Clamped
Nominal value of dc link voltage	6.5kV
Maximum ripple of dc link voltage	±5%
Maximum variation of dc link voltage in transient conditions	±9%
Output voltage waveforms from the inverters	Three level square waves, with variable duty-cycle
Inverters frequency	150 Hz
Equivalent dc/ac inverter output decoupling + stray inductances, for each phase	110 μ H
Maximum output dc current component from inverters	1% of the rated output current of the inverter
Step-up transformer connections	Delta/star
Step-up transformer short-circuit inductance, measured at secondary side	0.2 H for the first two stages 0.22H for the other three stages
Step-up transformer turn ratio (primary/secondary)	1/18.2

3.2.5 AGPS-DCGs scheme

Each AGPS-DCG have a step-up three phase transformer to raise the voltage with a turn ratio of 18.2 between primary and secondary. The parameters of these transformers are reported partly in table 3-9. Notice from table 3-9 that they have different nominal powers, to avoid the oversizing since previous stages require more power, having the beam a higher current.

Except this, basically the transformers can be subdivided in two groups of similar characteristics: the two of the first two stages are bigger transformers, with higher no load and short circuit losses and no load currents than the other three. They have also quite different resistance of the winding, leakage inductance and stray capacitances.

Table 3-9 Step-up transformers parameters

Stage	-1MV/ -800kV	-800kV/ -600kV	-600kV/ -400kV	-400kV/ -200kV	-200kV/ 0kV
Connection	Delta/star	Delta/star	Delta/star	Delta/star	Delta/star
Turn ratio	1:18.2	1:18.2	1:18.2	1:18.2	1:18.2
Total leakage inductance (see at secondary side)	0.20H	0.20H	0.22H	0.22H	0.22H
Resistance of the primary winding	5m Ω	5m Ω	6.2m Ω	6.2m Ω	6.3m Ω
Resistance of the secondary winding	2.4m Ω	2.4m Ω	2.9m Ω	3m Ω	3m Ω
Nominal power	13.3MVA	12.9MVA	11.9MVA	11.3MVA	10.9MVA
No load current	0.5%	0.5%	0.3%	0.3%	0.3%
No load losses	64.2kW	65.9kW	32.9kW	33.6kW	32.8kW
Short circuit losses (with 150Hz sine wave)	68.5kW	55.8kW	52.2kW	41.0kW	44.9kW
Stray capacitance between screens	18.5nF	18.1nF	14.9nF	14.1nF	14.4nF
Stray capacitance between HV windings and second screen	1.7nF	1.6nF	2.1nF	2.0nF	2.0nF

The output of the transformer is connected to a three phase diode bridge which provided at its output a six pulse voltage waveform with an average voltage rated for 200kV. At the output of the diode bridge there is a filter, based on capacitors, to reduce the voltage ripple on the load to fulfil the requirements (table 3-3); the filter systems of all the stages are placed in a unique filter tank, insulated in SF6, and they are connected in series.

3.3 Layout of the AGPS-CS

The AGPS-CS is hosted in the "Building 3" of the PRIMA Facility. Fig. 3-9 is a CAD representation of the internal of that building, where the inverters' cabinets are the light grey cabinet and the dc link bus bars are in the elongated brown cabinet. The internal connections of the inverter cabinets with the dc link are not shown.

The blue cabinets are the thyristor bridges, supplied by the copper bars coming from the step-down transformers, which are outside the building. The output of these bridges are the three copper bus bars, having a rectangular cross section, that are connected to the dc link bus bars.

The light grey boxes are the inverter output cubicles, connected to copper lines which exit from the building connecting to the step-up inverters.

Next to the dc link and the inverters some space is foreseen for the eventual addition of other devices in the future, like the crowbar (represented with the yellow box in figure) or a chopper to mitigate the dc link voltage fluctuation by dissipating energy on resistors.

The dummy load, represented in the front part of the figure, is necessary to test the AGPS-CS before supplying the DCGs.

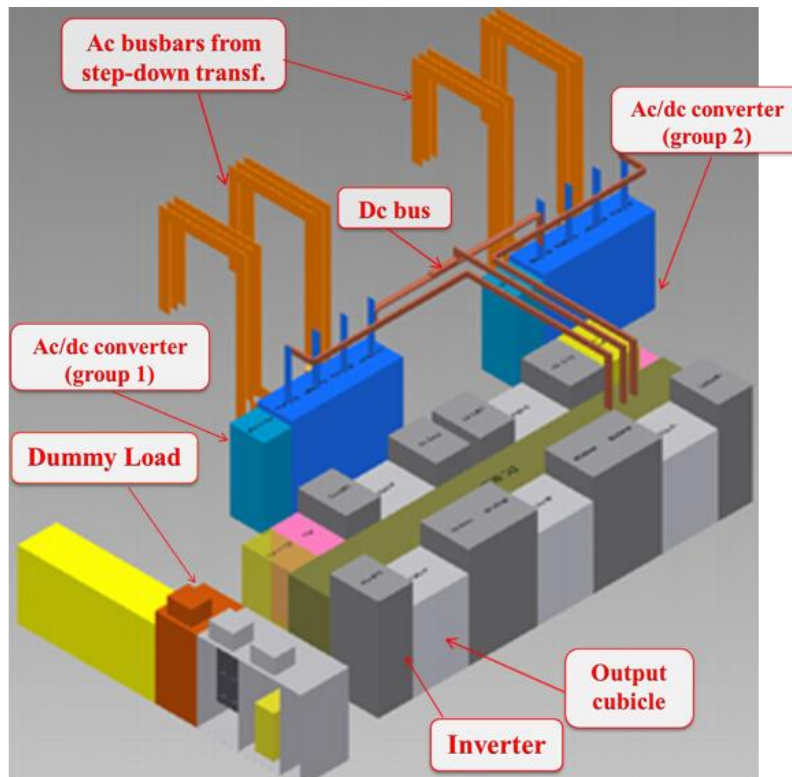


Figure 3-9 CAD view of building 3

The layout of the dc link with the connection to the inverters is shown in fig. 3-10. The dc link is composed by 3 bus bars, one at the voltage of 3250V, one to the ground potential and one to the voltage of -3250V. This structure is due to the use of three levels Neutral Point Clamped inverters that require a middle potential value, i.e. the ground potential. The capacitor bank is therefore made up of two half banks in series of 72mF: one connected to the positive voltage bar and the ground potential bar, the other connected to the ground potential bar and the negative voltage bar. The bank is distributed in the inverter cabinets to reduce the stray inductances between the bank and the inverters' legs.

Not all the cabinets are represented in fig. 3-10, but where they are not represented their presence is indicated by the bus bars connections and the fuses used at their input for protection against the internal short-circuits (one of the three protection systems considered, presented in paragraph 3.4.1).

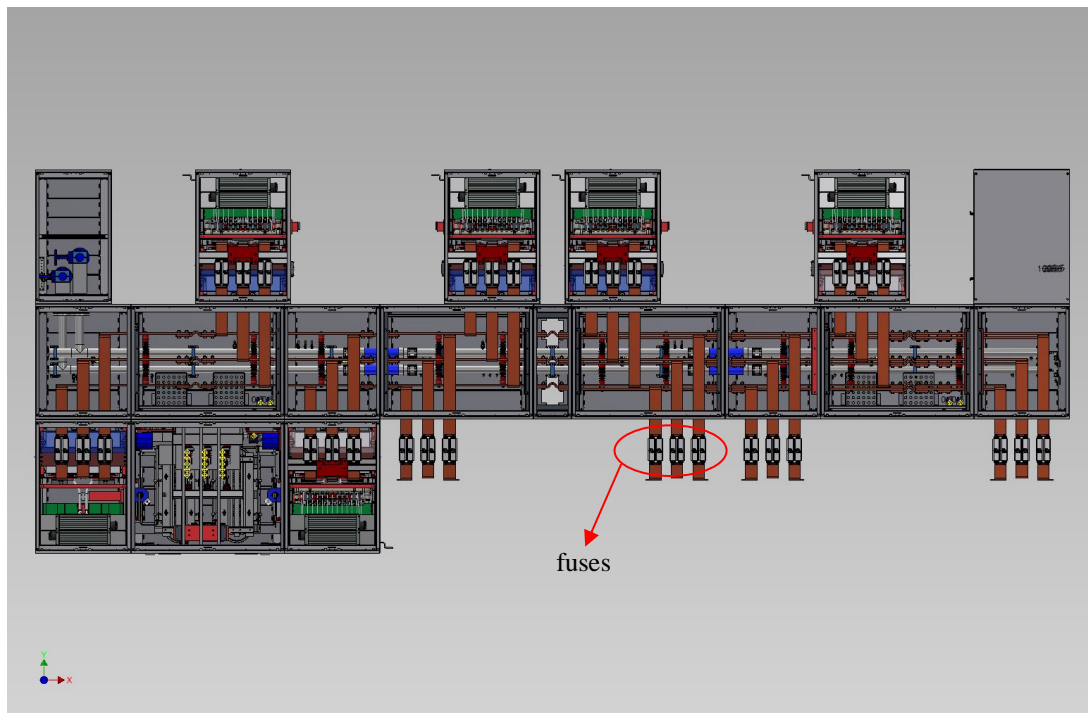


Figure 3-10 dc link layout, CAD representation seen from above

Each inverter cabinet is composed by three modules, each one containing the component of one leg and the capacitors of the bank. Each module has two capacitor banks of 2.4mF in series, therefore a total bank of 1.2mF is in parallel to each leg in a module. The 2.4mF bank is composed by three commercial capacitors of 800 μ F in parallel. The modules are 30 in total, each one having 1.2mF of capacitance of the bank: the overall dc-link bank has therefore the capacitance of 36mF. They are placed in the horizontal deck of the cabinet, as represented in fig. 3-11.

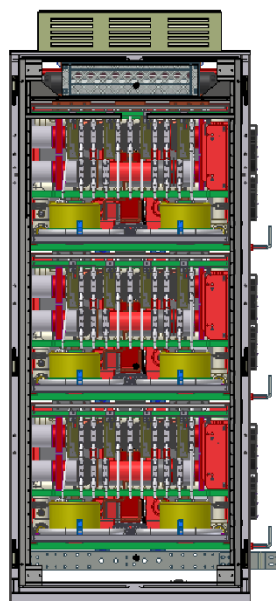


Figure 3-11 Front view of one inverter cabinet

3.4 Internal faults

Speaking about internal faults of the system, we mean the failures that can occur in the equipment composing the system itself. They can be of different types, concerning the different devices of the system: internal fault on the ac/dc converters, overvoltage on the dc link or internal fault on the inverter. The more important of these failures is the short circuit inside an inverter, because of the high energy stored in the capacitor bank of the dc link. The short circuit can occur when there is a failure of one or more of the switching components of the inverter's leg.

Considering the capacitance value (36mF) and the dc link nominal voltage value (6.5kV), using the well known formula of the energy stored in a capacitor:

$$W = \frac{1}{2} CV^2 \quad (3.1)$$

We obtain $W=760.5\text{kJ}$. This energy could become disruptive if an internal short circuit occurs in an NPC inverter, creating a low impedance path where the bank discharges.

We will consider the single fault situation, so the breakdown of only one of the four IGCTs of an inverter's leg. The case of a double fault is not analysed because it would occur if one IGCT has already undergone a breakdown and the control system has not detected it: the system continues to operate as if the fault had not occurred and when another IGCT of the leg is short circuited, the double fault would occur.

In the single fault situation only one of the two capacitor banks is discharging, while the other has not a closed path where the current can flow. Therefore one half bank discharges completely, while the other keeps its voltage to the nominal value of 3250V; which is the half bank discharging depends on which IGCTs of the damaged leg are closed or short circuited during the fault.

The current path on the damaged leg during the discharge of the bank is shown in the simplified fig. 3-12.

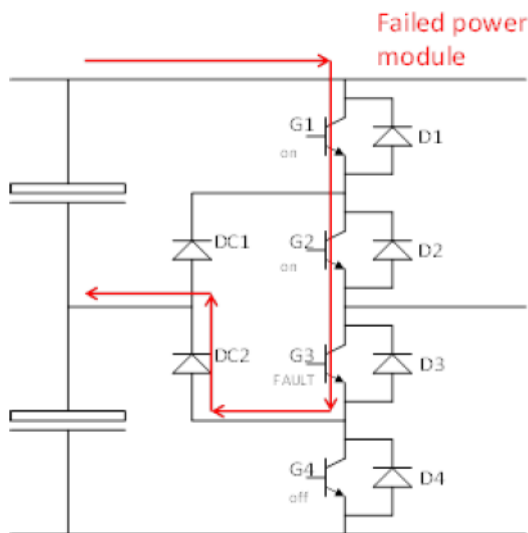


Figure 3-12 Current path on the damaged leg during the discharge

The dc link's energy would be quickly dissipated in the resistive components of the dc link itself and of the inverters, with the velocity of energy dissipation related to the R,L,C values present in the circuit: C is the capacitance of the bank while L and R come from the stray parameters of the circuit and the resistance of components.

The resistive components where the energy is dissipated are the resistance of the bus bars, of the connections, of the clamp resistors used in the inverters and of the semiconductor components of the inverters. Semiconductor components are the ICGTs, which are the fully controlled switches of the

inverters, the clamped diodes used for the NPC structure and the freewheeling diodes in antiparallel to the IGCTs.

Having the transient a RLC behaviour, the voltage of the dc link will oscillate causing an extremely high peak of current on the damaged leg with low impedance, followed by the oscillating decrease of the current.

It is necessary that the diodes and the IGCTs withstand the overall energy dissipated on them during the fault, without exploding: if an explosion occurs, the other components in the cabinet containing the faulty module can be seriously damaged and the fault can propagate to other parts of the system.

The current trend on the damaged leg during the fault is not easy to calculate because the circuit is complex. The main causes are the stray inductances and resistances introduced before, the unknown voltage value of the half dc-link at the fault time and the effect of snubber components of the inverters. Therefore it is necessary to simulate the circuit using a dedicated software, PSIM [7], which allows to study properly the fault, since it is very dependent on stray parameters.

In chapter 4 the models used for the simulations will be presented and in chapter 5 the main simulations that I have realized will be analysed.

As demonstrated in the previous paragraph, the internal short-circuit of the inverters is a serious fault that must be considered very carefully in the design of the system. The high energy involved calls for special provisions for protection, usually not considered for the industrial systems. As protection from these types of fault three system have been considered in this thesis: the protection system based on decoupling diodes, the protection system based on crowbar and the protection system based on fuses.

3.4.1 Protections from internal short-circuits of the inverters

The protection system based on decoupling diodes involves the use of diodes at the input of the inverters, in positive and negative voltage bars (fig 3-13). These diodes avoid the inversion of the current at the input of the inverters, therefore avoid the discharge of the capacitors of the healthy inverters in the faulty inverter through the dc link, thus dramatically reducing the energy into the fault.

An analysis of this solution has been carried out from the design point of view, highlighting the following critical points:

- increase of the required space, both because of the presence of additional components (diodes) and because having independent dc-link capacitors it is necessary to foresee five independent discharging systems, to be included in the cubicles with consequent increase of space for the layout.
- necessity of setting up a control system with five independent controls of dc link voltage, to avoid unbalances. In addition, obviously an individual control of each dc link would be necessary based on choppers with discharge resistors.
- during dynamic transitions it is possible to have unbalancing of voltages and currents

The critical points, given the constraints of layout and the necessity of meeting the requirements, led to the rejection of this system.

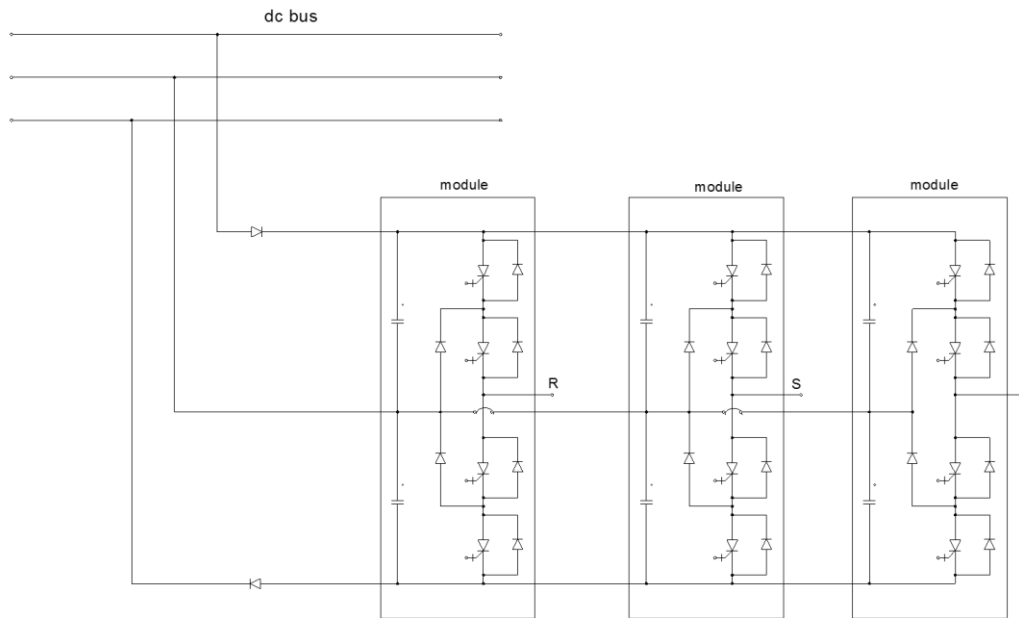


Figure 3-13 Scheme of the protection based on decoupling diodes

The second type of protection considered, is based on crowbars. This is a protection system usually used in middle voltage industrial systems to protect from internal faults. It consists in the insertion of low impedance paths in the dc link, activated at the fault time triggering some thyristors, which can be triggered quickly and with high reliability.

The crowbar is constituted by some dissipative resistances aside from the thyristors. Two thyristors in parallel are used in order to split the current (see fig 3-14). When this low impedance path is insert in parallel to the damaged leg, the current should flow mainly in this way rather than in the damaged leg. Therefore the energy dissipated on the components and the current peak on the damaged leg should be reduced.

Doubts on the use of this system come out because of the size of the crowbar, since it would need space for its own cabinet. Moreover, the dc link of the AGPS is a middle voltage drive having higher energy than the conventional systems, therefore in chapter 5 will be presented the analysis that I have done on the energy that the crowbar should manage.

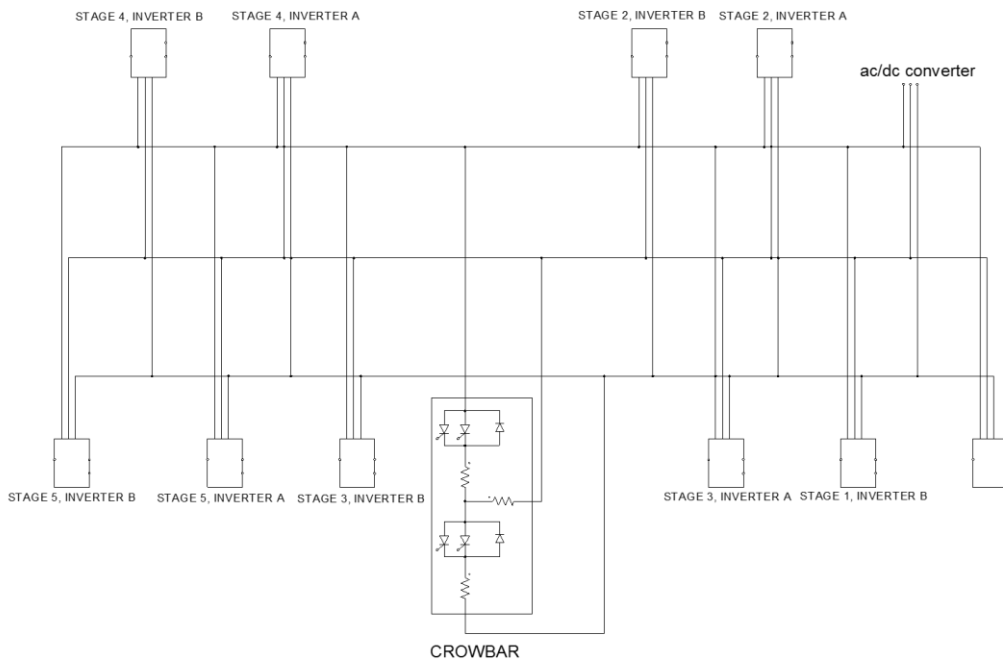


Figure 3-14 Scheme of the protection based on crowbar

Because of the doubts about the protection system based on crowbar, a third protection system has been considered, based on fuses. The fuses are placed at each input of the inverters, in the three bus bars connecting to the dc link (fig 3-15).

The fuse shall intervene when a certain energy has been transferred to the damaged module coming from the dc link. When the fuse intervenes, the relative input bar of the damaged inverter is detached from the dc link and no more energy is coming from it, reducing the energy dissipated on the components on the faulty module and the relative current peak.

Since it is not commercially available a fuse that can work with currents and voltages of the system in normal operation and which can manage the high energy involved during the internal fault considered, this fuse is being designed suitably.

The properly design of the fuses means:

- guarantee the selectivity of intervention, i.e. intervening only in the damaged inverter, without intervening in the other inverters
- guarantee the limitation of the current peak and the energy dissipated on the damaged leg to a level that is not dangerous for the components

The sizing of the fuse will be developed in chapter 5, with analysis of the prospective currents developing during the fault of an IGCT.

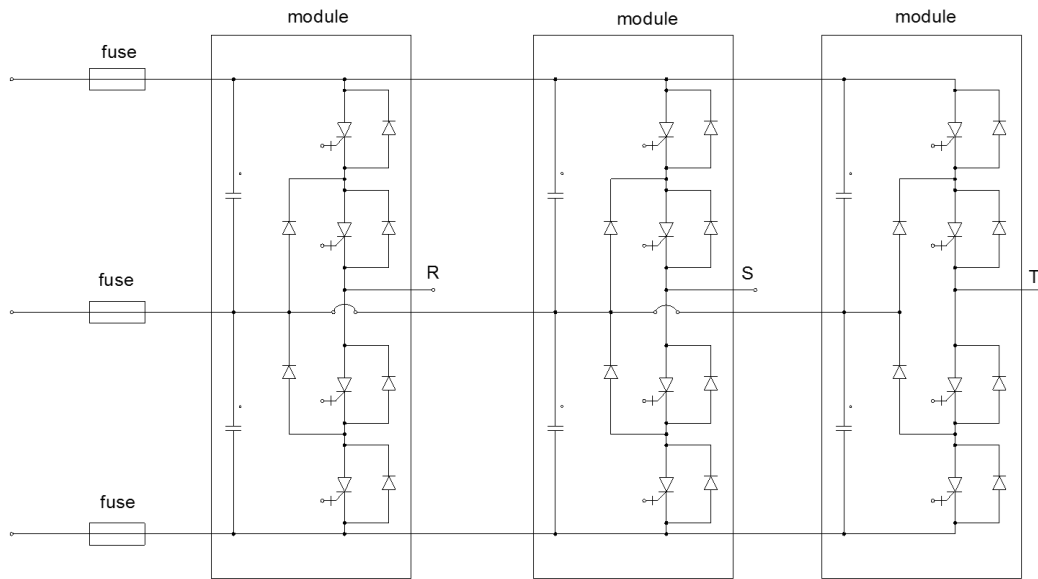


Figure 3-15 Scheme of the protection based on fuses

4 AGPS simulation model for the study of the internal faults

4.1 Model of the NPC inverters

The part of the AGPS circuit we are more interest in is the NPC inverters and the dc link. Therefore for this components a high detailed model has been derived, more detailed than for the other parts of the circuit.

I have simulated the three phase NPC inverters of the AGPS in PSIM using the circuit in fig. 4-1.

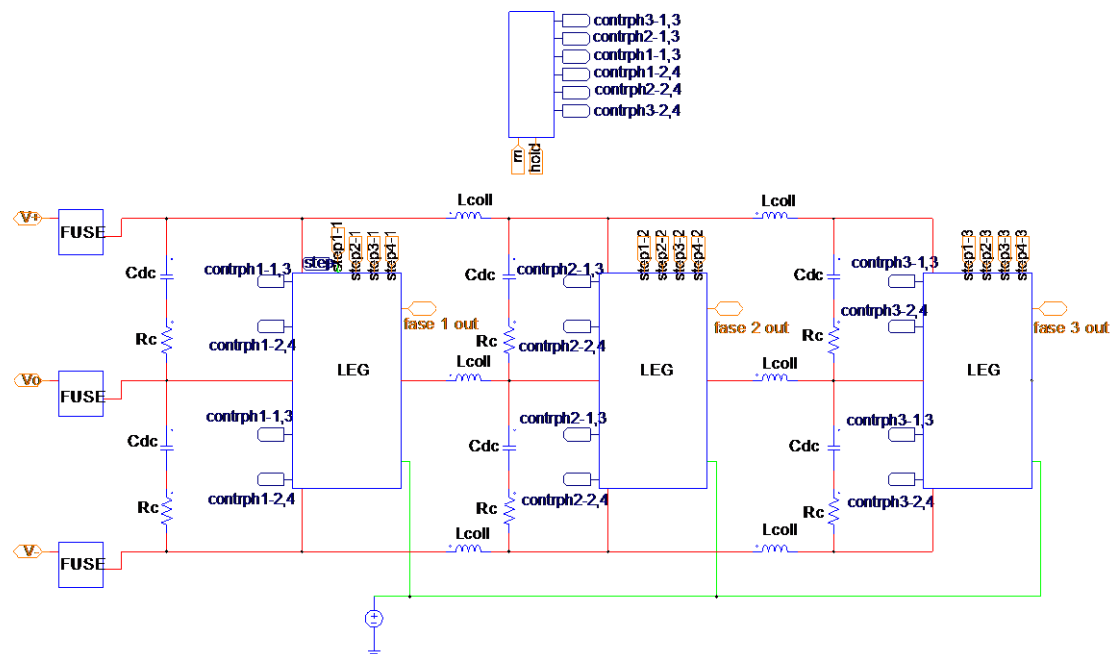


Figure 4-1 Model of the NPC inverter

The three sub-circuits named LEG are the model of the inverter's leg. The three subcircuit named FUSE simulate the fuses' behaviour and they are inserted only if the simulation foresees the use of fuses as protection.

In the model the stray inductances of the connections to the dc link are included (Lcollin), but they are not shown in figure because they are inside the subcircuits FUSE.

The stray inductances of the busbars between the legs, i.e. the modules (Lcoll), have been estimated from the layout of the inverter cubicle. [8]

In parallel to each leg there are the two capacitors of 2.4mF composing the bank. In simplified model simulations, they are pre-charged at the nominal value of 3250V to save the computational time for the energization of the bank.

In table 4-1 the parameters of the inverter scheme are summarized.

Table 4-1 Parameters of inverter scheme

Cdc=2.4mF
Lcollin=1000nH
Lcoll=500nH
Rc=0.1mΩ

The model of a leg is shown in fig. 4-2. While in fig. 3-7 the only main components of an NPC inverter were represented, here the elements used as clamp circuit are represented too.

In particular the leg in this figure is the damaged leg, having the upper IGCT a different resistance than the nominal resistance taken from the datasheet of the component. While the nominal resistance is $0.56\text{m}\Omega$, the resistance of the short-circuited IGCT is here reported at the value of $0.1\text{m}\Omega$, used in the great part of simulations. This value is actually difficult to be estimated. $0.1\text{m}\Omega$ represents an estimation based on the indications of the supplier of the IGCTs (ABB Semiconductors), but the supplier itself is not fully confident on the value due to the lack of experimental data. Since the behaviour of the internal short-circuit transient is dependent on this parameter, some sensitivity simulations have been carried out to assess the impact of the uncertainty.

The reason why there is uncertainty on the resistance of the IGCT after a failure of the component is explained in the following, according to private communication from ABB:

During the time point where the IGCT fails, typically the semiconductor wafer gets a melting crater. A melting crater is a local hot spot, where more current flows comparing to the rest of the wafer. The melting crater in hot condition with fluid silicon has a lower impedance than the rest of the wafer, therefore the wafer has a lower on-state resistance compared to the healthy one.

The current changes the direction during the fault. The faulty IGCT might cool down during this changed condition and the melted silicon gets solid again. The solid silicon as such is not a good conducting material. The faulty IGCT might no longer conduct like a healthy one, because the IGCT control might no longer be able to keep the IGCT in conduction condition.

In conclusion, when the melted crater cools down, it is not possible to give a clear statement, what is the on-state condition, we only know that probably the resistance decreases. Therefore in the analysis we have considered different values of this resistance.

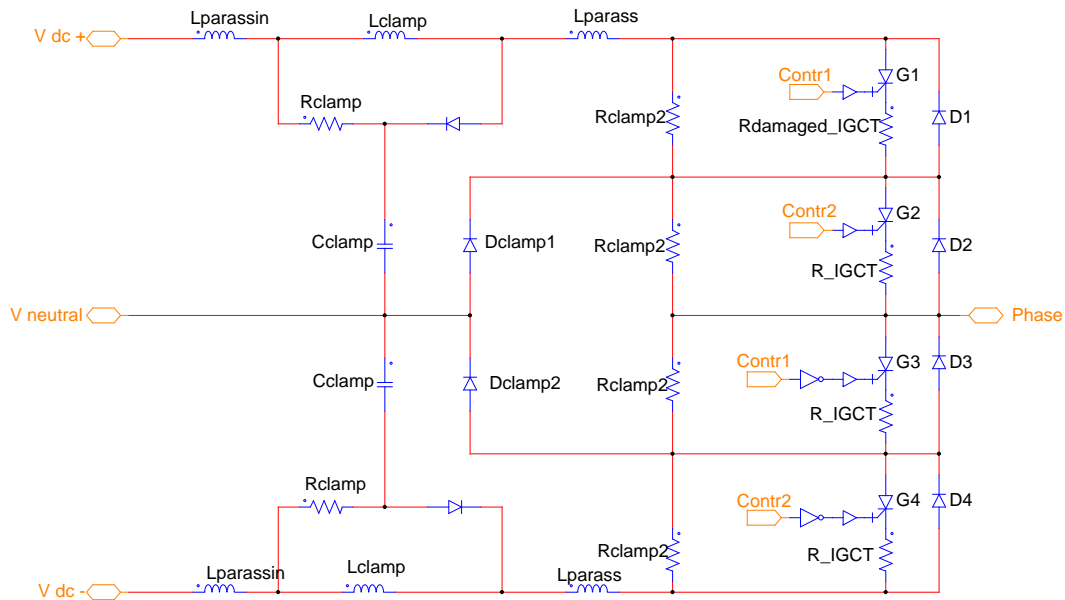


Figure 4-2 Model of NPC inverter

In table 4-2 the values of the parameters of this model are reported. There are:

- The resistances of the basic components of the NPC inverters: of IGCTs (R_{IGCT} for G2,G3,G4, and $R_{damaged_IGCT}$ for the damaged one, G1), of freewheeling diodes D1,D2,D3,D4 and clamped diodes Dclamp1, Dclamp2 (R_{diode}); the same type of diode is used for both the functions. These values are taken from the datasheet of the components (annexes 1 and 2) and for the damaged IGCT we assume a value lower than the one which it has in nominal operation, as explained above
- the components of the clamped circuit: they are inductances (L_{clamp}), resistances (R_{clamp1} and R_{clamp2}) and capacitors (C_{clamp}). These values results from estimations provided by the supplier, NIDEC [8]

- stray inductances owing to the connection of the module to the external lines ($L_{parassin}$) and the connection of the snubber circuit to the IGCT series (L_{parass}). These values results from estimations provided by the supplier too. [8]

Table 4-2 Parameters of module scheme

$L_{clamp}=4\mu H$
$R_{clamp}=0.7\Omega$
$R_{clamp2}=33k\Omega$
$C_{clamp}=4\mu F$
$L_{parassin}=350nH$
$L_{parass}=200nH$
$R_{igct}=0.56m\Omega$
$R_{diode}=1.364m\Omega$
$R_{damaged_igct}=0.1m\Omega$

As explained in chapter 3, the inverters are modulated in squared wave to obtain an alternated output voltage of 150Hz of frequency. In the model, the control system (fig 4-3) is based on the comparison of a tern of triangular voltages having amplitude equal to 1 and frequency equal to 150Hz with a constant value coming from the difference between 1 and the modulation index, which is obtained from the output of the regulator of the voltage on the grids (not shown in fig 4-3). This signal is then extracted and multiplied by -1 to have the comparison of the triangular voltages with the two opposite constant values, to control in pairs the 4 IGCTs of the leg, having in this way the unipolar modulation. As it can be seen from figure 4-2, the signal triggering the 2 lower IGCTs passes through the logical port NOT to control the other IGCT pairs.

The capacitors shown in figure have been used to simulate the behaviour of the control when the fault is detected, i.e. freeze the commands to the IGCTs of the faulty module.

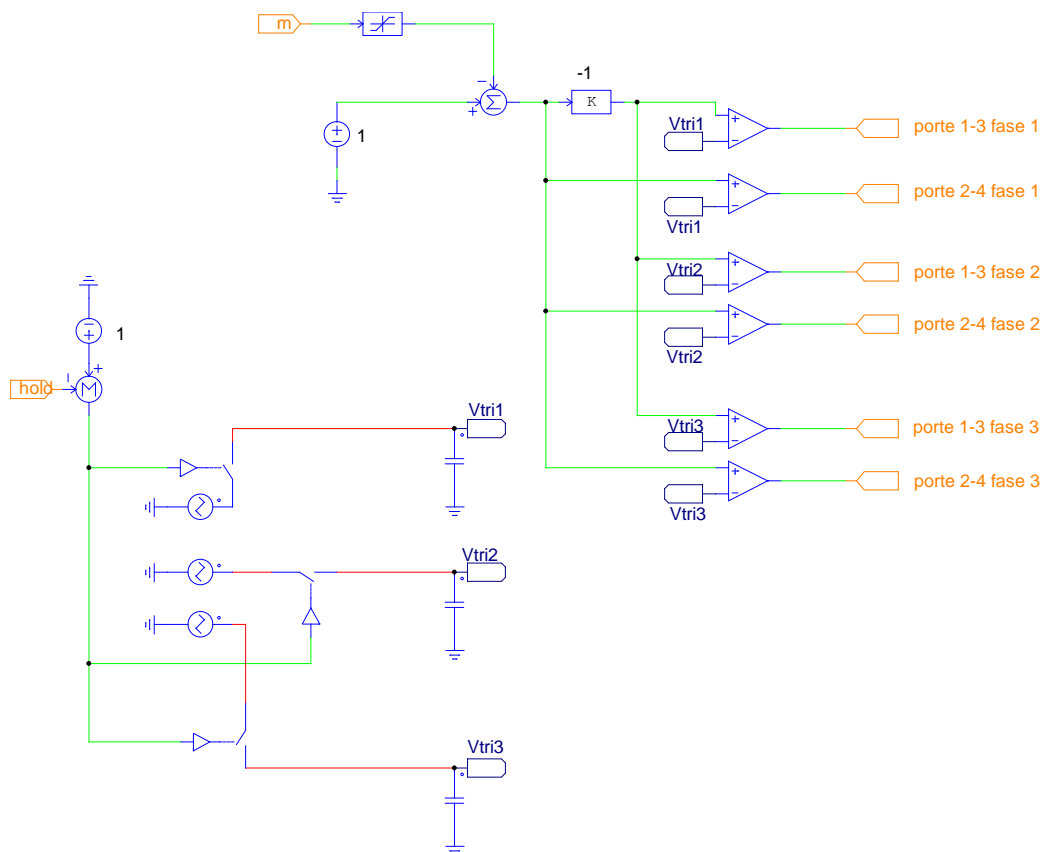


Figure 4-3 Simulation model of the control circuit of the inverter

4.2 Model of dc link

The inverters are connected to the dc link through a busbar system. The stray resistance and inductance of the different busbars have been estimated from the layout of the system, assuming the simplified geometrical model shown in fig. 4-4 and estimating the dimensions of each busbar from available design data [8]: a rectangular cross section whose sides are B=20cm and C=2cm. These busbars are made up of coppers, a material having magnetic properties similar to air.

The self-inductance (in μH) of a straight conductor of length l (in centimetres) is given with good accuracy by the general formula [9]:

$$L = 0.002l \left[\log_e \frac{2l}{r} - 1 + \frac{\delta_1}{l} \right] \quad (4.1)$$

In which r is the geometric mean distance and δ_1 is the arithmetic mean distance of the points of the cross section. The last term is usually negligible.

Using the geometrical mean distance for rectangular section wire [9]:

$$\log_e r = \log_e (B + C) - \frac{3}{2} + k \quad (4.2)$$

We get the formula for a wire of rectangular cross section of sides B and C and with a low magnetic permeability [9]:

$$L = 0.002l \left[\log_e \frac{2l}{B + C} + \frac{1}{2} - k \right] \quad (4.3)$$

Where k depends on the ratio B/C, but it has a negligible value with respect to the first two terms. The electric resistance is calculated using:

$$R = \rho \frac{L}{S} \quad (4.4)$$

Where L is the length of the bar, S its section and ρ its resistivity, which for copper is $1.68 \cdot 10^{-8} \Omega\text{m}$. The length of the bars connecting each module to the dc link comes from the geometrical hypothesis (fig.4-4) and they are: 1467mm, 1100mm and 2066.5mm. Then I take the average value to calculate a single impedance value for the three connections between dc link and inverters.

The resistance and the inductance related to the connection between the modules and the bars of the dc link calculated using equations 4.3 and 4.4 are accordingly $R_{st}=6.3\mu\Omega$ and $L_{st}=0.97\mu\text{H}$.

These are approximate values and I have compared to the values obtained by NIDEC, which are $R_{st}=18.7\mu\Omega$ and $L_{st}=0.65\mu\text{H}$. The order of magnitude is the same and for such small values the difference between the values is negligible for the aim of the simulation. Moreover, having the resistance I have calculated a lower value and the inductance a higher value, this is a precautionary situation for the discharge of capacitor bank in one inverter, as happens for the internal fault in an inverter.

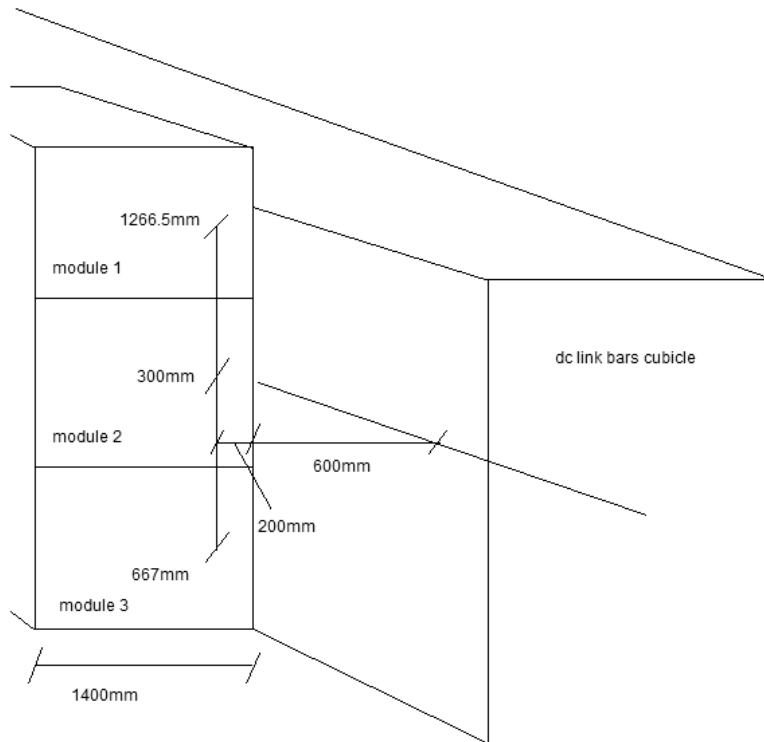


Figure 4-4 Hypothesized geometry of the connection between the dc link and the capacitors in the modules

The ac/dc conversion system is connected to the dc link busbar system, as shown in fig. 4-5. The stray resistances and impedance of the dc link sections are taken from calculations made on the precise measures of the geometry of the bars, provided by NIDEC. [8]

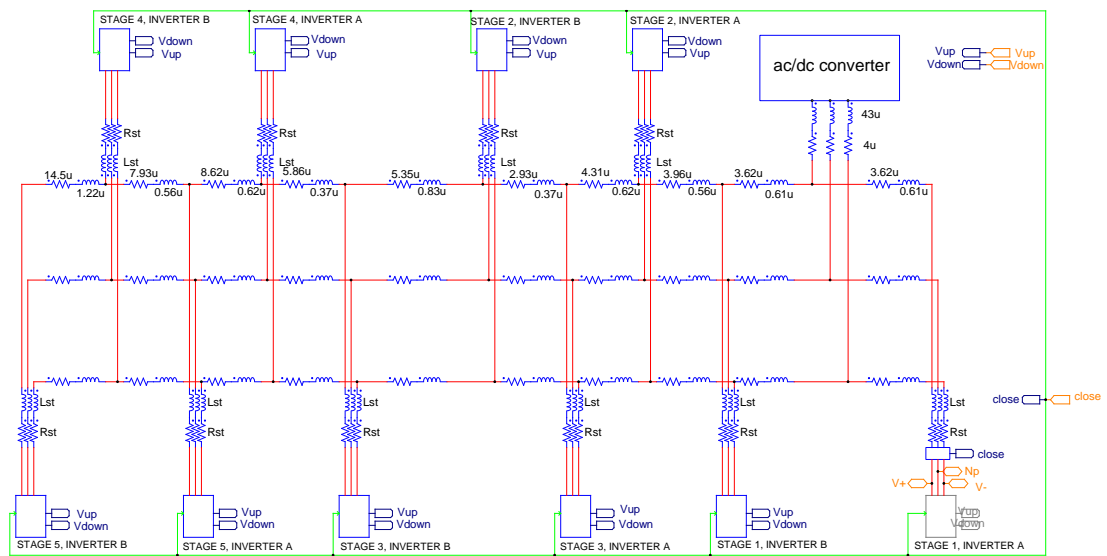


Figure 4-5 Model of the dc link

4.3 AGPS-DCG and load model

All the simulations are done using only one AGPS-DCG stage connected downstream the inverter. This is because we are interested on the behaviour of the faulty inverter stage and to reduce the computational time.

I consider only one stage because I need the load of the faulty inverter to simulate the nominal and fault regimes of that section of the AGPS. In particular, I use the first stage because it is the stage requiring more power.

The inverter stage (two inverter modules in parallel) is connected through medium voltage cables (five cables per phase, 240mm² each) to a step-up three phase transformer, having the parameters reported in table 3-9 in the column relative to the first stage (-1MV/-800kV).

Being the total ac/dc inverter output inductance $L_{inv}=110\mu H$ (table 3-8) and the stray inductance for each phase of the step up transformer $L_{sc2}=0.2H$ (table 3-9), the total equivalent inductance seen from the secondary side is:

$$L_{tot2} = \frac{(\sqrt{3})^2}{n} \cdot L_{inv} + L_{sc2} = 0.309H \quad (4.5)$$

Where n is the turn ratio. The value obtained is the line inductance used in the model between the transformer and the diode bridge (fig. 4-6).

The diode bridge connected to the transformer creates a dc component of the voltage at its output generating a six-pulse waveform, which for an input sinusoidal form has a medium voltage of [10]:

$$V_d \approx 1.35V_{LL} \quad (4.6)$$

Yet, the entering waveform has the shape created by the NPC inverter, therefore this law is not valid. The turn ratio of the step-up inverters has been chosen to obtain the nominal output voltage from the alternated voltage produced by inverters.

Considering the square-wave modulation of the inverters, the no load dc voltage at the output of the diode bridge is:

$$E_{0nom} = \frac{2}{n} V_{dc} = 2 \cdot 18.2 \cdot 6500 = 236.6kV \quad (4.7)$$

Since the dc link can have oscillations of $\pm 5\%$, the minimum no load output voltage is:

$$E_{0min} = E_{0nom} \cdot 0.95 = 224.8kV \quad (4.8)$$

The average voltage on the grids that can be reached in this condition is:

$$E = E_{0min} - 6 \cdot f \cdot L_{tot2} \cdot I_{out1} = 207.4kV \quad (4.9)$$

Where $I_{out1}=64.2A$ is the nominal current of the first stage considering the additional 5% margin, as reported in paragraph 3.1.1.

This confirms that the turn ratio and the requirements on the dc link ripple allow to achieve the required voltage at the output of the DCG.

The ripple of the output voltage is reduced using a high voltage dc filter, composed by a resistance of 68 Ω and a capacitor of 300nF.

The load of the DCG is MITICA accelerator, connected downstream of a high voltage transmission line, in particular each DCG stage is connected to one acceleration stage. The beam current flowing into one stage is the difference between the output current exiting from the previous stage and the current lost due to the collision of ions onto the acceleration grid connected to the two stages. The load can be therefore modelled as a current generator. The value of the current is set to 62.4A for the first stage, which is the current of the first stage in the case of nominal D⁻ operation considering the 5% margin with respect to the nominal value (table 3-2). This current is obtained through the perveance law

(equation 2.9), considering the nominal acceleration voltage of 200kV. The simulations have been carried out starting directly from the nominal conditions, without simulating the start-up. After a short transient the system is ready for the fault simulation, saving computational calculations.

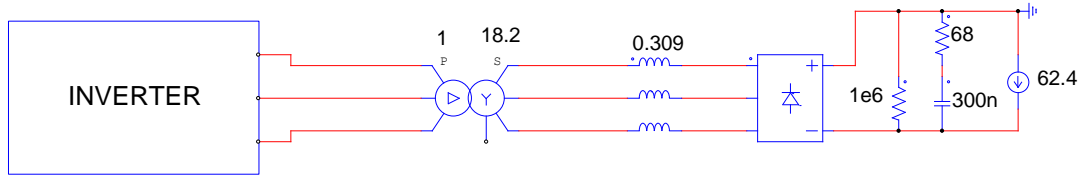


Figure 4-6 AGPS-DCG simulation model

4.4 Simplified model

Being the model of the inverter and of the dc link very detailed, current and voltage have to be calculated on a great number of elements of the circuit. The simulation of the circuit composed by dc link, inverters and DCG is therefore computationally expensive, especially during the fault when there is a not periodical voltages and currents, which are expected to have quick variations.

If I have to simulate also the model of the ac/dc converter, the simulation time would be very high, due to the introduction of that quite complex circuit upstream the dc link.

Hence the first simulations have been done using a simplified model (fig. 4-7) instead of the ac/dc conversion system supplying the dc link. Since the average value of the power at the output of the DCG stage is known, related to the beam current and output voltage, I have simulated the power supplied by the ac/dc converter with a current generator supplying the dc link and providing the request output power.

These simulations are a good approximation of the system behaviour, having the advantage of being computationally less expensive.

I simulate only one DCG stage, supplied by only one inverter, instead of two in parallel, because I need just to reach the nominal work condition of the inverter, when I need to simulate the fault. In this way, the inverter's components are interested by double currents with respect to the real values, but it does not matter for the aim of this simulation.

When the fault is simulated in this inverter, all the modules of the inverters are connected to the dc link, to simulate the discharge of the capacitors distributed in the different modules.

The additional energy contribute stored in stray inductances inside the inverter where the fault is simulated, caused by the presence of the double values of currents at the moment of the fault, is negligible with respect to the energy stored in the capacitor bank.

The capacitor bank is already charged at 6500V at the beginning of the simulation to start from stationary conditions. In the same way, the voltage on the capacitor filter on the output is pre-charged at the nominal 200kV.

The current provided by the generator has been calculated knowing that the power at the output of the first acceleration stage is about 12.6MW, which are almost completely given by the acceleration of the beam:

$$P_{out} = V_{grid} \cdot I_{beam} = 12.48MW \quad (4.10)$$

Where $I_{beam}=62.4A$ and $V_{grid}=200kV$.

Considering also the small power absorbed by the filter the total output power is about 12.6MW.

The current provided by the generator must be:

$$I = \frac{P_{out}}{V_{dc}} \cong \frac{12.6MW}{6500V} \cong 1940A \quad (4.11)$$

The resistive component of the circuit are not so big to create a considerable dissipation, so I assume the input power equal to the output power. If the current generator delivers the proper current, after the

short initial transient the system will reach the equilibrium having the nominal voltages on the dc link and at the output.

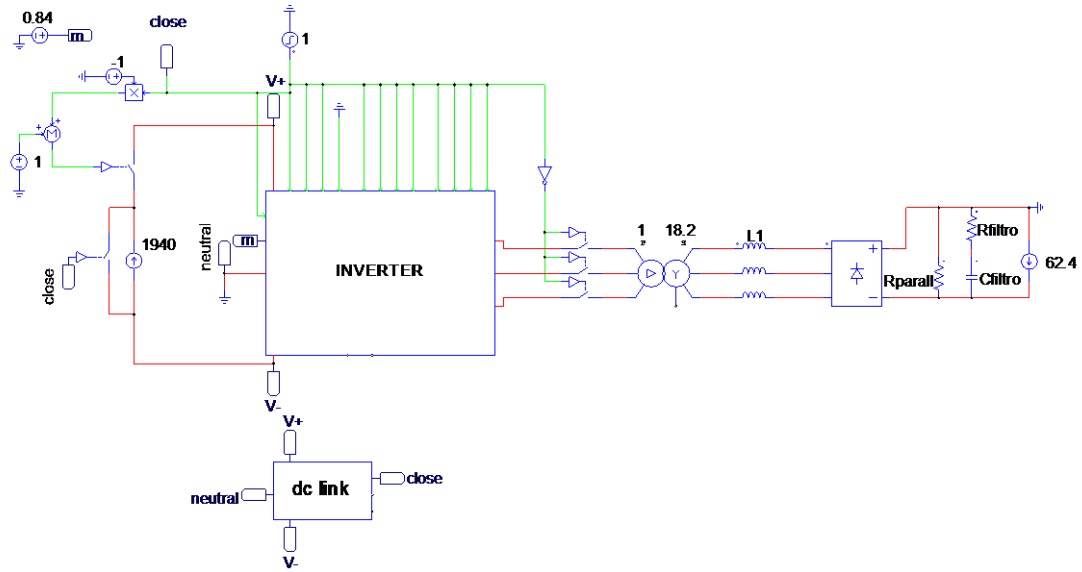


Figure 4-7 Simplified model

The inverters connected to the dc link at the fault time are represented only in their passive components (fig 4-8).

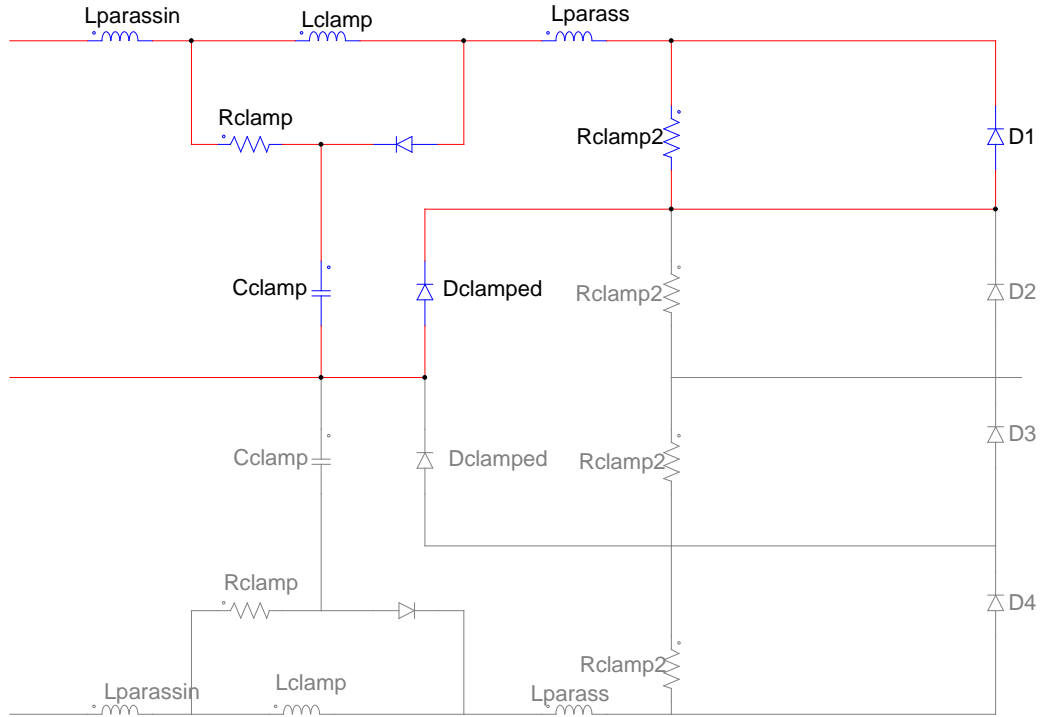


Figure 4-8 Simulation model of healthy inverters' leg

4.5 Detailed model

With the simplified model it is not possible to simulate the contribution of power coming from the ac/dc converter, which is present until the fault is detected and the protection system is activated.

To consider also this contribution I designed the detailed model (fig. 4-9), composed by the a sinusoidal voltage tern simulating the 22kV ac distribution grid, the step down transformers, the ac/dc converter and the lines connecting to the dc link. For a well detailed simulation, the parameters of the impedance between the transformers and the converter and between the converter and the dc link have been considered and modelled.

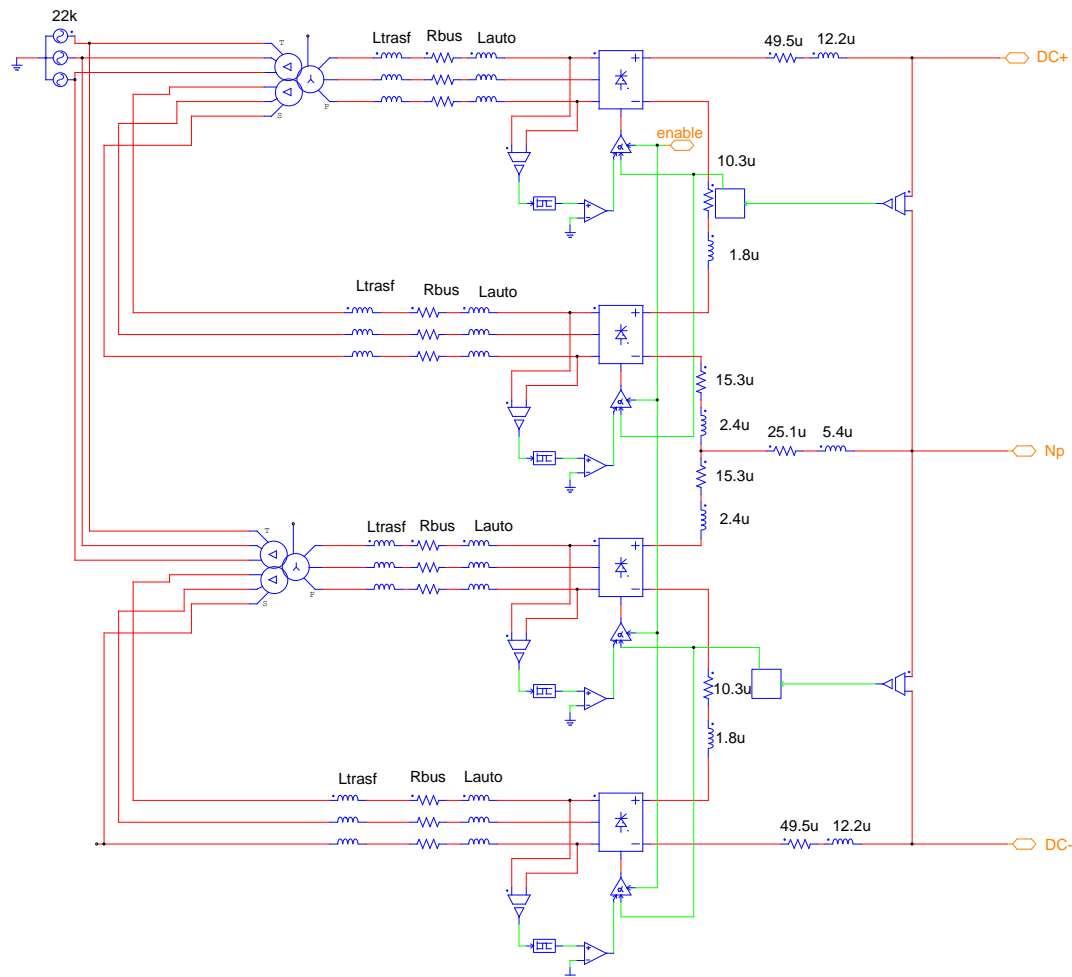


Figure 4-9 Detailed model of the ac/dc conversion system

4.5.1 Step down transformers model

Each 12 pulse rectifier is supplied by a transformer with two decoupled secondary windings, which reduces the 22kV voltage of the medium voltage grid supplying PRIMA and RFX-mod to 1.5kV. The main parameters of these 2 transformers are reported in table 3-5.

Knowing the primary and secondary voltages and the connection of the windings, I obtain the turn ratio between the primary and the two secondary windings.

Being not known from datasheet the turn ratios, but only the primary and secondary voltages, I have calculated it as explained below.

As for the Dd0 connection, assuming the number of spires of the secondary $N_{S'} = 1$, using the relationship:

$$\frac{N_p}{N_{S'}} = \frac{V_p}{V_{S'}} = \frac{22}{1.5} \quad (4.12)$$

I obtain $N_p=14.67$.

As for the Dy11 connection, I have to consider that the turn ratio is not equal to the voltage ratio, but it is:

$$\frac{N_p}{N_{s''}} = \frac{\sqrt{3} \cdot V_p}{V_{s'}} = \frac{\sqrt{3} \cdot 1.5}{22} \quad (4.13)$$

Being $N_p=14.67$, it results $N_{s''}=0.577$.

4.5.2 Impedances between transformers and ac/dc converters

The impedances are constituted by the resistances and the inductances between the secondary of the transformer and the input of the ac/dc converter, i.e. the secondary winding equivalent short-circuit impedance of the step down transformers and the impedance of the busbars connecting the secondary of transformers with the thyristor bridges.

The transformers have a nominal power of 38.2MVA, 19.1MVA for each secondary, and a short circuit impedance of about 10% with respect to the base power of 19.1MVA (table 3-5).

Therefore the equivalent short-circuit impedance can be calculated:

$$Z_{eq} = \frac{u_{cc\%} U_n^2}{100 S_N} = 0.01178\Omega \quad (4.14)$$

Where $u_{cc\%} = 10$, as previously said, $U_n=1500V$ is the nominal secondary voltage and $S_N=19.1MVA$. By neglecting the resistive component, the inductance value is:

$$L_{trafo} = \frac{Z_{eq}}{2\pi f} \cong 37.5\mu H \quad (4.15)$$

Where $f=50Hz$ is the frequency of the national grid.

The line impedances are imposed by the values calculated from geometry. [8]

It results $R_{bus}=36\mu\Omega$, where the asymmetry is neglected.

As for the inductances, they have different values because of their different length and the mutual inductances between the different cables should be considered. The resulting inductances coupling matrix is:

Table 4-6 Stray inductances of the line between step-down transformers and thyristor bridges

μH	1	2	3	4	5	6
1	5.1167	2.8147	1.8424	0.37747	0.44488	0.51966
2		5.2980	2.9135	0.33955	0.39165	0.44508
3			5.7458	0.30187	0.33942	0.37753
4				5.6911	2.9138	1.8430
5					5.2937	2.8134
6						5.1229

This matrix refers to the busbar 1-2-3 supplying a 6 pulses bridge and to the bus bar 4-5-6 supplying the other 6 pulses bridge forming the 12 pulses bridge of a half dc link. The same matrix is valid for the other 12 pluses rectifier of the other half dc link (see fig. 4-10).

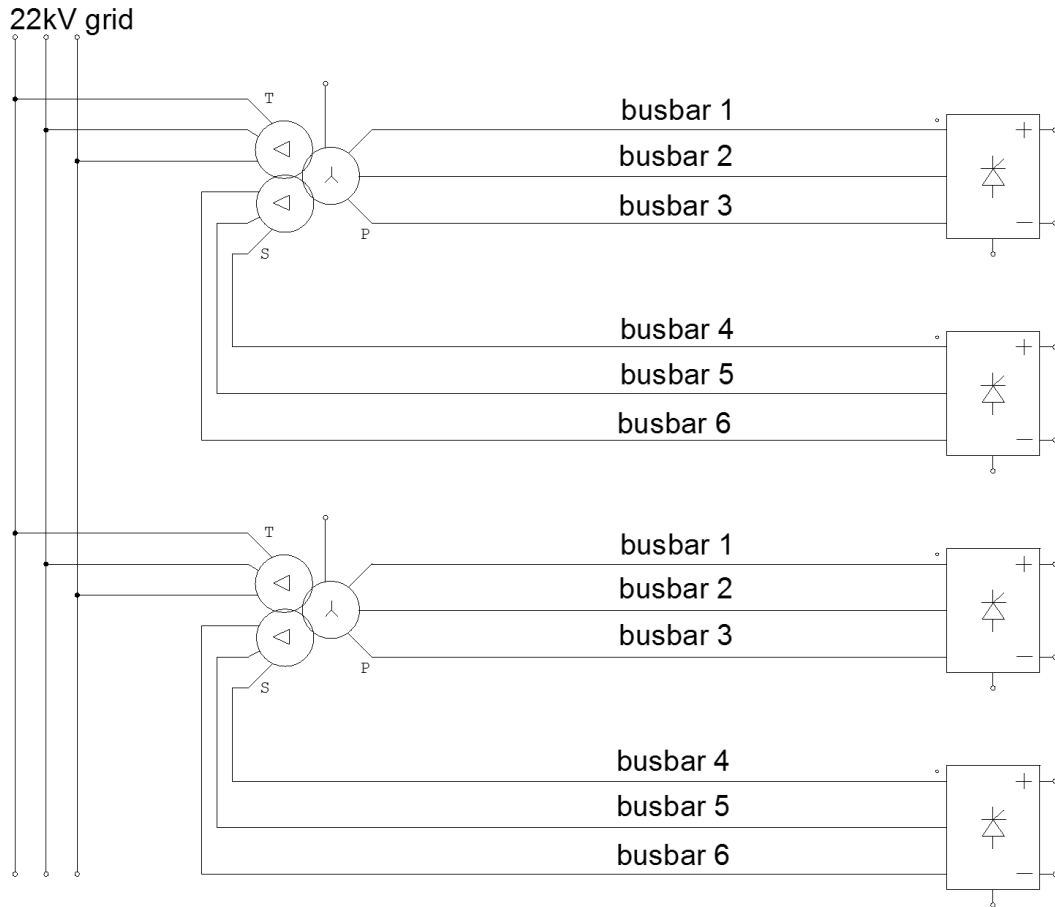


Figure 4-10 Layout of the connection between step-down transformers and thyristor bridges

These values are very small, since these inductances belong to the part of the system working at 50HZ. For this reason to simplify the scheme without losing much accuracy, we chose $L_{\text{auto}}=5.4\mu\text{H}$ for all the lines, which is more or less the average of the average value of the self-inductances, and the mutual inductances have been neglected. These are the parameters used in the model of fig. 4-9.

4.5.3 Ac/dc converter

The ac/dc converter is composed by two 12-pulse converters in series, each one supplying one half of the dc link, the central point of the series is connected to the Neutral Point of the dc link. Each 12-pulse converter is made by two 6-pulse thyristor bridges in series, each supplied by one of the two secondaries of a step down transformer and since the windings are one star connected and one delta connected, the supplying voltages have a phase displacement of 30° to obtain the 12-pulses dc voltage at the output.

If the 12 pulse converter supplied a load requiring a constant current, therefore an inductive load with high inductance, the dc output voltage would be given by:

$$V_{\text{out}} = 2.7V_{\text{LL}}\cos\alpha - 12fL_sI_d \quad (4.16)$$

Where V_{LL} is the line to line voltage input voltage (in our case would be 1.5kV), L_s the inductances at the dc side, I_d the current at the dc side, assumed constant, f the frequency of the voltage at the input and α is the activation angle of the thyristors.

However, in this case the load of the ac/dc converter is a large capacitor bank, with a downstream system absorbing active power. The operation of the converter with such a load can be discontinuous and not

easy to control like the inductive load. It can be demonstrated that the maximum value of the alpha that controls the bridges is 120° . [11]

In the model, the control system of the ac/dc converter has been implemented as shown in figure 4-11. The feedback control commands the value of alpha having as input the difference between the reference voltage and the output voltage of a 12 pulses converter. It is made up basically by a PI controller, whose gain and time constant are chosen tentatively by simulations, in order to have a good compromise between time of rise and a reduced voltage peak: $\tau = 43\text{s}$ and $k = 2.63 \cdot 10^{-4}$. The measured voltage is filtered with a second order low pass filter with cut-off frequency of 300Hz to avoid contributes by the 600Hz component created by the converter.

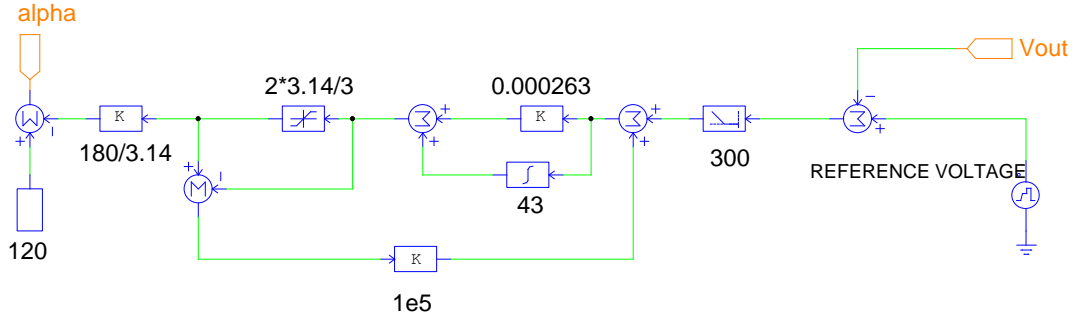


Figure 4-11 Control system of the ac/dc converter

The control system has an anti-windup circuit to avoid the saturation of the control signal and consequently the divergence of the output voltage.

The value obtained is subtracted to the value of 120, in order to have $\alpha = 120$ when the output voltage is equal to the reference voltage, to nullify the output in that situation.

4.5.4 Stray inductances between the ac/dc converter and the dc link

The ac/dc converters are connected to the dc link with three bars as shown in the simplified scheme of fig. 4-12.

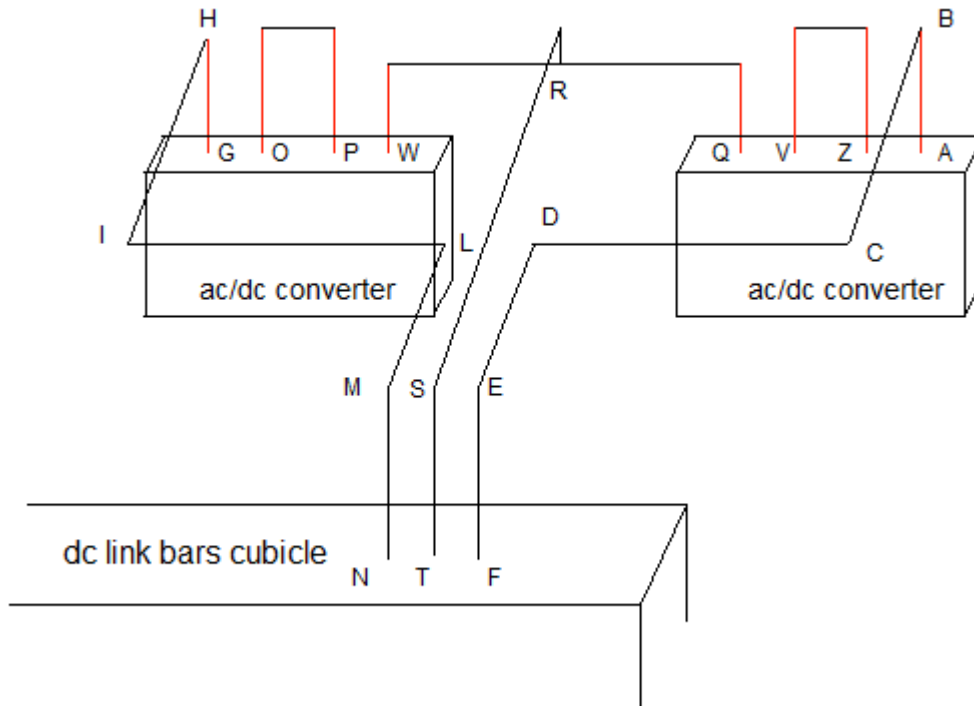


Figure 4-12 Layout of connection between ac/dc converters and dc link

The busbars are three: one for the connection to the positive polarity of the dc-link, one for the connection to the negative polarity and one for the connection to the neutral point. These bars are made up of coppers (ad only small parts in silver highlighted in red in fig. 4-12), a material with magnetic properties similar to air, with a rectangular cross section of dimensions $B=20\text{cm}$ and $C=2\text{cm}$. The difference between silver and copper parts will be considered only for the silver relevant length parts.

The segments represented in figure have the following length: AB is 155cm long, the same for GH which is symmetrical, BC and HI are 80cm long, CD and IL are 440 cm long, DE and LM are 348cm long, EF and MN are 155 cm long

We want to calculate the inductances of the busbars connecting the ac/dc converter to the dc link busbars that feed all the inverters' modules (see layout in section 3.3). All calculations have been done neglecting the curvatures of the corners.

The self-inductance (in μH) of a straight conductor of rectangular cross section is given with good accuracy by the general formula 4-3. The electric resistance is calculated using the equation 4-4.

The busbar from A to F is 1178cm length, so from formula: $L=12.19\mu\text{H}$. The inductance of the connection to the negative polarity (from G to N) has the same value, since the two bars has the same length.

These two busbars have a resistance of $49.48\mu\Omega$.

For the busbar connecting to the neutral point from Q to R has a length of 598cm, therefore $L=5.38\mu\text{H}$. Its resistance is $R=25.12\mu\Omega$.

The two connectors between R and Q (and W) have a length of 369cm and always the same section. It comes out $L=2.45\mu\text{H}$ and considering the mean value of resistivity of $1.66 \cdot 10^{-8}\Omega\text{m}$, being this part made up about half and half by copper and silver, $R=15.31\mu\Omega$.

For the busbar connection to the negative polarity of the first bridge and the positive polarity of the second bridge at their outputs the design is not completed yet (segments OP and VZ). Therefore we suppose a similar geometry of the other connection, with the same section and a length of 250cm, 1/3 in copper and 2/3 in silver (mean resistivity of $1.65 \cdot 10^{-8}\Omega\text{m}$). The result is: $L=1.81\mu\text{H}$ and $R=10.31\mu\Omega$.

These values have been used in the model, shown in figure 4-9.

All the mutual inductances are neglected because their values are much smaller than the ones calculated for the self-inductances.

4.6 Protection systems

4.6.1 Crowbar

A current crowbar is typically used in these applications for the protection against internal faults. In the following, the model of a crowbar implemented in the simulations for comparison with other protection strategies (e.g. fuses) is presented. The crowbar scheme is shown in figure 3-13. The principle of operation is based on the insertion in the middle of the dc link of a low impedance path to quickly discharge the dc-link capacitors in case of faults. It is inserted in the middle to avoid to have too distance between it and the short circuited leg, which would slow down the discharge on this device.

The circuit used for the simulation is represented in figure 4-13.

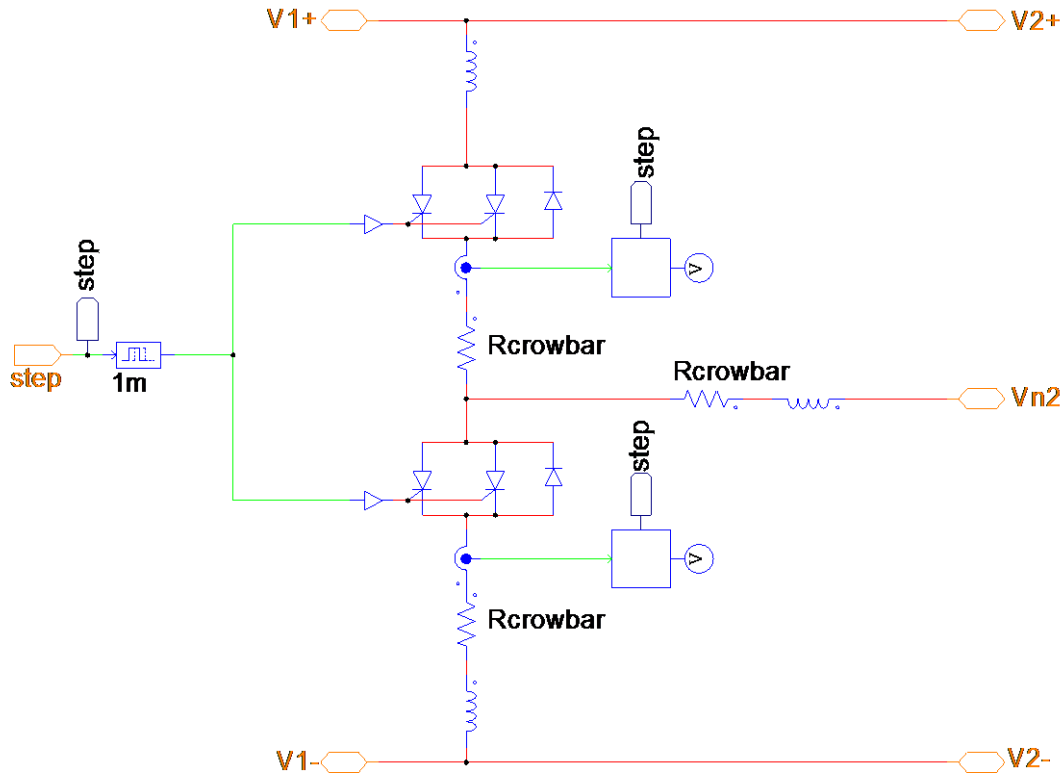


Figure 4-13 Model of the circuit of the crowbar

The subcircuits are used just to calculate the I^2t in case of crowbar intervention.

The values of the resistance are estimated to $R_{\text{crowbar}}=3.7\text{m}\Omega$, a typical value for these protection system. In typical applications, each resistance is composed by two parallel bars in Inconel with rectangular cross section ($13.5\text{mm}\times 28.5\text{mm}$) and 1.2m length; two thyristors in parallel per leg are used to withstand the stresses during the intervention. Usually, due to the large dimensions of the bars and to the need of cooling them, the resistances are placed on the top of the crowbar cubicles, in air.

The diodes allow the flowing of the current when the upper capacitor bank has a negative voltage, preventing the flowing of the current on the freewheeling diodes of the healthy modules during the fault of an IGCT of an inverter.

The time of intervention of the crowbar is estimated to be 1ms, by knowing the typical operation of these devices.

4.6.2 Fuses

An alternative protection studied in this thesis and compared to the crowbar is the fuse protection. The idea is to place the fuses at the input of each inverter, on each of the three input bars, as shown in figure 3-15.

Their intervention is based on the I^2t on the fuses.

The value of I^2t is related to the prospective current, which is the current flowing in the branch where the fuse would be insert when fuses are not installed. From the prospective current a proper fuse will be chosen, or designed, if there were not a commercial fuse available with the required characteristics.

Once the fuse will be chosen, the intervention current can be determined from the datasheet and the fuse can be modelled as explained below.

When the fuses intervene and an arc is generated inside them, the current is forced to decrease and we suppose a linear decrease to 0A in 10ms, which is a good approximation, by information on fuses behaviour.

Imposing roughly the wanted current in that branch produces computational instabilities because the fuses are in series to stray inductances, which do not allow instantaneous variations of the current. These computational errors would generate high voltage peaks at the input of the inverter and this alters the current trends that we want to analyse.

To simulate their intervention, without creating computational instabilities downstream the fuses to have the proper voltage supplying the damaged inverter, the current on the stray inductance at the input of the inverter is deviated on a short circuit, where a current generator imposes the value of current extracted from the circuit.

This gives us the correct voltage trend downstream the fuses but upstream them the voltage has peaks due to computational errors. Nevertheless this voltage is less relevant for our aim.

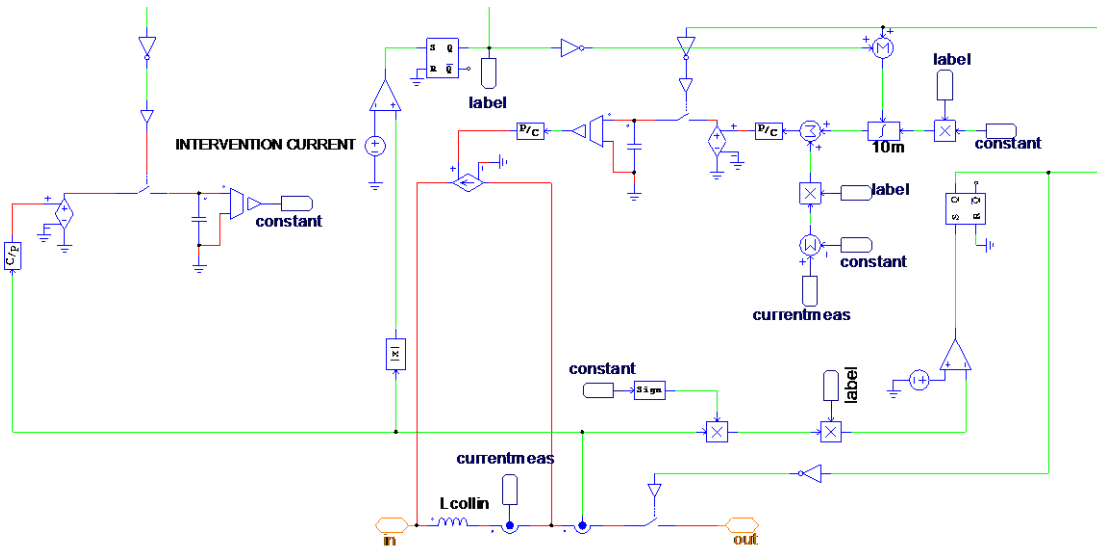


Figure 4-14 Circuit to simulate the intervention of one fuse

The circuit of figure 4-14 has the only purpose of deviating the current away from the input of the inverter to have the linear decay of the current. So when the current overcome the limit, that is the intervention current of the fuse, in absolute value, the current generator is controlled to produce the difference between the current measured in every instant on the inductance and the current measured in the instant when the limit has been overcome. A component linearly increasing from 0 to the intervention current value (the value of the generator 'INTERVENTION CURRENT' in figure) in 10ms is added to this value. Finally, 10ms after the intervention of the generator a switch is opened to nullify the small value of current coming from the discrete structure of the control, based on the time step of the simulation.

5 Simulations

5.1 Nominal operation in steady-state

5.1.1 Simplified circuit

The simplified circuit is simulated starting directly from steady state nominal conditions, as explained in chapter 4. The most interesting parameters of the steady state condition are analysed in this paragraph. The steady state condition is reached after a short transient, when the system settles.

In fig. 5-1 the voltage at the input of the inverter and the voltage at the output of the AGPS are shown. The voltage at the input is the voltage measured at the input of the inverter, downstream the fuses. It is basically the voltage of the dc link, even if there are different oscillations of voltages on the capacitors in the different modules due to the stray inductances.

Anyway, hereafter we will consider this value as reference value of the dc link voltage.

The output voltage is the one applied to the grid of the acceleration stage.

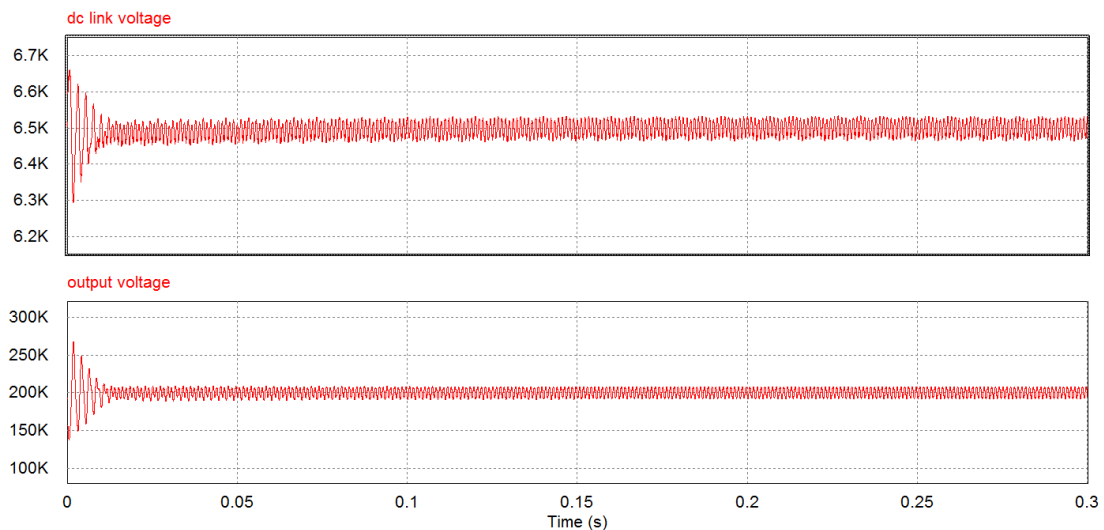


Figure 5-1 Simulated dc link voltage and DCG output voltage of the simplified circuit in steady state nominal condition.

The two voltages are oscillating around their mean values of 6.5kV and 200kV, with ripple produced by the inverter and by the diode rectifier. Being the inverter working at 150Hz and the rectifiers producing a six pulse output voltage, the resulting oscillations have a frequency of 900Hz. Moreover small components at 150Hz and 300Hz are present too due to the operation of the inverter in unipolar modulation.

The current flowing into the switches of the inverter during nominal operation is reported in fig. 5-2. Notice that the peak values are almost 3000A for IGCTs, and a little more than 1000A for the diodes. We are simulating one stage using only one inverter (as explained in paragraph 4.4), therefore the real current will be half these values.

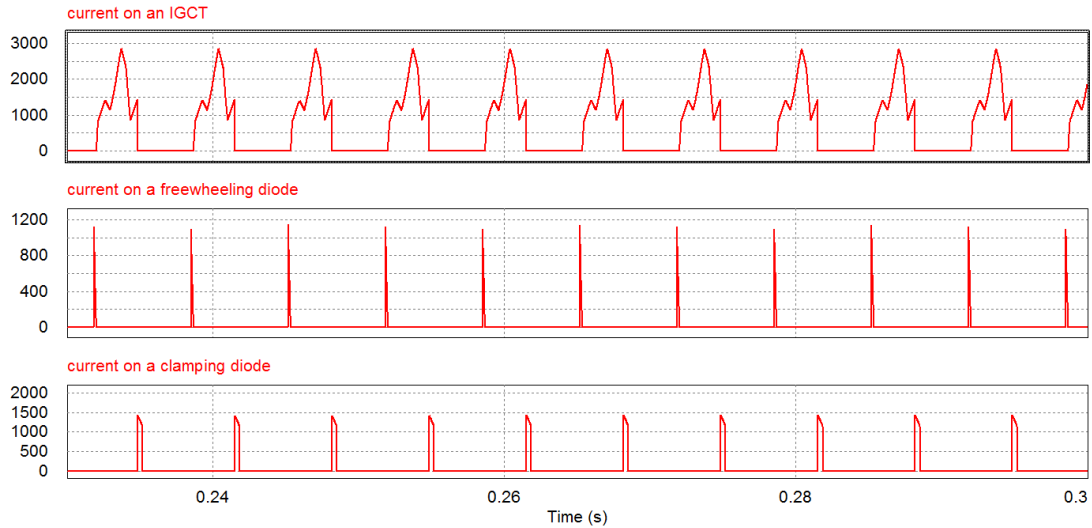


Figure 5-2 Simulated current on the switches of the inverter in the simplified circuit: IGCT G1 (upper plot), freewheeling diode D1 (middle plot) and clamping diode Dclamp1 (bottom plot)

The output voltages produced by the inverter are represented in fig. 5-3. The trend has some differences with respect to the ideal trend of fig. 3-8, because of the clamping components and stray parameters.

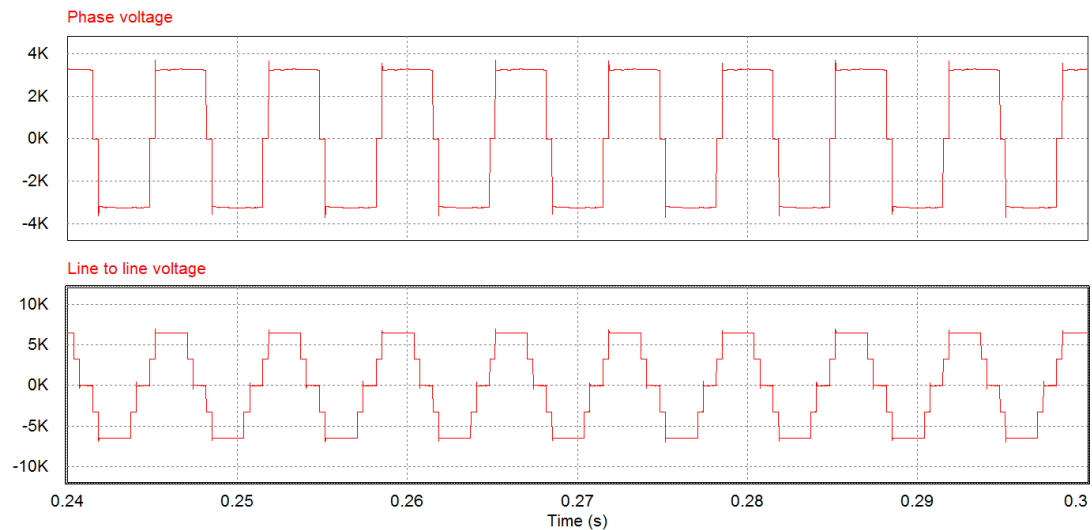


Figure 5-3 Phase voltage and line to line voltage at the output of the inverter

At regime situation, with the nominal voltage on the dc link and at the output voltages and the nominal value of beam current (therefore 62.4A provided by the current generator placed at the output), the resulting modulation index of the inverter is about 0.9.

To calculate this value I have used:

$$E_d = V_{dc} \cdot \frac{2}{n} \cdot f(\delta) - 6 \cdot f \cdot L_{tot} \cdot I_{DGC} \quad (5.1)$$

Where E_d is the output voltage, V_{dc} is the voltage on the dc link, n is the turn ratio of the step up transformer, f is the frequency of inverter operation, I_{DGC} is the beam current and L_{tot} is the inductance downstream the step up transformer. The only unknown is $f(\delta)$, which is a function that express the output inverter voltage by varying the modulation index δ .

The interval of the modulation index during the normal operation allows a linear approximation of this relationship, expressed by:

$$f(\delta) = \left(\delta - \frac{1}{3}\right) \cdot \frac{3}{4} + \frac{1}{2} \quad (5.2)$$

Having obtained $f(\delta)$ from equation 5.1, the modulation index can be calculated.

5.1.2 Detailed model

In the detailed model the inverter is supplied by the ac/dc converter and the control of the voltage on the dc link is guaranteed by the feedback control of the thyristor bridges.

To reach the steady-state condition, the capacitor bank is initially energized, increasing the dc link voltage from 0V to 6500V in a quite short time (to reduce the simulation time), but avoiding that the fast raise creates an overshoot. Once the bank is charged at the nominal voltage, the inverter is switched on to control the AGPS output voltage. According to the requirements, the voltage reference is a 80ms ramp (see fig. 3-2) and the start-up is performed in perveance matching. The load current is set to half the maximum nominal value because only one inverter is simulated per stage, in order to set the correct values of current in the inverter components.

In fig. 5-4 the voltage on the dc link and the AGPS output voltage of one stage resulting from the simulation are reported. When the system has reached the regime, at about 0.5s, the voltages are oscillating around the nominal values; now there is not only the oscillating component at 900Hz, but also the component at 50Hz produced by the supplying grid and the component of 600Hz produced by the 12 pulses thyristor rectifier. The superposition of all these oscillating components results in the obtained voltage.

Anyway, the filtering action of the capacitor bank and the feedback action allow keeping the voltage ripple within required $\pm 5\%$.

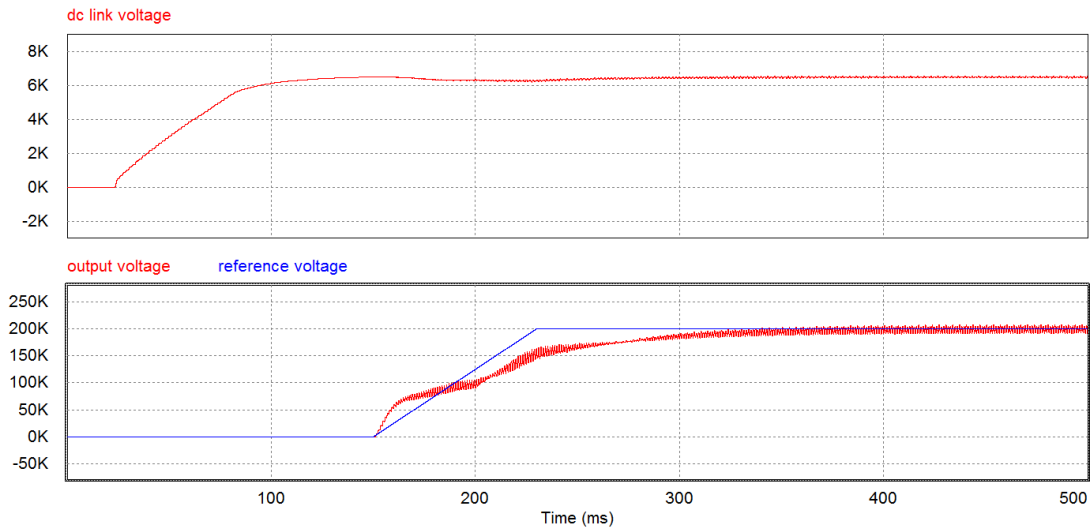


Figure 5-4 Voltage on the dc link and output voltage of one stage, for nominal operation.

The current flowing through the switches of the inverter is shown in fig. 5-5 and it has the same behaviour than the one obtained for the simplified model, but is half the value due to the fact that the load current is halved.

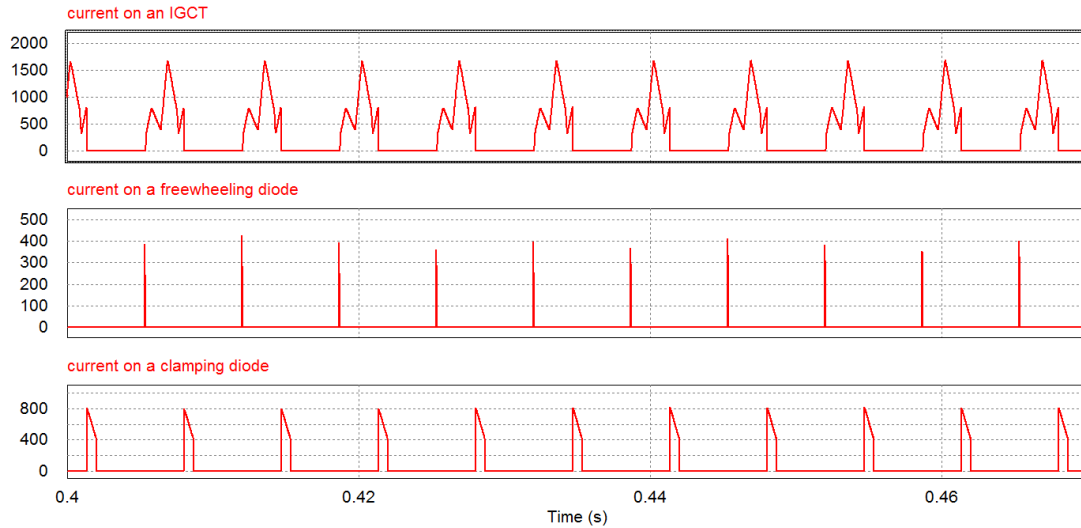


Figure 5-5 Current on the components of the inverter in the detailed model: IGCT G1 (upper plot), freewheeling diode D1 (middle plot) and clamping diode Dclamp1 (bottom plot)

5.2 Fault analysis

In this paragraph we are going to study the breakdown of one IGCT of an inverter, firstly from a theoretical and qualitative point of view, while in following paragraphs a more accurate analysis based on the simulations is developed.

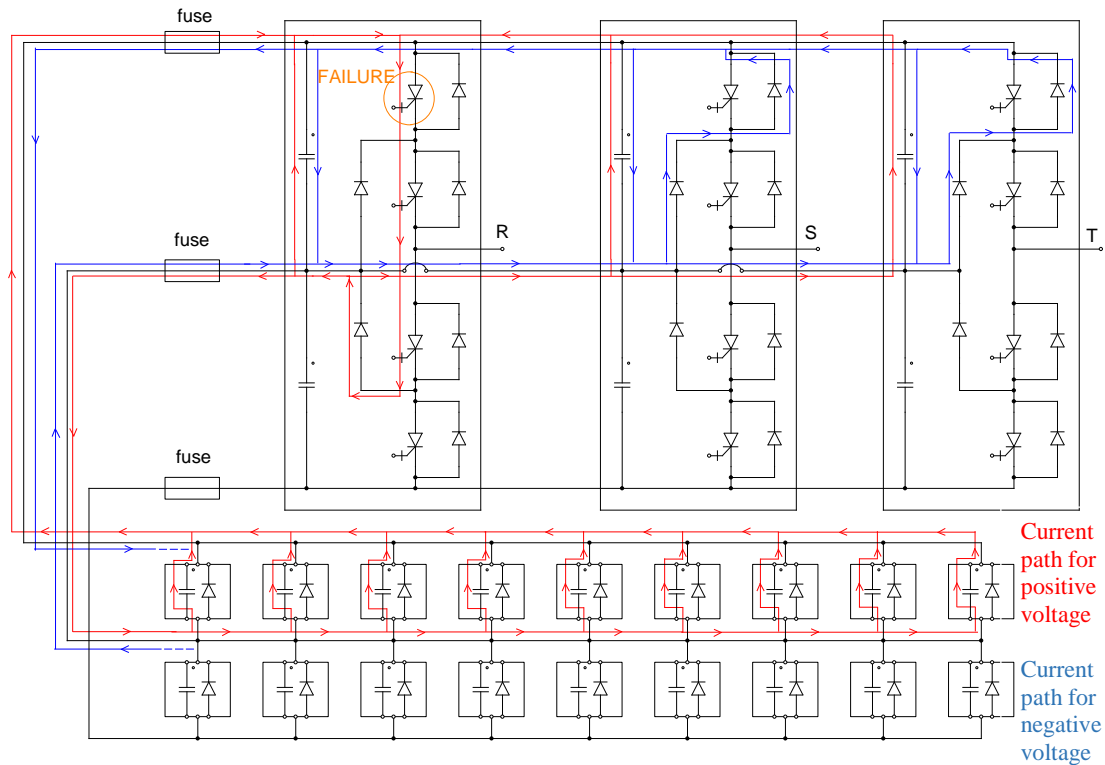


Figure 5-6 Current distribution during the fault

Assuming that the fault occur in the bottom central IGCT or in the upper IGCT of the leg (G2 and G1 of fig. 4-1), during the fault the damaged leg has a low impedance connection between the positive voltage busbar and the middle voltage busbar, being the bottom IGCT kept open.

In fact, when the fault occurs, the IGCTs of the faulty module which are conducting, continue to conduct, while all the other IGCTs are opened, both in the damaged modules and in all the other modules. Therefore, the upper capacitor bank is discharging through this low path impedance, made up of the three IGCTs (one is faulty) and the clamped diodes, that is connecting the high voltage dc busbar with the middle voltage dc busbar, grounded (see fig. 5-6).

Instead, the lower capacitor banks are not discharging because they have not a low path impedance allowing the reclosing of the current. Therefore they have the nominal voltage at the end of the transitory.

The symmetrical situation would occur if the fault cause the closure of the bottom three IGCTs.

The upper capacitor bank discharge is not just a RC discharge, with an exponential decay of the capacitors voltage, because of the presence of the inductances: they are the inductance of the clamped circuit and the line inductances. These inductances create an oscillation of the capacitor voltage, because the circuit is a RLC series. Moreover these inductances cause the slowing down of the discharge of the more distant capacitors' modules from the fault: for the higher presence of stray inductances in the longer path the LC parameter results to be higher, therefore the oscillations have a higher period and the oscillating discharge is evolving slowly than the capacitors nearer to the fault.

Due to the oscillation not too smoothed by the low value of resistance of the circuit, the capacitors' voltage became negative in certain intervals of time.

When the capacitor voltage of healthy modules is negative, the current reverses its direction in these modules flowing through the freewheeling and clamped diodes (showed in fig. 5-6).

A rough, simplified model of the fault, without considering stray inductances and resistances of the connections of the capacitors of the different modules, is represented in figure 5-7:

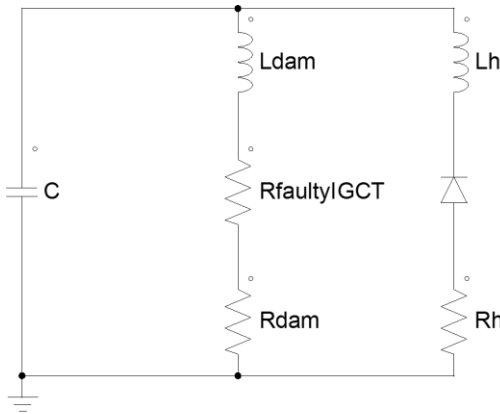


Figure 5-7 Equivalent circuit of the fault under study

C represents the total upper half bank capacitance. The capacitor is in parallel to the faulty leg, represented with the inductance obtained adding the stray and clamp inductances of the leg, shown in fig. 4-2, and by the resistances of the components of the path: the two healthy IGCTs, the clamping diode and the faulty IGCT.

It is in parallel also with the other two legs of the inverter. Here, to simplify, only one leg is represented. It is made up of a series of an inductance, a resistance and an ideal diode. The inductance and resistance values are obtained by considering the stray and clamp inductances (also the one connecting the healthy leg to the faulty leg) and the resistance of the component.

The values of the parameter of the circuit are reported in table 5-1.

Table 5-1 Parameters of the equivalent circuit

C=72mF
L_{dam} =4.5μH
R_{dam} =2.484mΩ
L_h =6.5μH
R_h =2.728mΩ

Before the diode is switched on (i.e. when the capacitor has a negative voltage), the circuit is a simple series RLC circuit. The current peak on the faulty leg is obtained by solving the differential equation of this circuit.

The circuit has the natural frequency:

$$\omega = \frac{1}{\sqrt{LC}} \quad (5.3)$$

The solution is a damped oscillation because we are in the situation:

$$\frac{R^2}{4L^2} < \frac{1}{LC} \quad (5.4)$$

Introducing the parameters:

$$\alpha = \frac{R}{2L} \quad \beta = \sqrt{\frac{1}{LC} - \frac{R^2}{4L^2}} \quad (5.5)$$

The value of the current in function of the time is:

$$I(t) = \frac{q_0\omega^2}{\beta} e^{-\alpha t} \sin(\beta t) \quad (5.6)$$

q_0 is the initial charge inside the capacitor and it can be obtained by:

$$q = C \cdot V \quad (5.7)$$

Where C and V are the capacitance of the capacitor (36mF) and the initial voltage on the capacitor (used the nominal 3250V).

The maximum value occurs at 1/4 of the oscillating period, which is:

$$T = \frac{2\pi}{\omega} \quad (5.8)$$

I use this value of time and the parameters L and C of table 5-1; as R I take the value reported in that table summed to the value of resistance of the damaged IGCT. I have considered 5 equally distributed values between the resistance that it has when it is healthy and a value 100 times lower, according to the considerations explained in paragraph 4.1. In this way I have obtained the values of the current peak in function of this resistance, shown in table 5-2.

Table 5-2 Current peaks on the equivalent model at the variation of the resistance of the damaged IGCT

Resistance of the faulty IGCT	Current peak
0.5mΩ	311.1kA
0.1mΩ	323.7kA
0.05mΩ	325.3kA
0.01mΩ	326.6kA
0.005mΩ	326.8kA

Notice that the first decreasing step of the resistance causes a high increment of the current peak, after that the reductions of the resistance do not influence the peak very much. This is because the resistance is becoming more and more small compared to the total resistance of the faulty leg (about 2.5mΩ). Therefore this resistance does not influence very much the fault transient.

To get the real solution of the circuit of figure 5-7 we should take into consideration the leg with the diode too; in such a way we can estimate the current in the freewheeling diodes during the fault with the current flowing in that branch.

Anyway, the solution of this simple circuit would be not very significant, since the capacitor bank is supposed concentrated and not distributed, neglecting the influence of the stray parameters between modules. These parameters slow down the discharge, reducing the peaks of current on the faulty modules and on the healthy modules, which would result exaggerate from the solution of the circuit of figure 5-7.

5.3 Fault simulations with the simplified circuit

5.3.1 Prospective currents during the fault

Starting from the nominal operation, in steady state, I have simulated the single fault of a breakdown of an IGCT of an inverter's leg. Using the simplified model of the circuit, I simulate the short circuit current and the energy dissipated on the components due to the energy stored in the capacitor bank. With this model, the energy coming from the ac/dc converter is neglected.

I simulate the fault using the simulation items represented in the top part of the fig. 4-7. A step voltage generator changes its value from 0 to 1 commanding a series of events:

- In the first leg to the left composing the faulty inverter in fig. 4-1, G1 is closed, simulating the breakdown of the switch, while G2 and G3 continue to be closed (the fault time is chosen to have this situation) and G4 is left open. This is because the IGCTs of the faulty leg are frozen in the condition they are at fault time, according to the fault protection policy, because fault currents are too high to be interrupted opening the healthy switches, and dangerous arcs could be generated in that situation;
- In the other legs all the ICGTs are opened to stop the transfer of power to the load. Actually they take a short but not null time to open, yet, being this time very short, in simulations it will be neglected;
- The input current generator is instantly isolated, not providing power to the inverter during the fault;
- The DCG is disconnected from the inverter, because during the fault the current does not exit from the inverter, since the capacitor bank is discharging in a closed path;
- Dc link is connected (the subcircuit 'DC LINK' of fig. 4-7) to the input nodes of the faulty inverter, with all modules (represented only in their passive components) having their capacitors charged at the value that the capacitors of the faulty module have at the fault time.

The results of the simulation are discussed in the following.

As we can see from fig. 5-8, the dc link voltage after a short transient characterized by oscillations reaches a value that is the half of the nominal one. That is because, as previously said, the upper capacitor bank discharges on the damaged leg.

The voltage on the upper half bank is 3.33kV when the fault occurs, because to avoid a long time of simulation I have simulated the fault at 0.1s and at this time the voltage on the dc link is not completely at the nominal value, but it is oscillating around a mean value a little higher than the 6.5kV, anyway within the requirements.

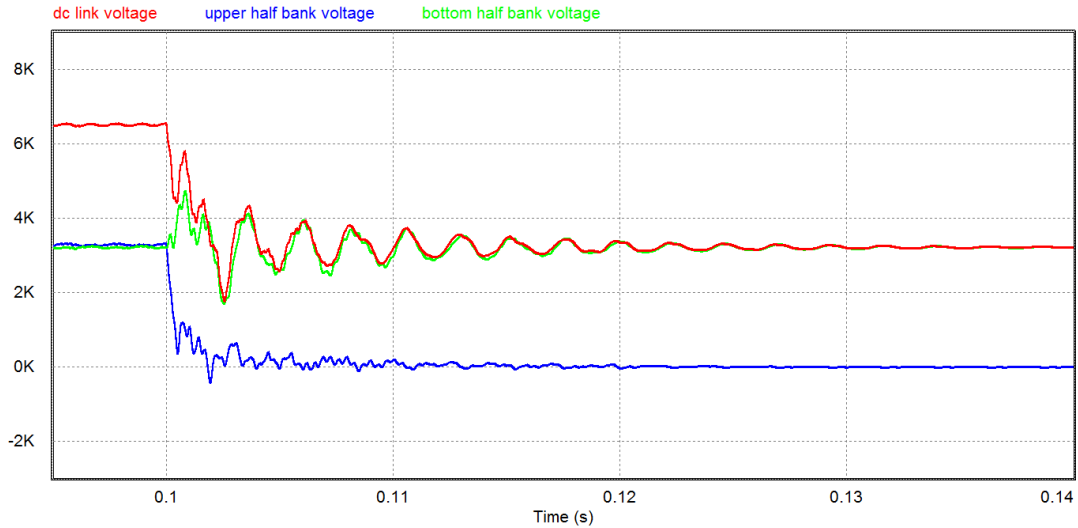


Figure 5-8 Dc link voltage, voltage on the upper and bottom capacitor half bank during the fault

However we are not interested on the voltage on the dc link, but we need to know the values of current on the components that can be damaged from the fault and the energy there dissipated.

We have seen in the previous paragraph that the current is influenced by the value of resistance of the faulty IGCT, but this value is uncertain. Previously we did an analysis of the peak of current in the damaged leg based on the study of an equivalent RLC circuit. In this paragraph we present the results obtained by simulations, which take into account the effects caused by all the elements of the circuit.

The simulations are done setting the resistance to $0.5\text{m}\Omega$ (which is the resistance of the IGCT in healthy state), $0.1\text{m}\Omega$, and $0.01\text{m}\Omega$. The voltage plot of figure 5-8 is obtained using $0.1\text{m}\Omega$ just to show the behaviour of the voltage, which is obviously influenced by this resistance too.

As shown in the previous analysis of the RLC circuit, we expect that the more the resistance of the damaged component is low, the more the peak of current on the faulty leg is high because it is less smoothed by the resistance and consequently the peak of negative voltage on the capacitor will be higher, producing a higher peak of current on the healthy legs. Anyway, we expect a not very high dependence on this parameter.

In fig. 5-9, 5-10 and 5-11 the currents on the faulty leg for the selected values of faulty IGCT resistance are represented.

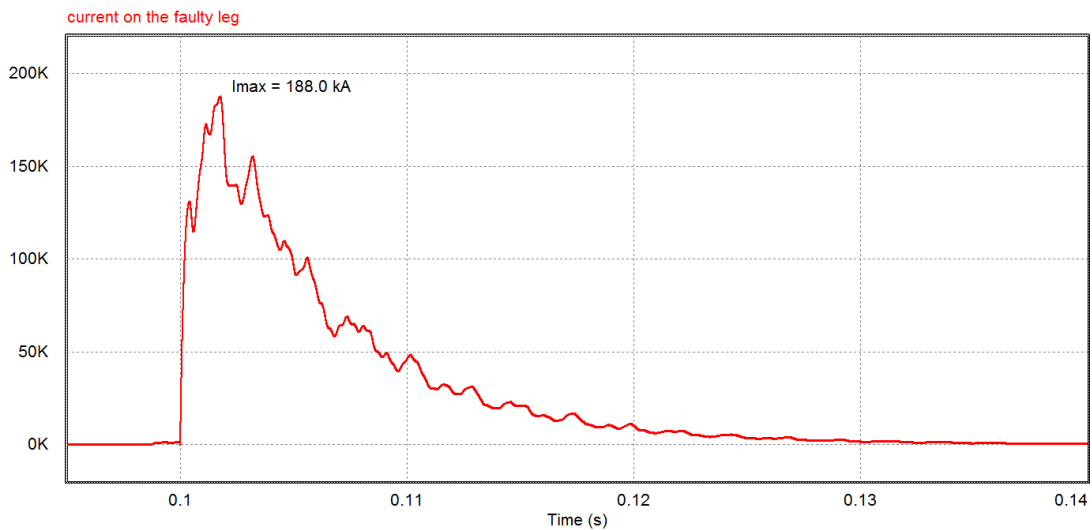


Figure 5-9 Current on the faulty leg, with the faulty IGCT having $0.5\text{m}\Omega$ of resistance

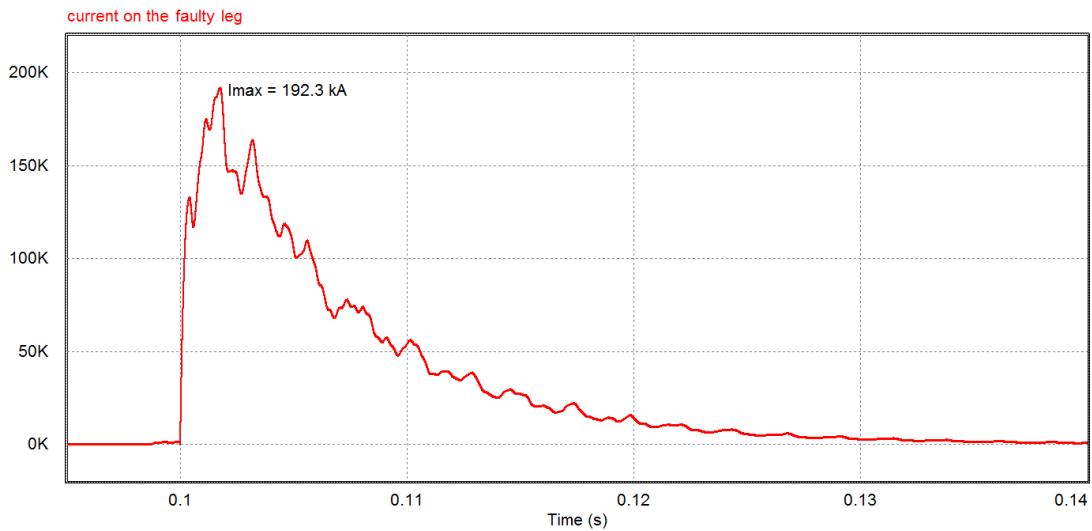


Figure 5-10 Current on the faulty leg, with the faulty IGCT having $0.1\text{m}\Omega$ of resistance

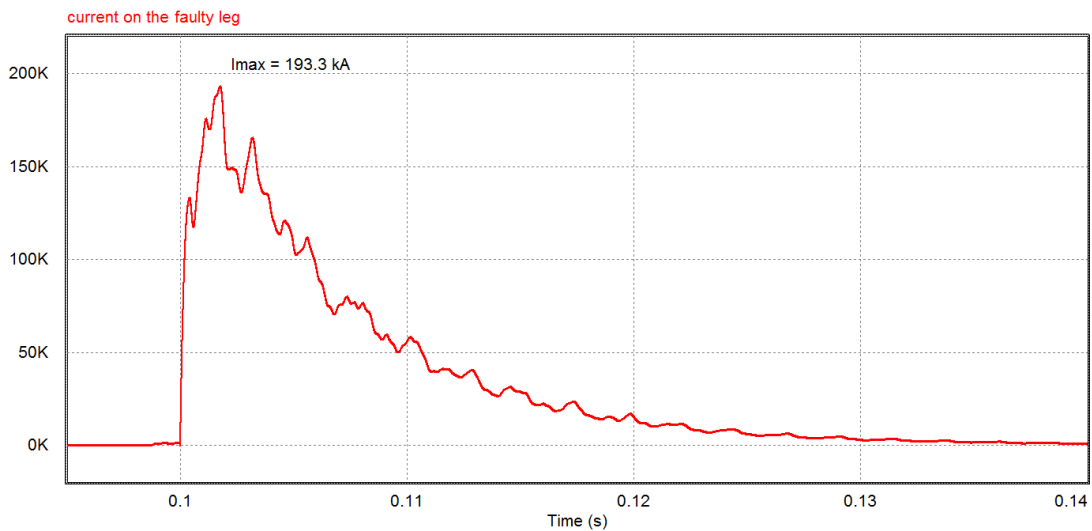


Figure 5-11 Current on the faulty leg, with the faulty IGCT having $0.01\text{m}\Omega$ of resistance

This is the current flowing through the damaged IGCT (G1), the two healthy closed IGCTs (G2 and G3) and the clamping diode (Dc2).

From the resulting plots we can see that the behaviour is the same and the current peak does not change so much: passing from the resistance of $0.5\text{m}\Omega$ to the value of $0.01\text{m}\Omega$, 50 times smaller, the peak increases only of 2.8%. This means that the reduction of this value has not so much influence compared to the whole resistance of the leg, which is indeed about $2.5\text{m}\Omega$.

The fault current causes a dissipation of energy on the components and the semiconductor devices have to withstand not only the current peak, but also the energy that they are dissipating. Semiconductor components in particular have a limitation on the maximum specific let-through energy I^2t allowable to avoid the explosion of the case and the consequent damage on nearby equipment. Therefore the value I^2t on the faulty leg is obtained in the simulations for the three different resistance values. This is an important parameter, since it allows the calculation of the energy dissipated on the components by multiplying this value for the resistance of the relative component.

The fault lasts for a very short time but the current involved is so high that the I^2t reaches extremely high values on the faulty leg.

In fig. 5-12, 5-13, and 5-14 the I^2t is reported for the analysed cases. The unit of measurement of the plots is $[\text{A}^2\text{s}]$.

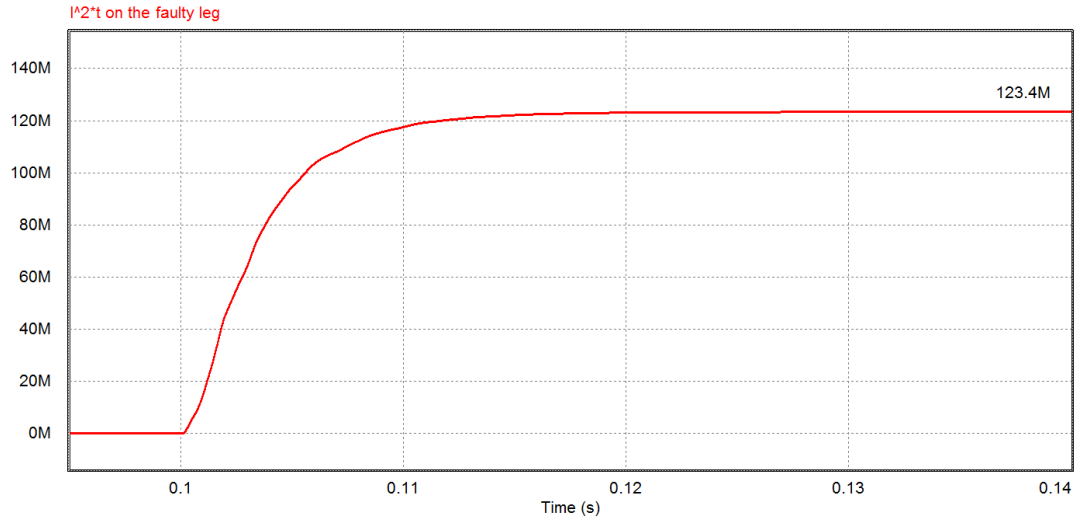


Figure 5-12 I^2t on the faulty leg, with the faulty IGCT having $0.5m\Omega$ of resistance

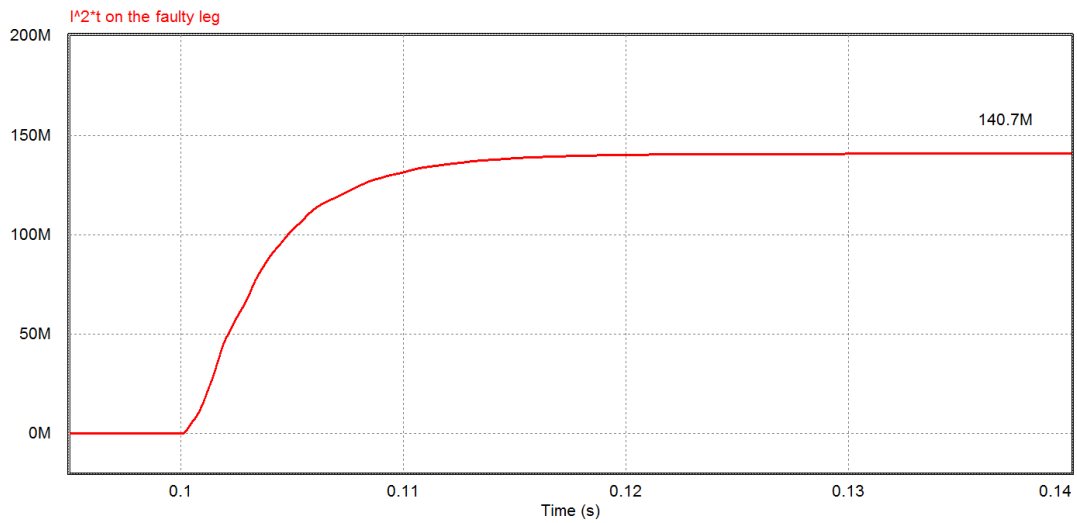


Figure 5-13 I^2t on the faulty leg, with the faulty IGCT having $0.1m\Omega$ of resistance

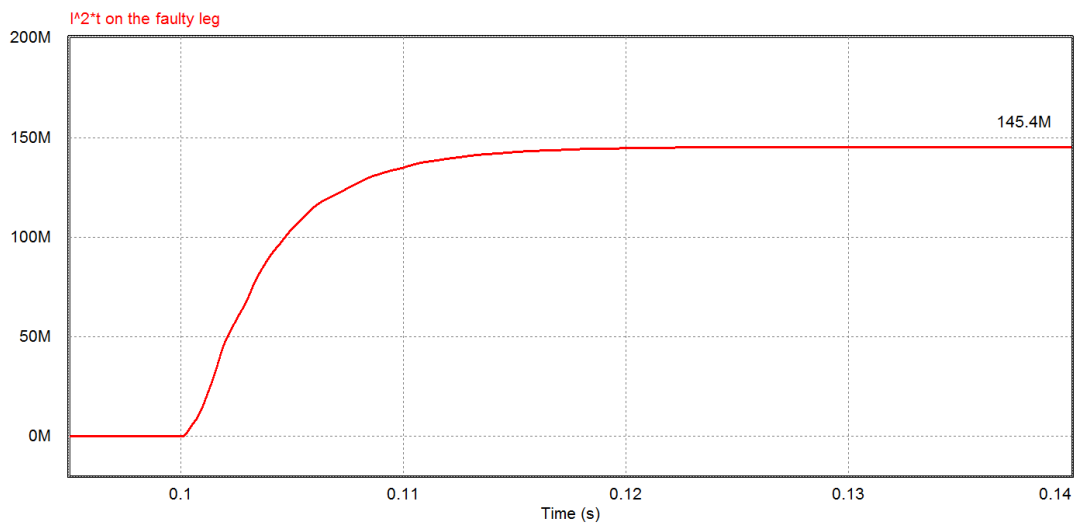


Figure 5-14 I^2t on the faulty leg, with the faulty IGCT having $0.01m\Omega$ of resistance

We can see that the variation of the resistance affects more significantly the value of I^2t , and therefore the energy dissipated on the components during the fault: passing from the resistance of $0.5\text{m}\Omega$ to the value of $0.01\text{m}\Omega$, this value has increased about 18%.

This means that the variation of such a small resistance is not able of modify largely the peak, but modifying the current values in all the period of the fault it causes a high variation on the integration of the current.

Anyway, the stresses on the IGCT components are extremely high both in terms of peak currents and let through specific energy. Such levels of energy in particular can lead to the explosion of the components and the propagation of the fault.

Being the voltage oscillations of the capacitor half bank causing the flowing of current also in the 2 healthy legs of the damaged inverters when the voltage of the half bank becomes negative, we must analyse the current on other two legs too, because it could damage the diode where it happens (see fig. 5-6).

The currents on the other two legs for the different values of resistance of the faulty IGCT are represented in fig. 5-15, 5-16 and 5-17.

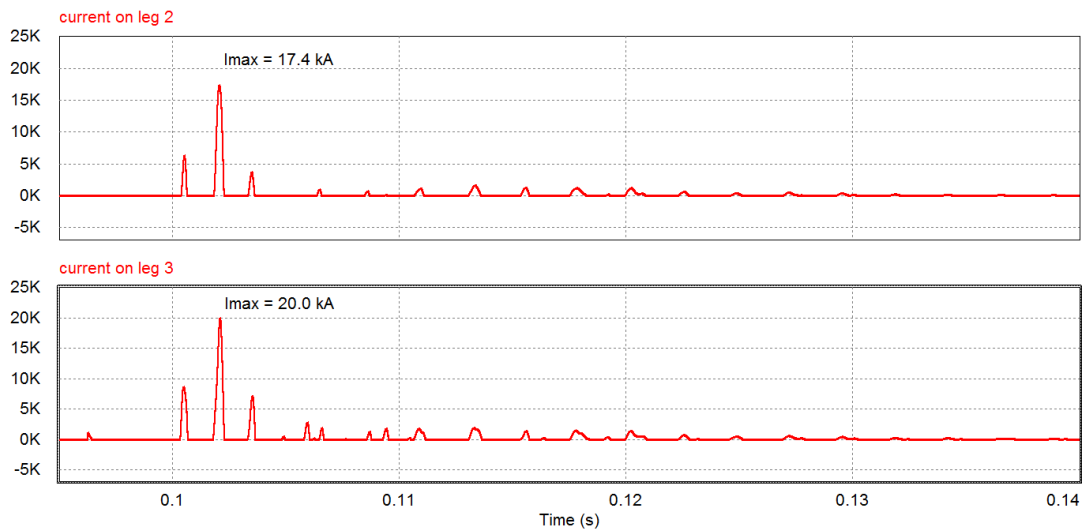


Figure 5-15 Currents on the two healthy legs of the faulty inverter, with the faulty IGCT having $0.5\text{m}\Omega$ of resistance

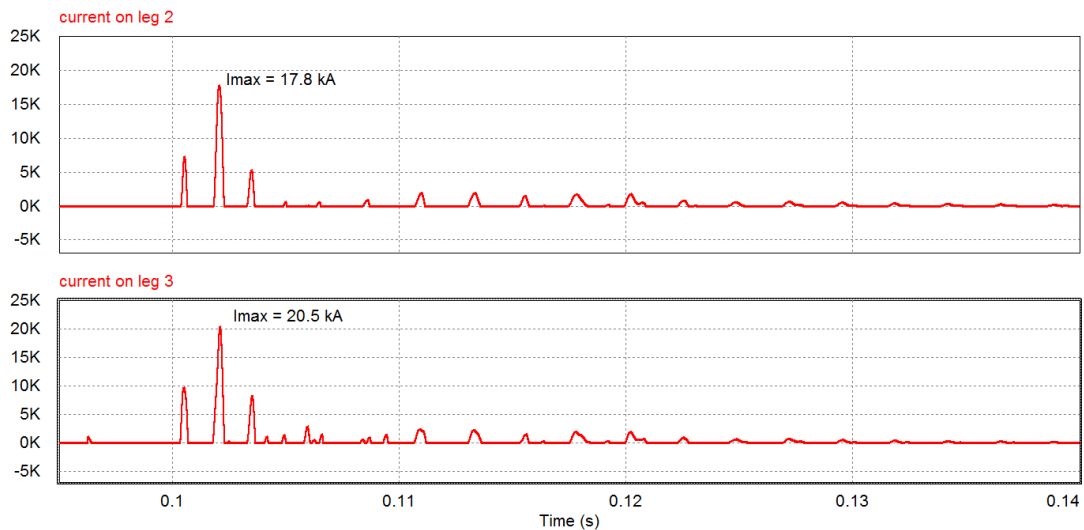


Figure 5-16 Currents on the two healthy legs of the faulty inverter, with the faulty IGCT having $0.1\text{m}\Omega$ of resistance

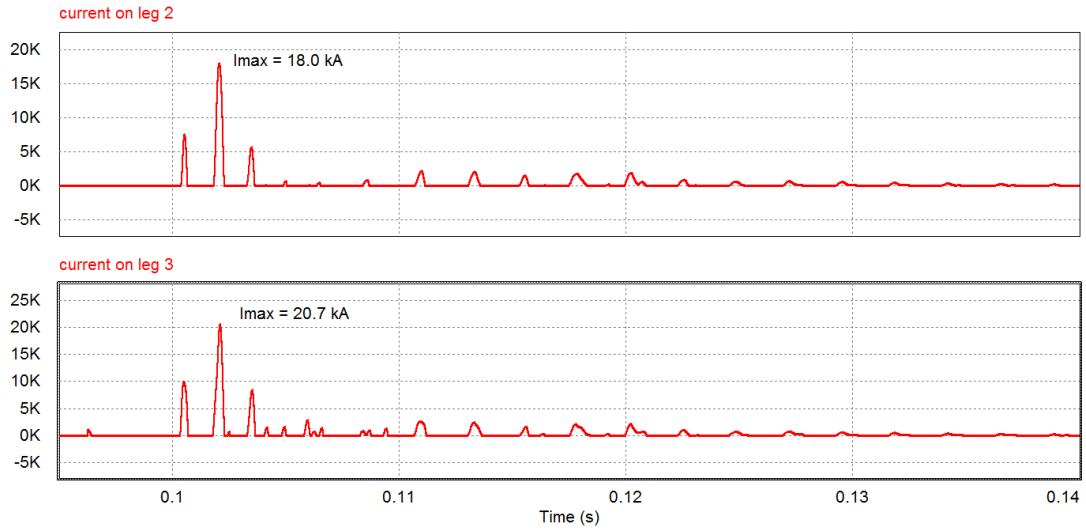


Figure 5-17 Currents on the two healthy legs of the faulty inverter, with the faulty IGCT having 0.1mΩ of resistance

The values of specific let through energy I^2t in the diodes in the three cases are represented in fig. 5-18, 5-19 and 5-20.

As in the faulty leg, the variation of the resistance does not affects very much the maximum current in the healthy legs, while the passing energy is more affected, for the same reason explained before.

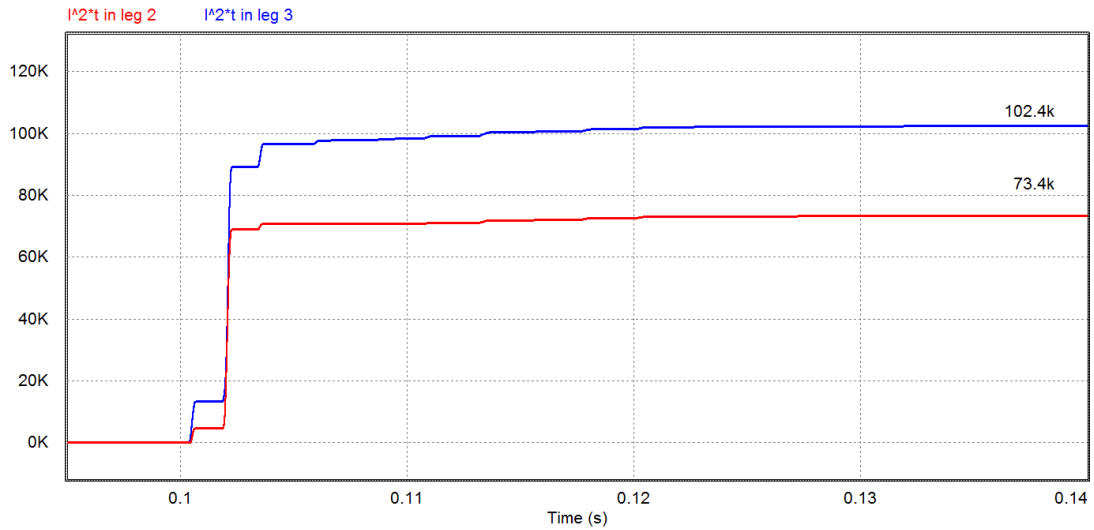


Figure 5-18 I^2t on the healthy legs during the fault, with the faulty IGCT having 0.5mΩ of resistance

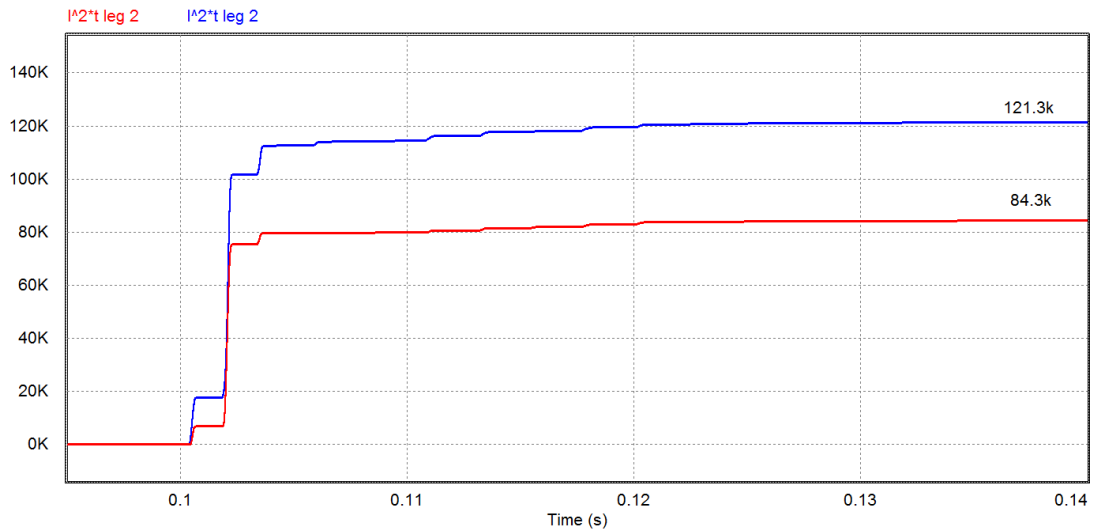


Figure 5-19 I^2t on the healthy legs during the fault, with the faulty IGCT having $0.1m\Omega$ of resistance

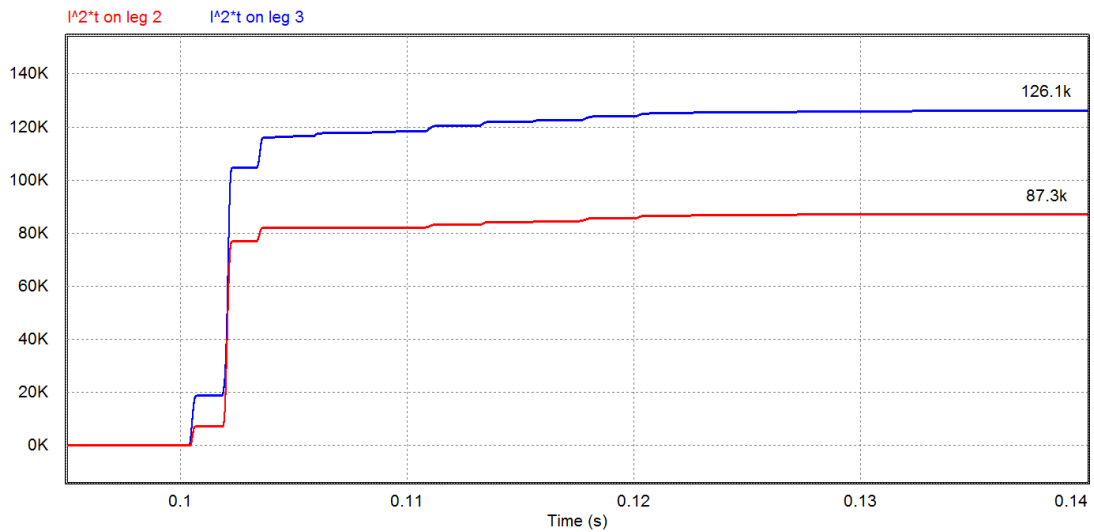


Figure 5-20 I^2t on the healthy legs during the fault, with the faulty IGCT having $0.01m\Omega$ of resistance

Hereafter, to compare the different situations and to analyse the electrical stresses, I have used mainly the resistance of the faulty IGCT equal to $0.1m$, which is the middle values of the considered cases and we have seen that further reductions do not cause very high variations on electrical stresses.

Not only the two healthy legs of the faulty inverter are subjected to the phenomena of the flowing of current in the freewheeling diodes, but also the other modules connected to the dc link. The peak of current flowing in these diodes occurs at different times and with different behaviours, because they depends on the voltage of the inverter module capacitors. We have to verify if during the discharge of the bank, the freewheeling diodes of the healthy inverters are interested by excessive current peaks. Fig. from 5-21 to 5-25 shows the current flowing in the freewheeling diodes during the fault, for all the modules connected to the dc link, in the case of resistance of the faulty IGCT equal to $0.1m\Omega$.

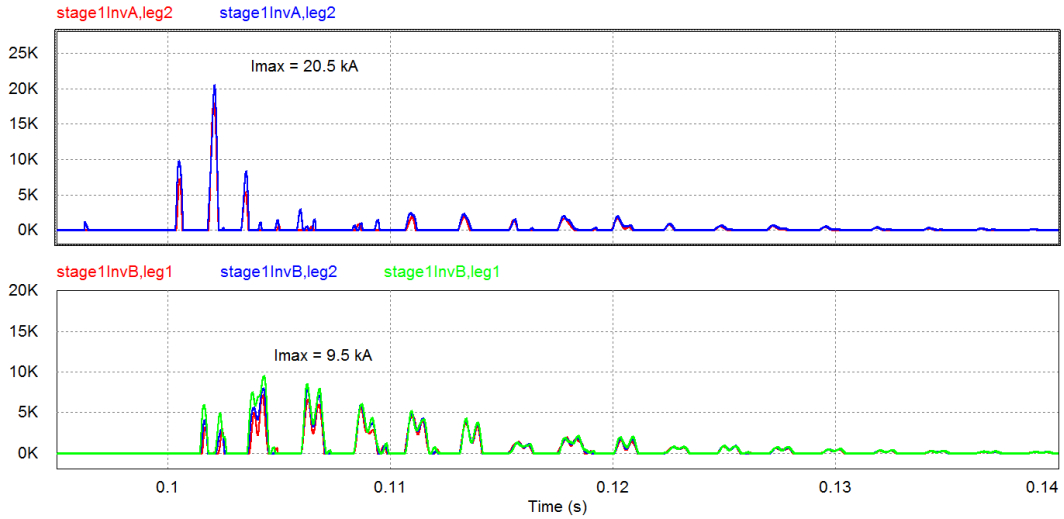


Figure 5-21 Current on the freewheeling inverters of stage 1, where inverter A is the inverter where the fault occurs

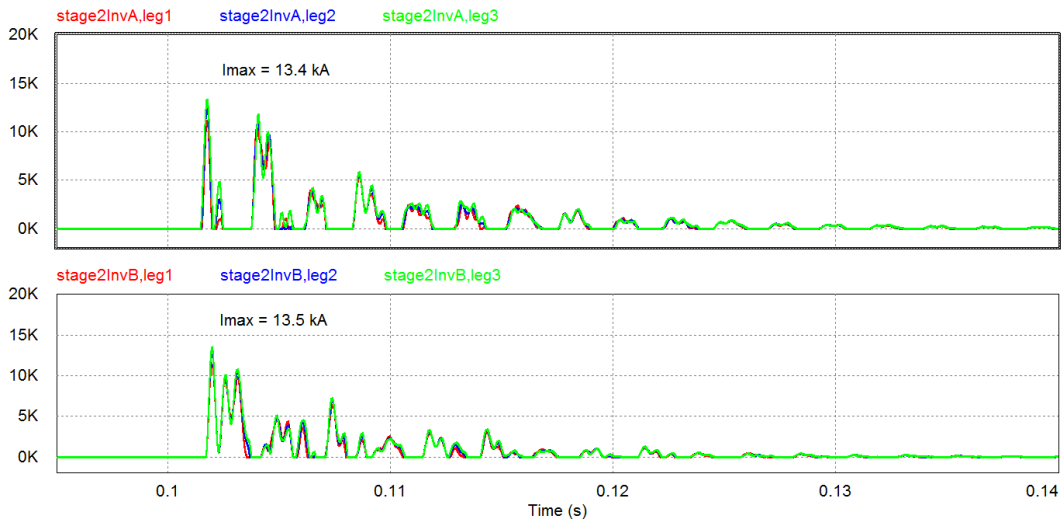


Figure 5-22 Current on the freewheeling inverters of stage 2

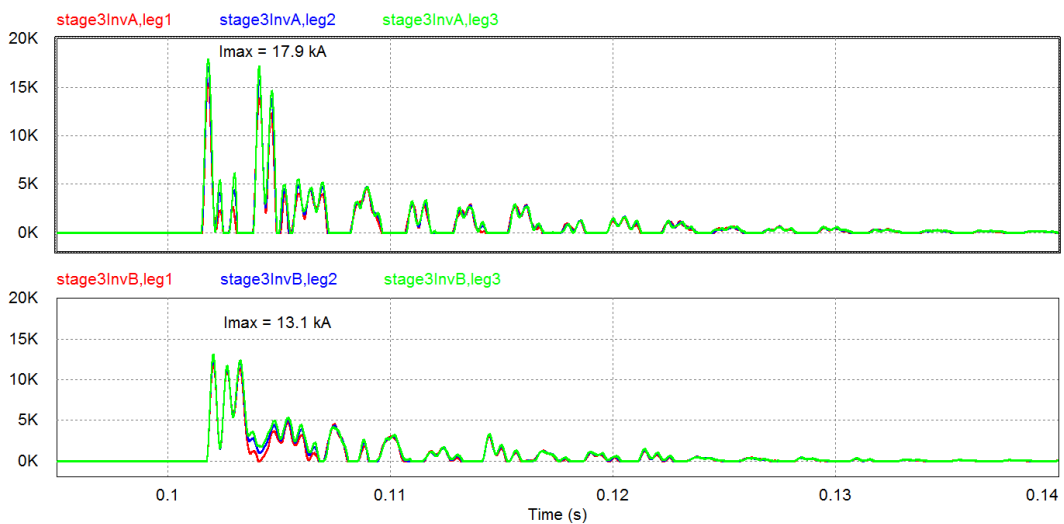


Figure 5-23 Current on the freewheeling inverters of stage 3

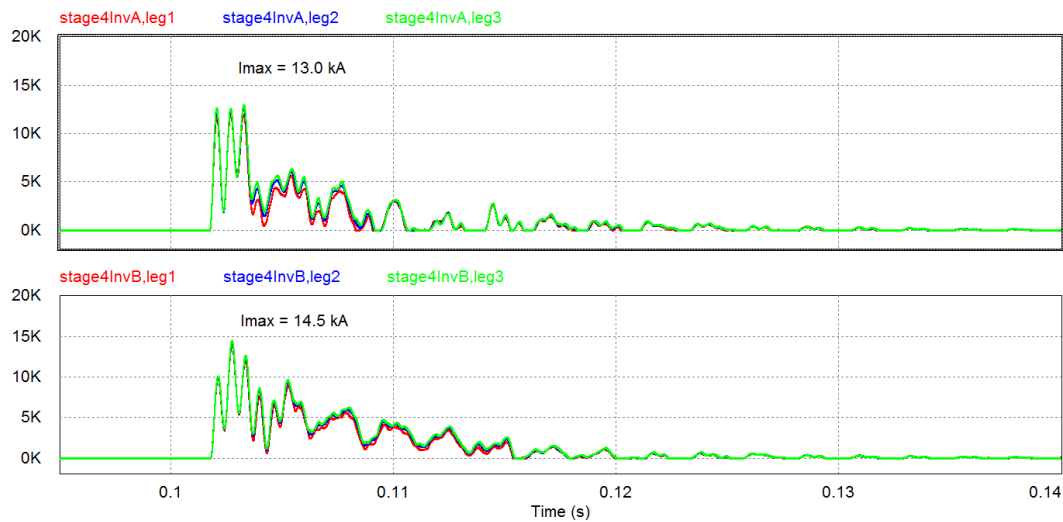


Figure 5-24 Current on the freewheeling inverters of stage 4

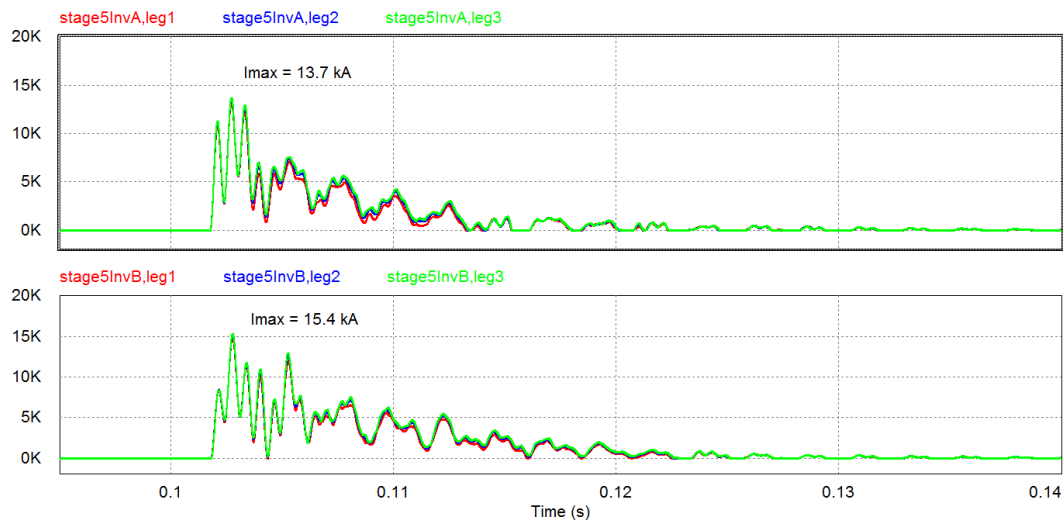


Figure 5-25 Current on the freewheeling inverters of stage 5

The current behaviour and the maximum values are quite different in the inverters; that is due to the current distribution on the dc link, related to the stray inductances values.

We notice that the current peak on the freewheeling diodes is lower in the healthy inverters than in the damaged inverter. In this situation the maximum value is lower than 18kA, while in the damaged inverter the current peak is more than 20kA (fig. 5-16). Moreover in the other modules the current peaks are even lower.

Therefore, the worst case for the freewheeling diodes occurs for the healthy modules of the faulty inverter, since they are subjected to the highest stress.

The values of I^2t I have obtained by the simulation for these freewheeling diodes are reported in table 5-3, with the values of the current peak.

Table 5-3 Maximum current peak and I^2t in the freewheeling diodes of all the inverters

INVERTER'S FREEWHEELING DIODE:	Current peak	I^2t
Stage 1, inverter A (faulty)	20.5 kA	121 KA ² s
Stage 1, inverter B	9.5 kA	137 KA ² s
Stage 2, inverter A	13.4 kA	149 KA ² s
Stage 2, inverter B	13.5 kA	157 KA ² s
Stage 3, inverter A	17.9 kA	263 KA ² s
Stage 3, inverter B	13.1 kA	196 KA ² s
Stage 4, inverter A	13.0 kA	236 KA ² s
Stage 4, inverter B	14.5kA	363 KA ² s
Stage 5, inverter A	13.7 kA	305 KA ² s
Stage 5, inverter B	15.4 kA	447 KA ² s

The highest stress in terms of I^2t occurs in the stage 5, inverter B. However, both in terms of peak current and of let-through energy, the stresses on the diodes are not relevant and can be withstood by the components.

5.3.2 Prospective current and I^2t at the input of the inverter

In case the protection is based on fuses, the selection of a suitable fuse needs as input the prospective fault current and the rms fault current (proportional to I^2t), i.e. the current flowing in the place where the fuses will be put.

We see in this paragraph the prospective current behaviour and the rms values resulting from simulations to see how the fuses have been chosen. The fuses will be placed at the input of the inverter module in order to isolate, in case of fault, the faulty inverter from the rest of the inverters, in order to avoid the discharge of the dc-link capacitors of the healthy modules into the fault, thus limiting the let-through specific energy and the fault current peak.

Moreover, the fuses have to ensure the selectivity of the intervention: only the fuses of the faulty module has to intervene in case of fault.

The prospective currents at the input of the inverter resulting from simulations are shown in fig. 5-26. Only the result obtained with the resistance of the faulty IGCT equal to 0.1m Ω is reported, the middle of the considered values, because we have previously seen that the current trend is not very much affected by this parameter: there is just a small variation of the values keeping the same behaviour.

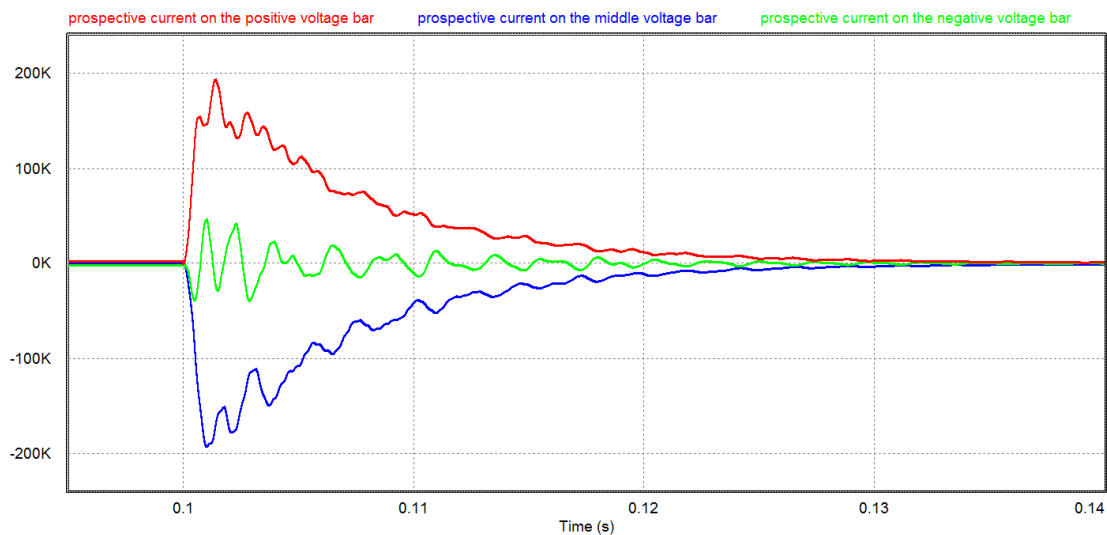


Figure 5-26 Prospective current on the three bars at the input of the damaged inverters

The value of I^2t at the inputs on the inverter, in fuses' positions, is shown in fig. 5-27. Obviously on the negative voltage input the value is very small, because it is the only result of the oscillations of the lower capacitor bank around the nominal value.

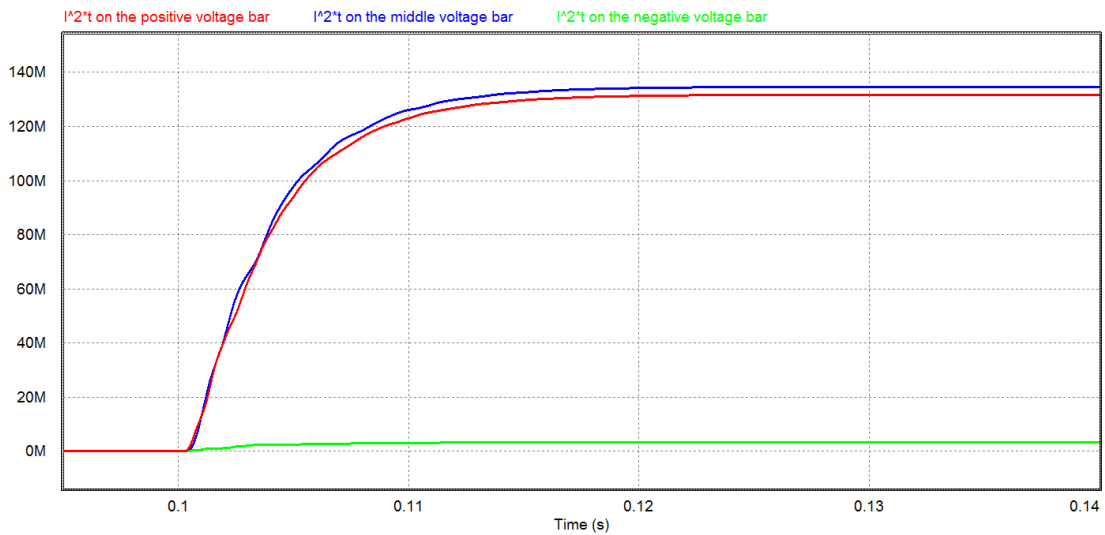


Figure 5-27 I^2t on the three inputs of the inverters

In fig. 5-28 are shown the rms values of the prospective currents, which will be used in the next paragraph to calculate the intervention current of the fuses, necessary to simulate the fuse behaviour.

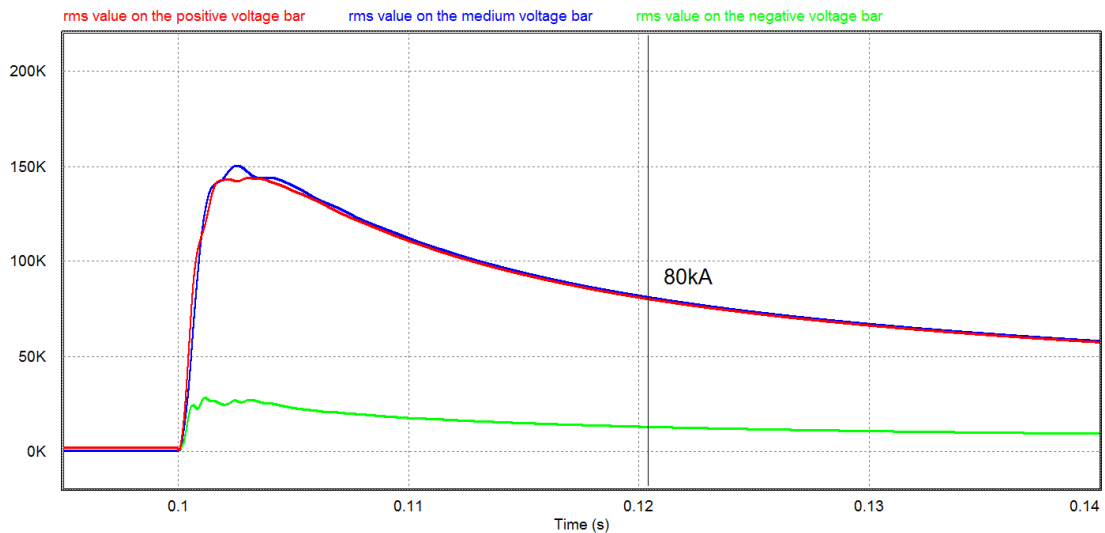


Figure 5-28 rms value of the prospective current

The rms value of the prospective current has been determined by choosing the value calculated with the simulation of $\sqrt{\frac{1}{T} \int I^2 t}$ at the instant when the I^2t value reaches the saturation

Let us analyse the prospective currents (fig. 5-29) at the input of the inverter B of stage 5, which is the more far away inverter with respect to the fault. These currents are needed as input for the selection of the fuses to verify the selectivity (the fuses have not to intervene in the healthy inverters).

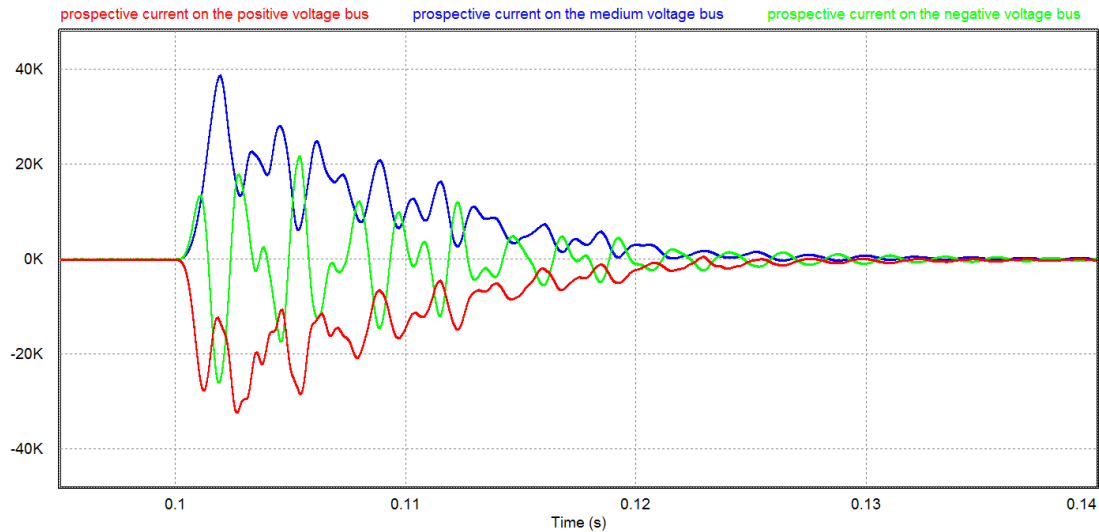


Figure 5-29 Prospective currents at the inputs of inverter B of stage 5

The I^2t at the input of other inverters are reported in fig. 5-30. They depend on the current distribution on the dc link, due to the presence of stray inductances.

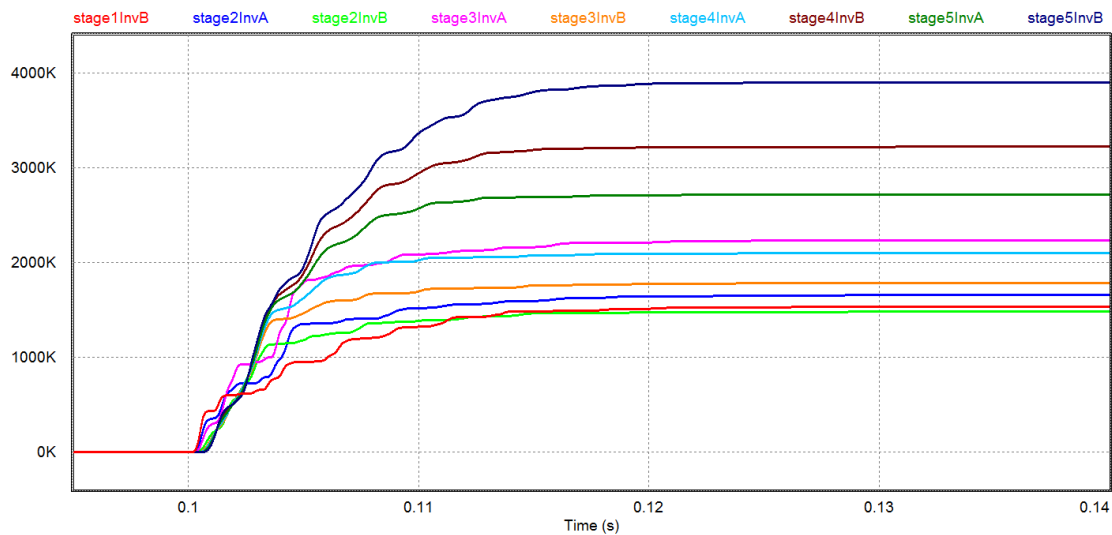


Figure 5-30 I^2t values at the input of the healthy inverters

We notice, as expected, that the current peak (about 40kA, from fig. 5-29) and the I^2t (about $4MA^2s$ from fig. 5-30) value are much lower than in the input of the damaged inverter, respectively about 200kA and $135MA^2s$, from fig. 5-26 and 5-27. The chosen fuse has to withstand these I^2t to ensure selectivity, i.e. the fuses must not intervene before the intervention of the fuses in the faulty inverter.

The values obtained in this paragraph will be used in the paragraph 5.3.3 to select the fuse.

5.3.3 Selection of the fuse

Based on the prospective fault currents determined with the simulations, a fuse has been searched in the market with the suitable intervention curve. Unfortunately, a fuse for such a high voltage, current and energy was not available.

A special custom medium voltage fuse from SIBA [12] has been developed on purpose, customized and tested to provide the protection and selectivity required, based on the expected prospective current. It is a double body fuse with rated current 500A per body (1000A in total), and rated voltage 6.5kV.

The fuse layout is shown in fig. 5-31.

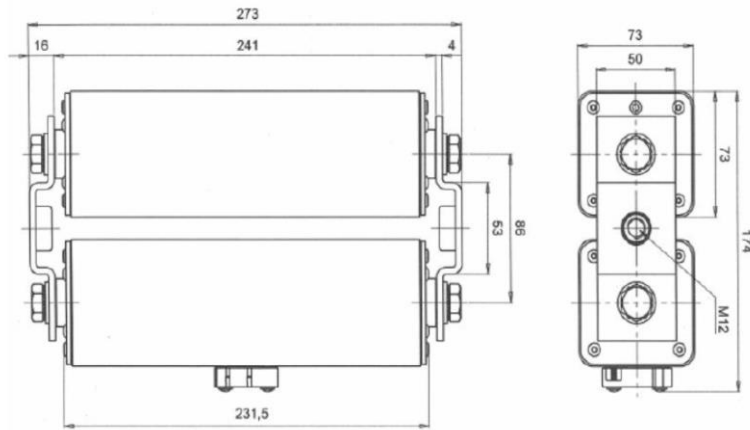


Figure 5-31 Fuse layout

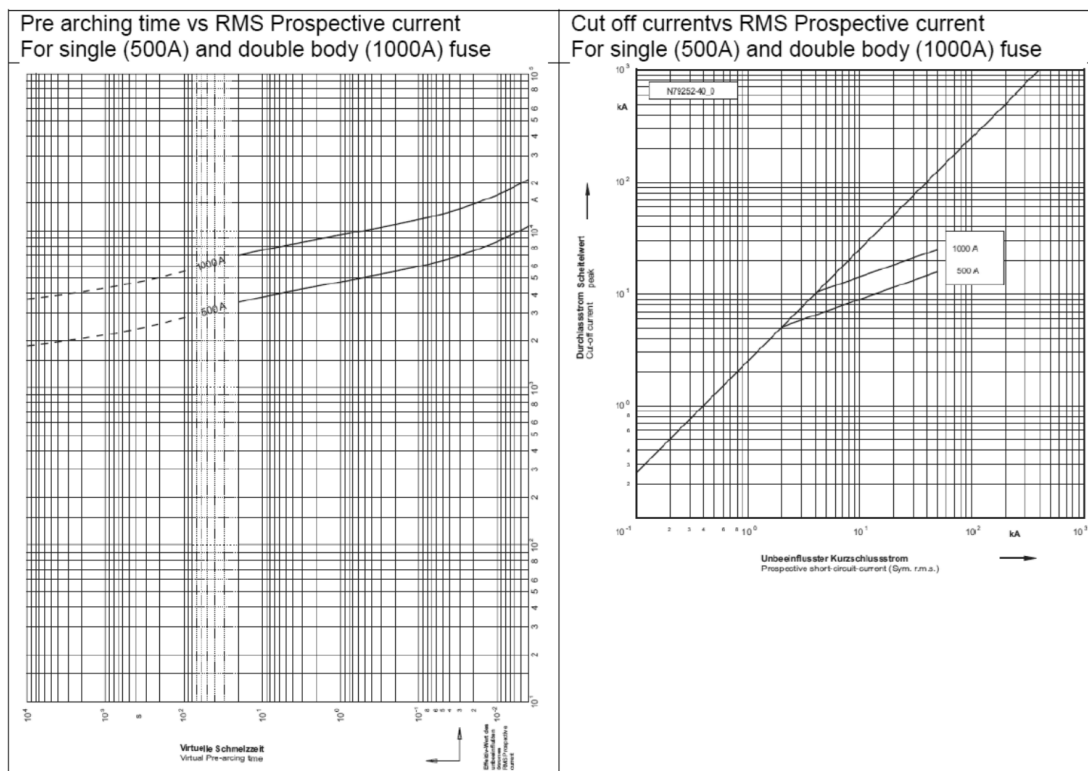


Figure 5-32 Intervention currents of fuses

The curves of the fuse are shown in fig. 5-32. The pre-arcing time as a function of the rms prospective current and the cut-off current as a function of the rms prospective current are represented. On the basis of these curves, we can determine the cut-off current: from the rms value of 80kA obtained from the simulation (fig. 5.28) the intervention current of the fuse of about 125kA has been obtained. This is the value that has been used in the circuit simulating the fuse in fig. 4-14.

5.3.4 Using the fuses as protection

On the basis of the cut-off current, we can verify the effectiveness of the selected fuse in protecting the circuit, i.e. limiting the current peak and the let-through specific energy in the faulty module below the limits for explosion.

The system that has been chosen is the insertion of fuses at the input of each inverter, in each one of the three bars, as showed in fig. 3-15. The fuses have been selected in paragraph 5.3.3.

The circuit is simulated with the presence of the fuses, simulated by circuits whose operation is explained in paragraph 4.6.2.

The resulting input voltage, downstream of the fuses, is shown in fig. 5-33.

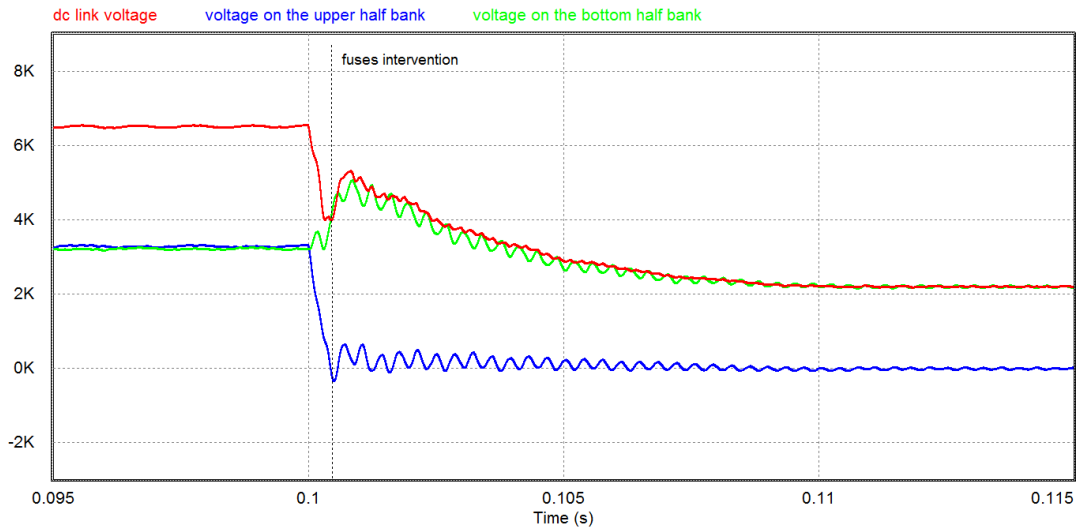


Figure 5-33 Voltage downstream the fuses during the fault, with fuse intervention

The voltage of the upper bank capacitor in parallel to the faulty leg is decreasing to 0V. The first quick drop causes the highest current peak and before the successive growth, when the voltage becomes negative, causes the highest peak of current on the freewheeling diodes of the healthy legs.

The voltages measured upstream the fuses are represented in fig. 5-34.

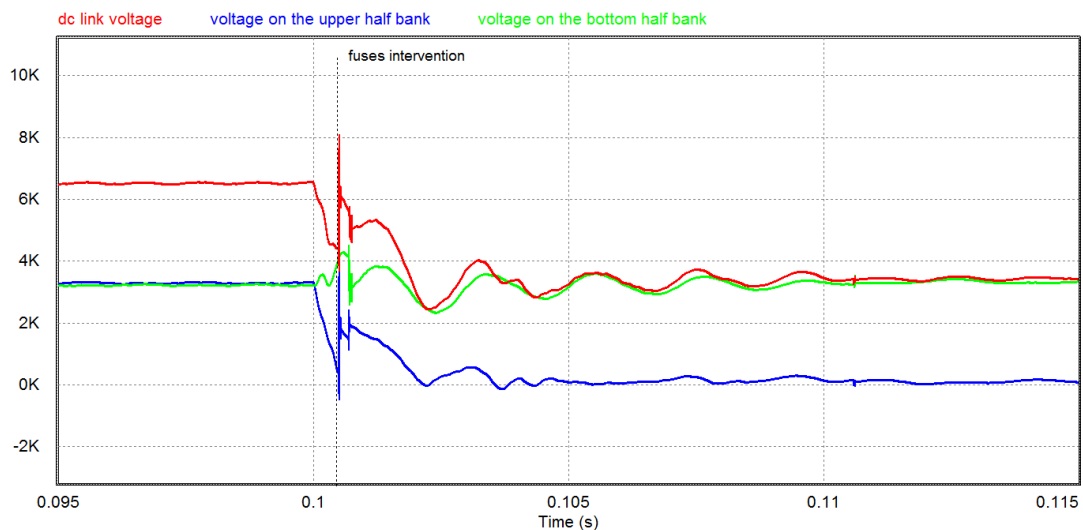


Figure 5-34 Voltages measured upstream the fuses during the fault, with fuse intervention

These trends are affected by numerical instabilities produced by the intervention of the circuit that simulates the fuses, but before that moment the dc link is properly described.

The trends of the current in the faulty leg for the three considered values of resistance of the faulty IGCT are reported in fig. 5-35, 5-36 and 5-37.

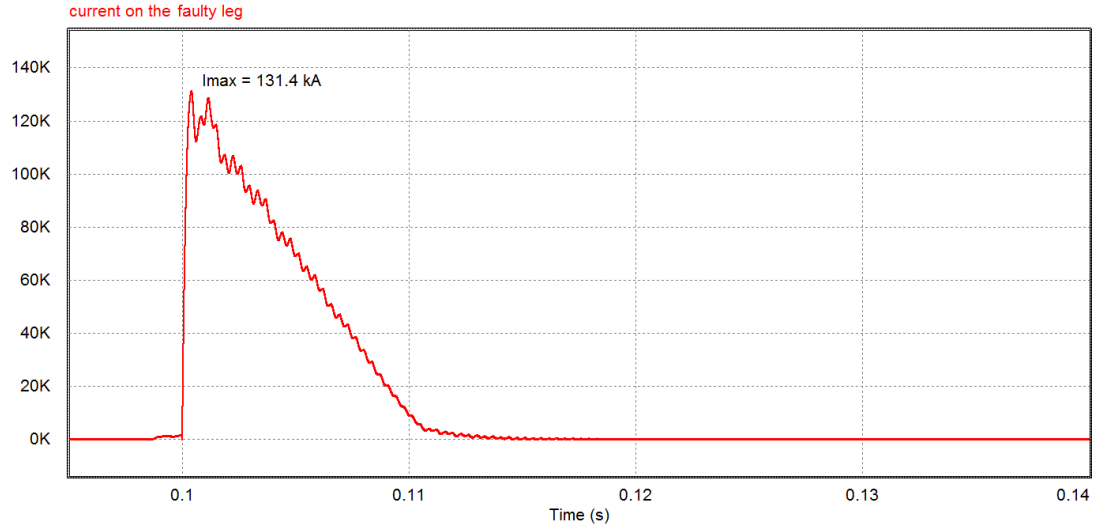


Figure 5-35 Current on the faulty leg using the fuses, with the faulty IGCT having 0.5mΩ of resistance

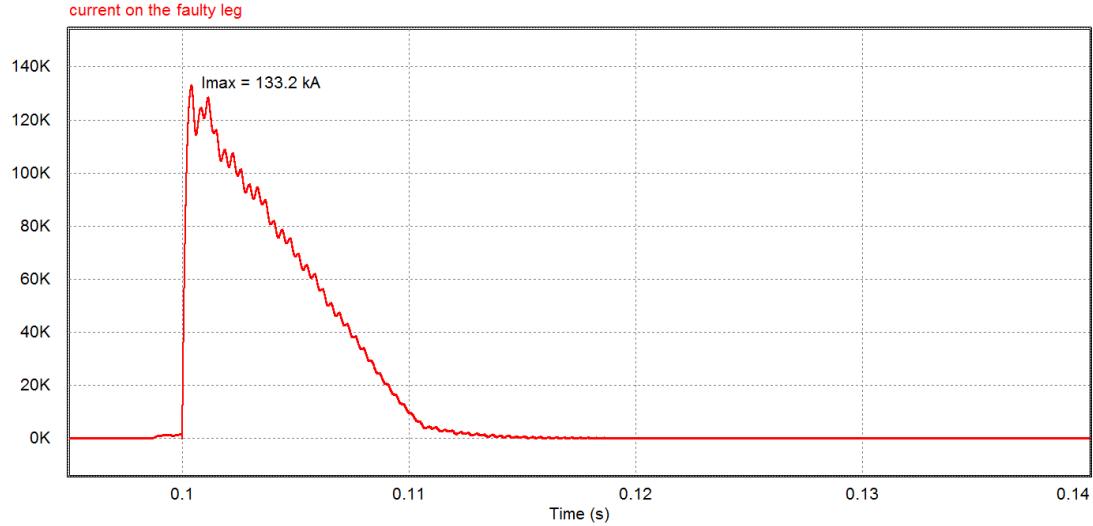


Figure 5-36 Current on the faulty leg using the fuses, with the faulty IGCT having 0.1mΩ of resistance

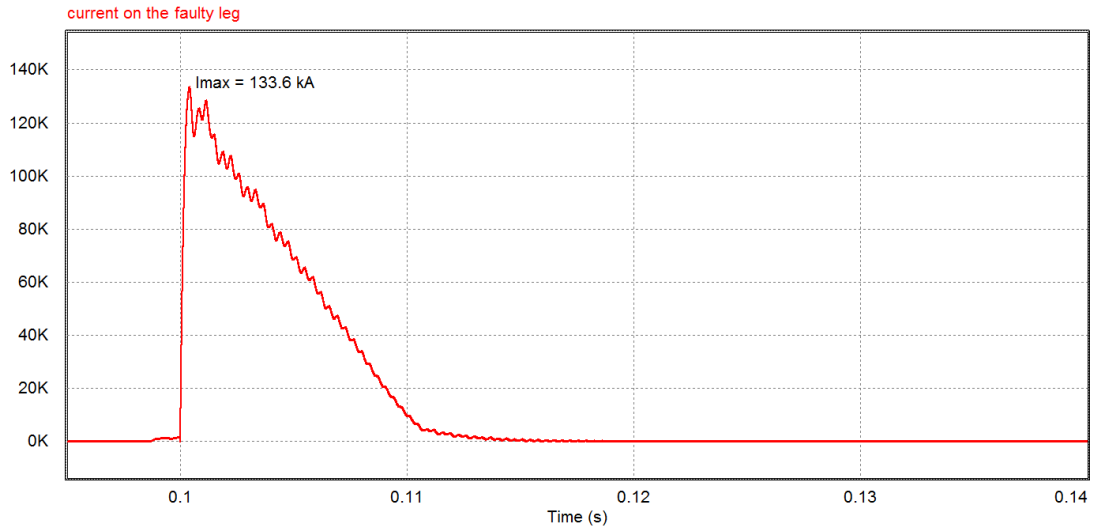


Figure 5-37 Current on the faulty leg using the fuses, with the faulty IGCT having $0.01\text{m}\Omega$ of resistance

Fig. 5-38, 5-39 and 5-40 show the relative values of I^2t in the faulty leg.

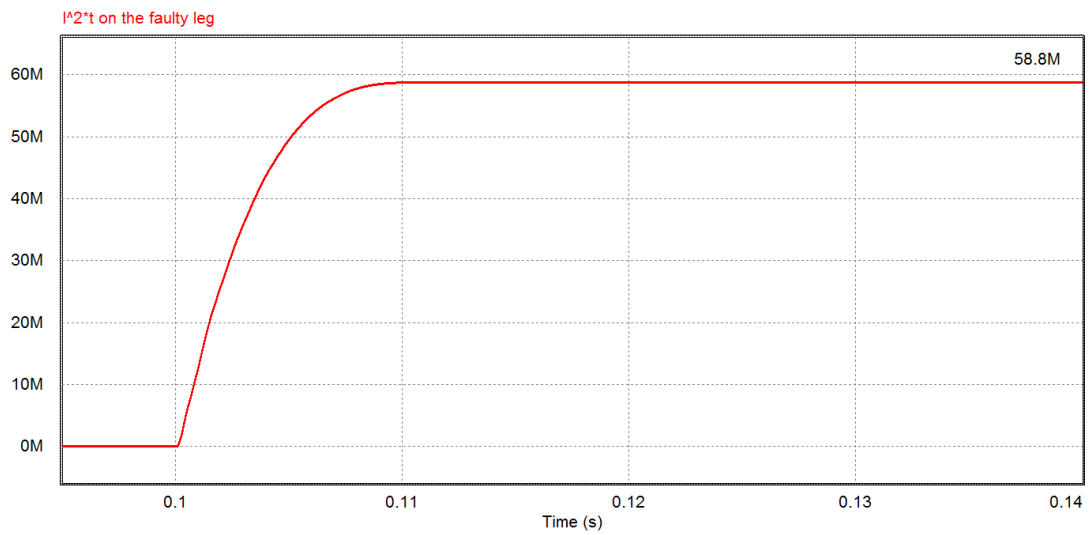


Figure 5-38 I^2t in the faulty leg using fuses, with the faulty IGCT having $0.5\text{m}\Omega$ of resistance

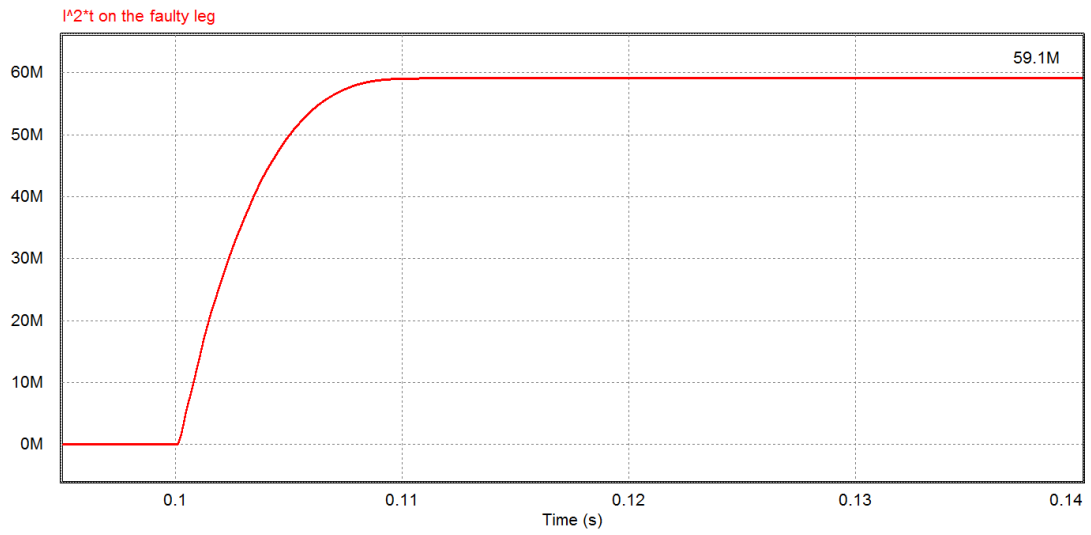


Figure 5-39 I^2t in the faulty leg using fuses, with the faulty IGCT having $0.1m\Omega$ of resistance

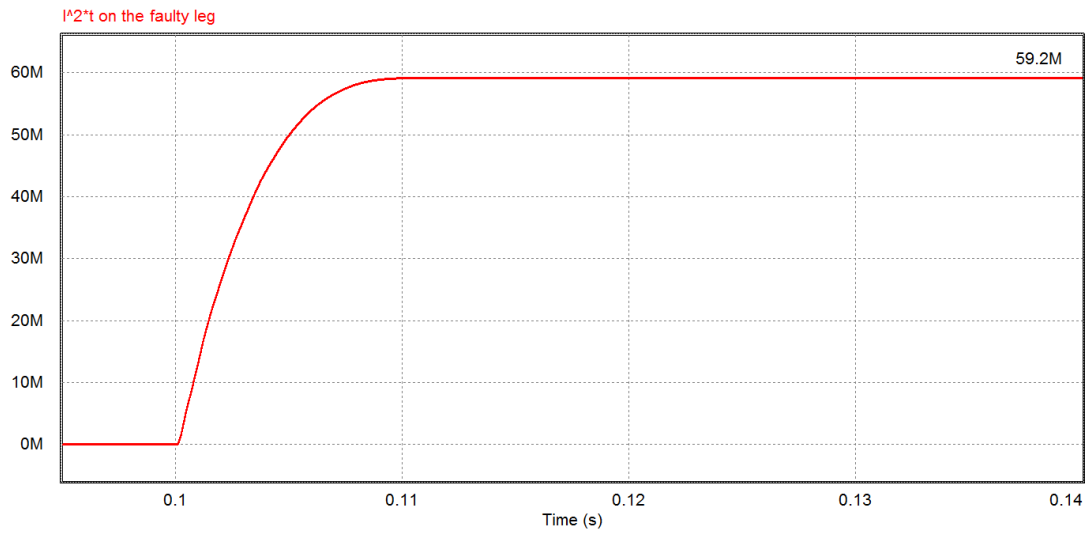


Figure 5-40 I^2t in the faulty leg using fuses, with the faulty IGCT having $0.01m\Omega$ of resistance

The same values, current and I^2t for different resistances of the faulty IGCT, are shown for the current flowing in the freewheeling and clamping diodes of the other two legs in fig. 5-41 to 5-46.

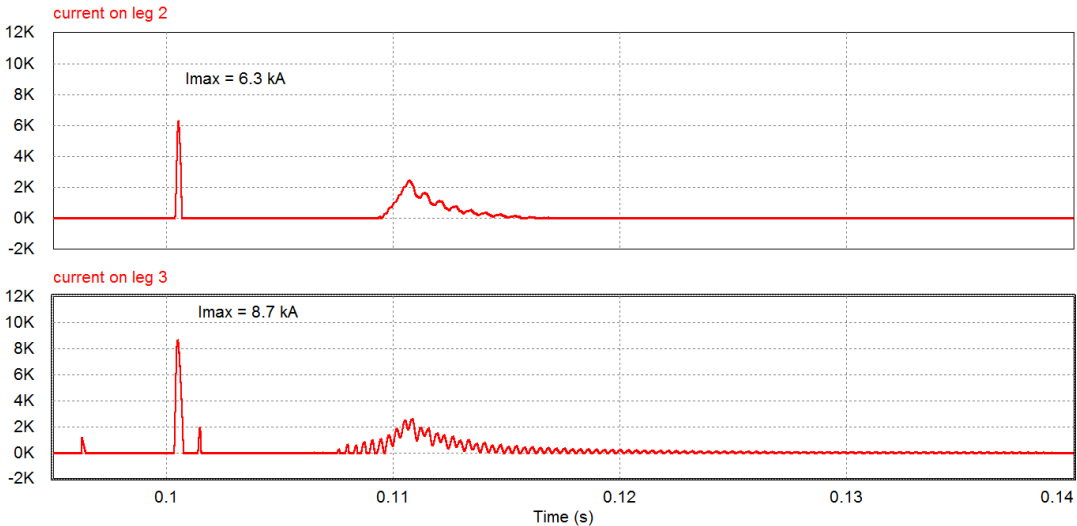


Figure 5-41 Currents on the two healthy legs of the faulty inverter using fuses, with the faulty IGCT having $0.5\text{m}\Omega$ of resistance

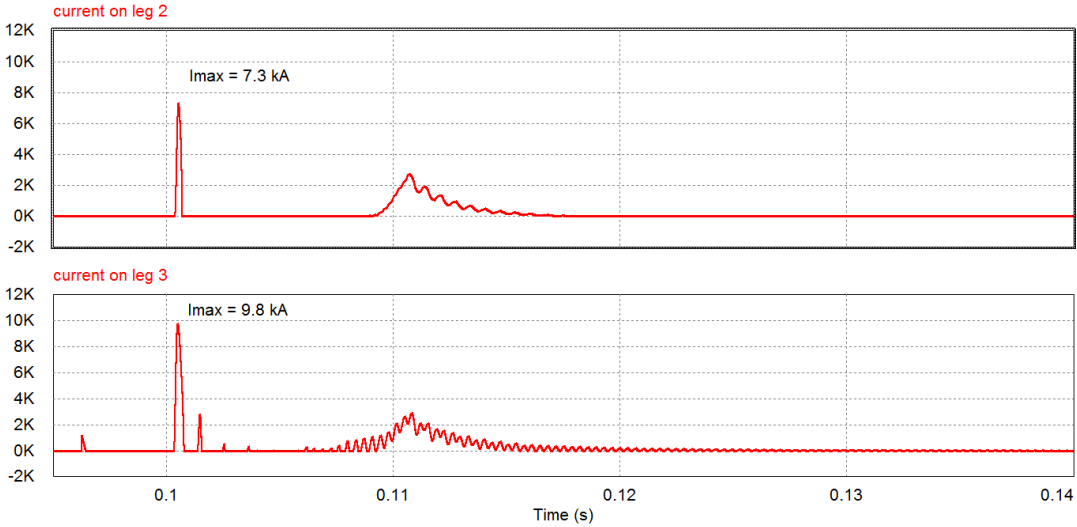


Figure 5-42 Currents on the two healthy legs of the faulty inverter using fuses, with the faulty IGCT having $0.1\text{m}\Omega$ of resistance

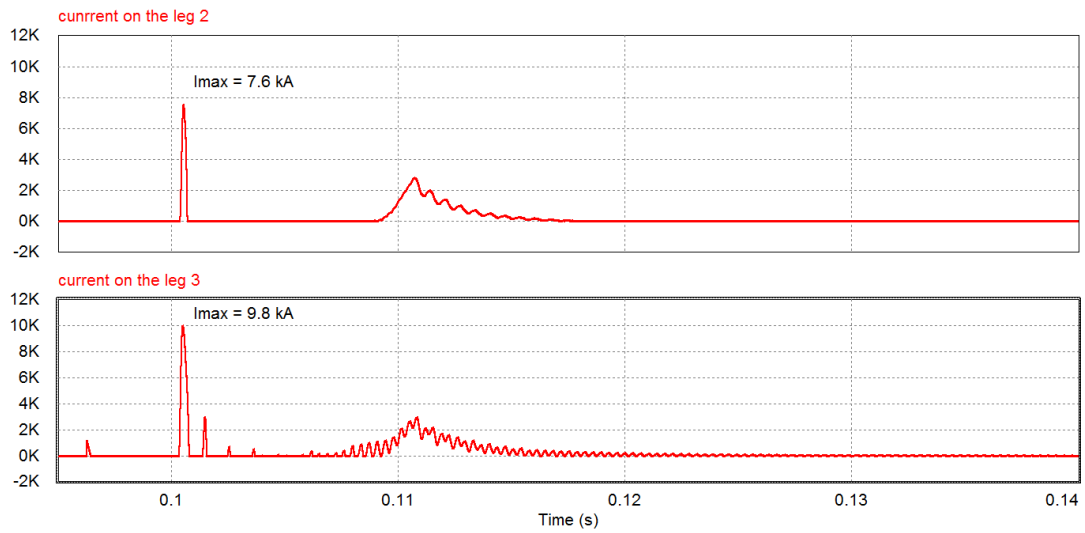


Figure 5-43 Currents on the two healthy legs of the faulty inverter using fuses, with the faulty IGCT having $0.01\text{m}\Omega$ of resistance

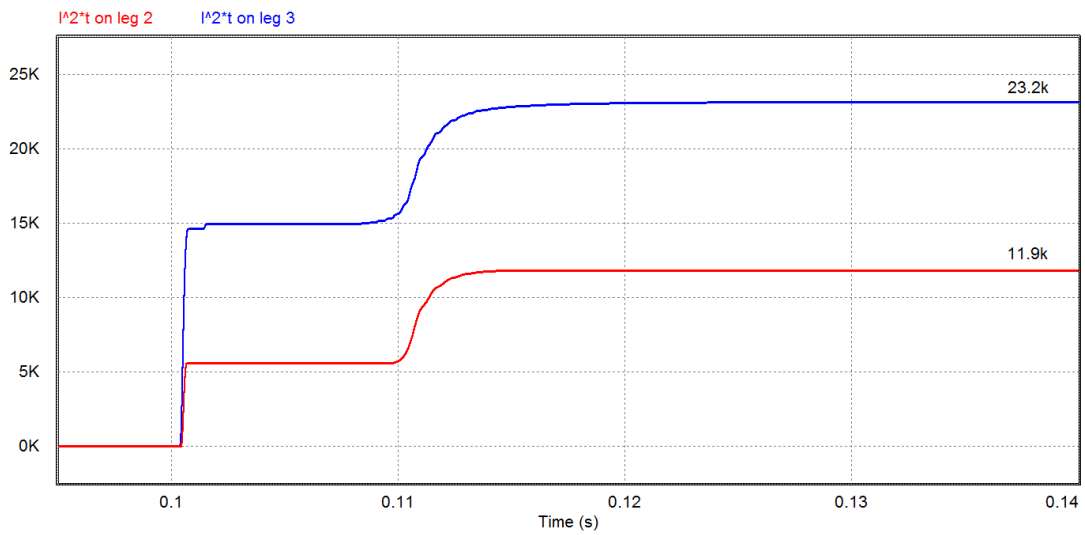


Figure 5-44 Currents on the two healthy legs of the faulty inverter using fuses, with the faulty IGCT having $0.5\text{m}\Omega$ of resistance

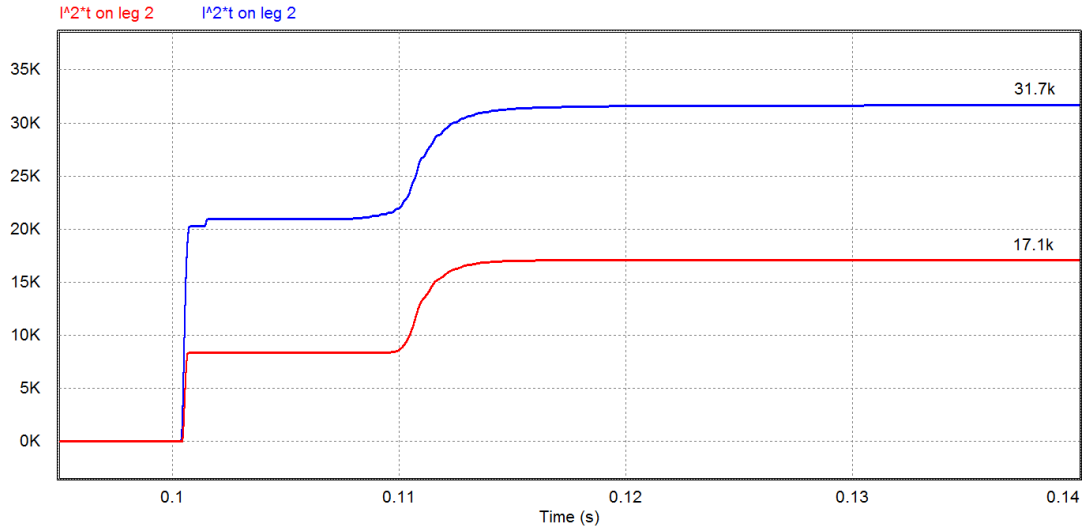


Figure 5-45 Currents on the two healthy legs of the faulty inverter using fuses, with the faulty IGCT having 0.1mΩ of resistance

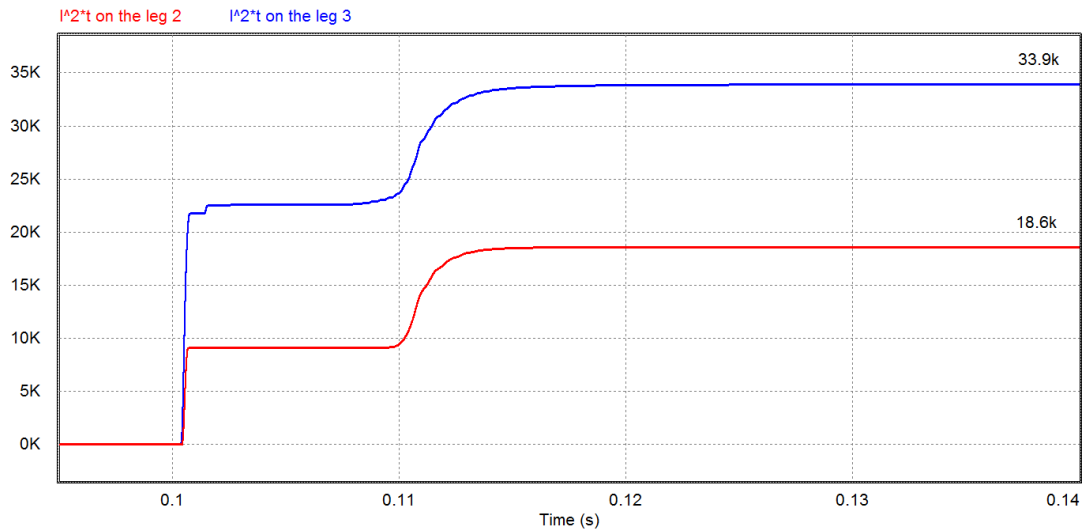


Figure 5-46 Currents on the two healthy legs of the faulty inverter using fuses, with the faulty IGCT having 0.01mΩ of resistance

From the comparison with figures of paragraph 5.3.1, it results that the presence of fuses reduce a lot the energy dissipated by components of the damaged leg, and reduces of more than 50kA the peak of current on it. As for the freewheeling diodes both the current peak and the energy dissipated on them are greatly reduced.

The comparison for the three cases of resistance is reported in tables 5-4, 5-5, 5-6.

Table 5-4 Electrical stresses comparison between the case with fuses and the case without, with 0.5mΩ as resistance of faulty IGCT

	Without fuses	Using fuses
Current peak on the faulty leg	188.0 kA	131.4 kA
I^2t on the damaged leg	123.4 MA ² s	58.8 MA ² s
Current peak on the freewheeling diodes	20.0 kA	8.7 kA
I^2t on the freewheeling diodes	102.4 kA ² s	23.2 kA ² s

Table 5-5 Electrical stresses comparison between the case with fuses and the case without, with 0.1mΩ as resistance of faulty IGCT

	Without fuses	Using fuses
Current peak on the damaged leg	192.3 kA	133.2 kA
I ² t on the damaged leg	140.7 MA ² s	59.1 MA ² s
Current peak on the freewheeling diodes	20.5 kA	9.8 kA
I ² t on the freewheeling diodes	121.3 kA ² s	31.7 kA ² s

Table 5-6 Electrical stresses comparison between the case with fuses and the case without, with 0.01mΩ as resistance of faulty IGCT

	Without fuses	Using fuses
Current peak on the damaged leg	193.3 kA	133.6 kA
I ² t on the damaged leg	145.4 MA ² s	59.2 MA ² s
Current peak on the freewheeling diodes	20.7 kA	9.8 kA
I ² t on the freewheeling diodes	126.1 kA ² s	33.9 kA ² s

Notice that the value of I²t on freewheeling diodes is low also in the case without protection: the only stress that can damages these components is the current peak.

5.3.5 Analysis of trends simulating the fault in different inverters

Until now we have always seen the result of the simulation of a fault occurring in the same inverter. In this paragraph the significant values obtained by simulating the fault in different inverters are reported to see how the stray inductances and resistances between the faulty module and the other modules affects the trend of the current and the let-through specific energy.

This analysis has been done using only one value of resistance of the faulty IGCT, R=0.1 mΩ.

Table 5-7 Current and I²t values for the fault occurring in the different inverters using the protection based on fuses

DAMAGED INVERTER	Damaged leg peak current	Damaged leg let-through I ² t	Healthy leg peak current	Healthy leg let-through I ² t
Stage 1, inverter A	133.2 kA	59.1 MA ² s	9.8 kA	31.7kA ² s
Stage 1, inverter B	143.7 kA	58.8 MA ² s	7.0 kA	16.7 kA ² s
Stage 2, inverter A	146.2 kA	58.9 MA ² s	7.0 kA	19.3 kA ² s
Stage 2, inverter B	146.7 kA	58.9 MA ² s	8.0 kA	20.8 kA ² s
Stage 3, inverter A	146.3 kA	58.9 MA ² s	7.9 kA	20.0 kA ² s
Stage 3, inverter B	148.8 kA	59.0 MA ² s	7.6 kA	22.7 kA ² s
Stage 4, inverter A	149.0 kA	59.1 MA ² s	8.5 kA	22.9 kA ² s
Stage 4, inverter B	144.4 kA	58.8 MA ² s	7.3 kA	17.6 kA ² s
Stage 5, inverter A	147.6 kA	59.0 MA ² s	8.2 kA	20.9 kA ² s
Stage 5, inverter B	133.5 kA	59.1 MA ² s	9.4kA	29.6 kA ² s

The values reported in table 5-7 show that the peak of current on the faulty leg is mildly affected by the location. In particular it is quite lower in the inverter at the two edges (the position are shown in fig. 4-5), the ones that have more stray inductances in the connection with other inverters, so the raise of current is slowed down. Instead the value of I²t is almost similar in all the cases: stray inductances modify the trend of the discharge current, but the integral of the current is quite similar. This means that the fuses work properly, isolating quickly the faulty inverter from the dc link.

Instead, the current peak and I²t in the freewheeling diodes of the healthy legs are more influenced by the position of the fault, but both the values are higher in the inverter at the edges, that is the case deeply analysed and therefore it provides the worst situation.

5.3.6 Using the crowbar as protection

On top of using fuses, another more conventional option is the use of a current crowbar, as explained in paragraph 3.4.1.

In this paragraph we analyse the possibility of using such a protection, simulating a crowbar intervention after 1 ms from the fault detection. This time interval is the usual intervention time of crowbars in middle voltage industrial systems protected in such way.

The crowbar has been simulated as explained in paragraph 4.6.1.

When the crowbar is triggered, the energy is quickly removed from the dc link and discharged into the crowbar, in particular in its resistances. Considering a typical crowbar used in industrial medium voltage system, the resistances are three Inconel bars positioned above the cabinet containing the crowbar, having a rectangular cross section ($13.5\text{mm} \times 4.5\text{mm}$) and a length of $l=1.2\text{m}$.

The purpose of the simulation is understanding if the crowbar is effective in protecting the IGCTs and if the crowbar components are able to withstand the associated stress due to the intervention.

The simulation has been done using the resistance of $0.1\text{m}\Omega$ of the faulty IGCT. The results will be compared with the equivalent simulation with no crowbar intervention.

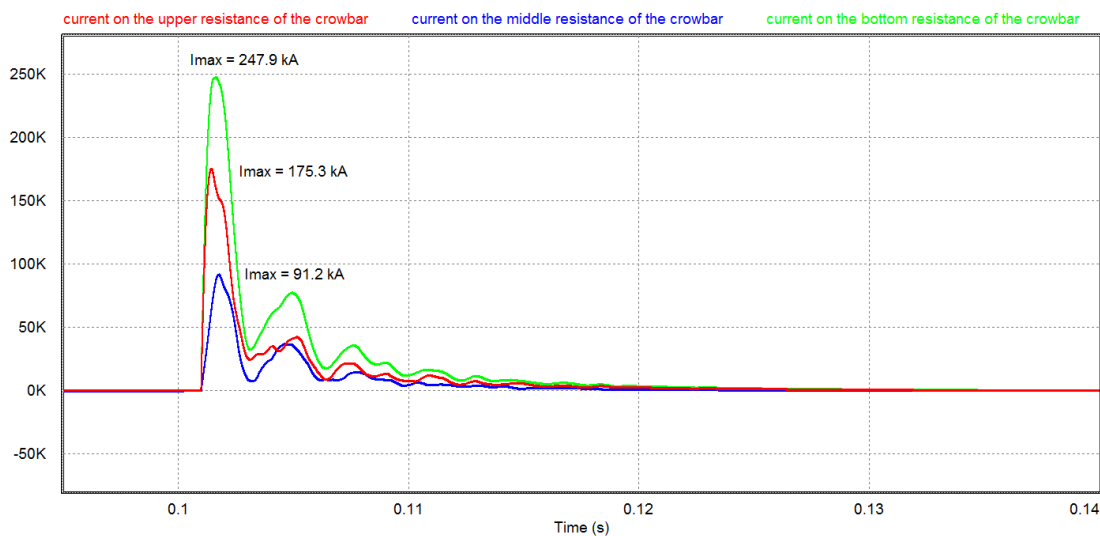


Figure 5-47 Currents on the three resistances of the crowbar

The currents of figure 5-47 are the currents on the three resistances of $3.7\text{m}\Omega$ composing the crowbar (see fig. 4-13).

The current has a much higher peak on the bottom half of the crowbar because the bottom half bank is discharging only there, while the upper half bank was discharging on the damaged leg until the crowbar intervention and then the current is split in the two path according to their impedance. Since the overall resistance of half of the crowbar is $7.4\text{m}\Omega$ and the resistance of the faulty leg is about $2.5\text{m}\Omega$, large part of the current flows in the faulty leg. (fig. 5-48).

In the middle resistance the current is lower, being the difference of the currents of the upper and bottom crowbar parts.

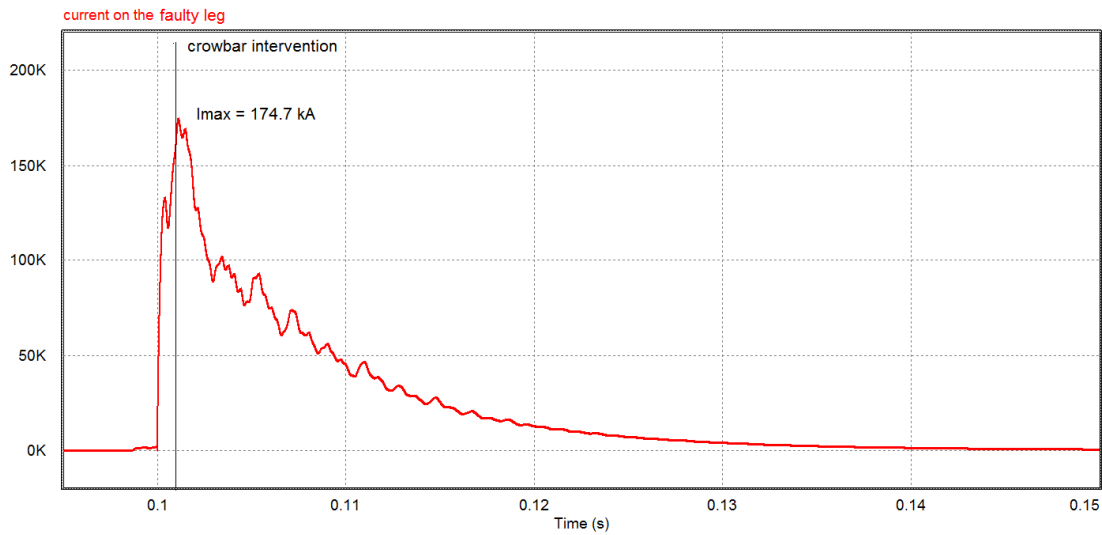


Figure 5-48 Current on the faulty leg using the crowbar

As you can see by comparing fig. 5-48 and 5-10, the current peak on the faulty leg has been reduced of only 9%. When the crowbar intervenes, the raise of current is stopped, but we can see that the crowbar is not effective in reducing the peak. This is due to the delay of the crowbar intervention, while the discharge during the fault occurs very quickly. The initial transient is therefore too fast to be limited by the crowbar.

The presence of the antiparallel diodes on the crowbar allows reducing the current on the freewheeling diodes. It is not nullified because the resistance of the healthy legs at the current inversion is about $2.7\text{m}\Omega$, lower than the $7.4\text{m}\Omega$ of the crowbar. The intervention of the crowbar, inserting a resistance in parallel to the damaged leg, decreases the resistance where the bank is discharging, increasing the voltage oscillations and consequently increasing the negative peaks of the voltage of the upper bank (see fig.5-49).

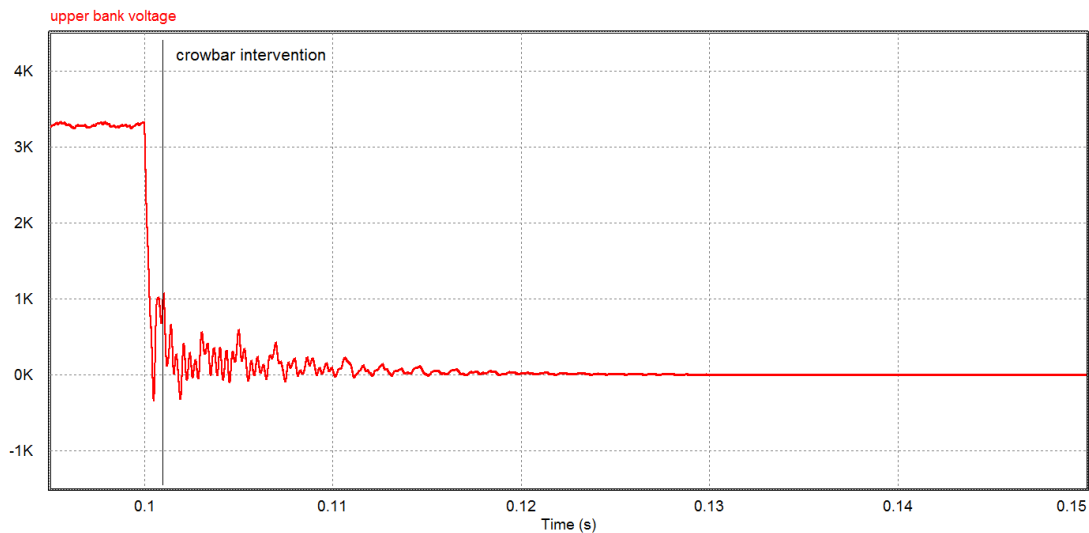


Figure 5-49 Voltage of the upper capacitor bank during the discharge

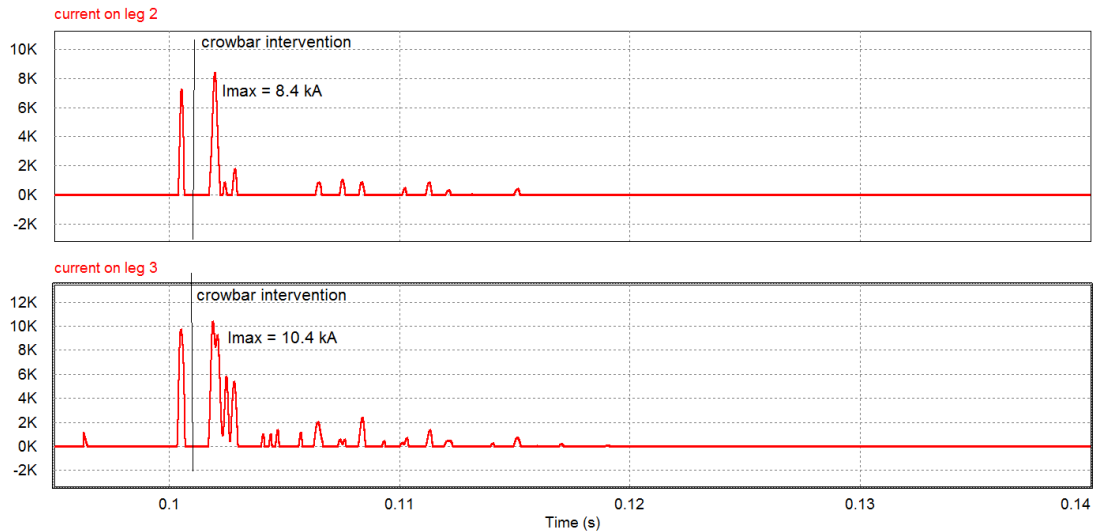


Figure 5-50 Currents on the healthy legs of the damaged inverters using the crowbars

Observing fig. 5-50 and comparing with the 5-16 we notice a reduction of the current peak on the diodes of the healthy legs.

In fig. 5-51 the values of I^2t for each one of the three branches on the two halves of the crowbar and on the damaged leg are shown.

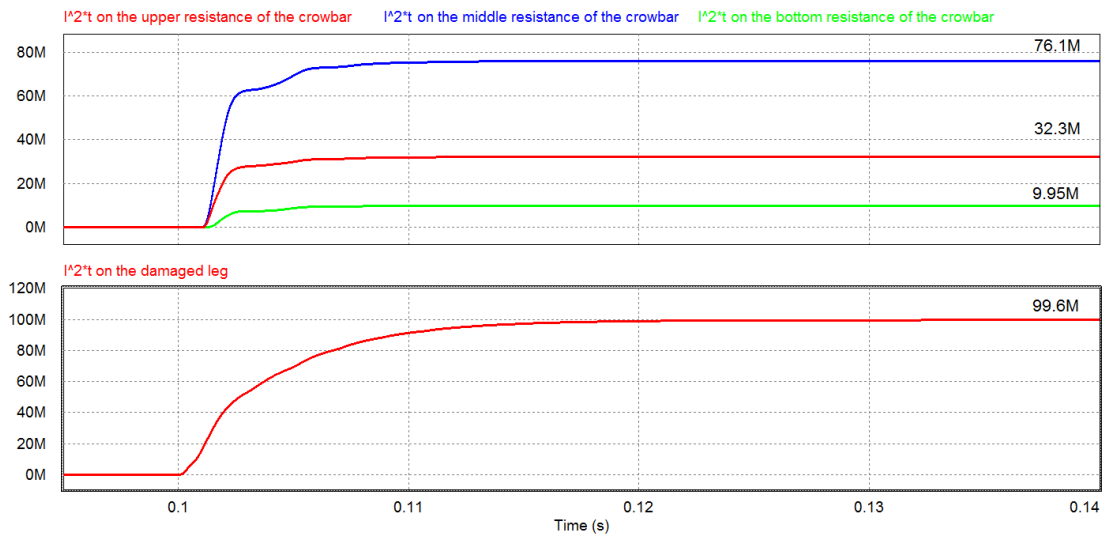


Figure 5-51 I^2t on the two parts of the crowbar and on the damaged leg

The I^2t on the damaged leg on has been reduced of about $40MA^2s$ (comparing the second graph of fig. 5-51 with fig. 5-13).

In table 5-8 the comparison of the stress parameters between the case without protections and the case with crowbar is shown. From that, we can notice that the electrical stresses are less reduced with respect to the protection with fuses (table 5-5), due to the delay on the intervention. A more detailed comparison will be done in paragraph 5.5.

Table 5-8 Comparison between the case without protection and the case with the crowbar

	Without protection	Using the crowbar
Current peak on the faulty leg	192.3 kA	174.7 kA
I^2t on the faulty leg	140.7 MA ² s	99.6 MA ² s
Current peak on the freewheeling diodes	20.5 kA	10.4 kA
I^2t on the freewheeling diodes	121.3 kA ² s	62.6 kA ² s

Yet, when the crowbar intervenes, the lower half capacitor bank has a low impedance path where the current can flow, the low half bank discharges entirely on that part of the crowbar, and its resistance should withstand a too high energy to be dissipated.

From simulation (fig. 5-51, upper graph) and knowing that the resistance value is $3.7m\Omega$:

$$W = (I^2t) \cdot R = (76.1 \cdot 10^6) \cdot 3.7 \cdot 10^{-3} = 281.6kJ \quad (5.9)$$

From private communication by NIDEC, the Inconel bars can withstand a maximum energy of 227kJ. The energy that they should withstand for the breakdown of an IGCT is higher than the limit value. Consequently this protection system cannot be adopted and it would be necessary to design a new type of crowbar, with bigger bars. This crowbar would take up too more space and problems of layout for the installation would derive.

Moreover, in the crowbar the activation may not occur, being related to the activation of thyristors. On the other hand the fuses are more reliable, since they are a passive protection system.

5.4 Fault simulations with the detailed model

The detailed model of the circuit is computationally very expensive; it has been used to understand the effect of the ac/dc conversion system turn-off time and to obtain more accurate results.

This model includes the contribution of the power coming from the AC/DC converter.

Yet, having simulated only one stage of the DCG and only for the power required to an inverter, the current delivered by the ac/dc converter is 1/10 of the total contribution it should provide in regime operation.

I simulate the fault when the voltage on the upper bank has the same voltage than in the case of the fault simulated with the simplified circuit, to have a comparison between the results and to quantify the influence that the energy provided by the ac/dc converter has on the electrical stresses.

Firstly I have analysed the situation without the use of protections simulating the case of resistance of the faulty IGCT equal to $0.1m\Omega$. In this case, the resulting voltage trend is shown in fig. 5-52.

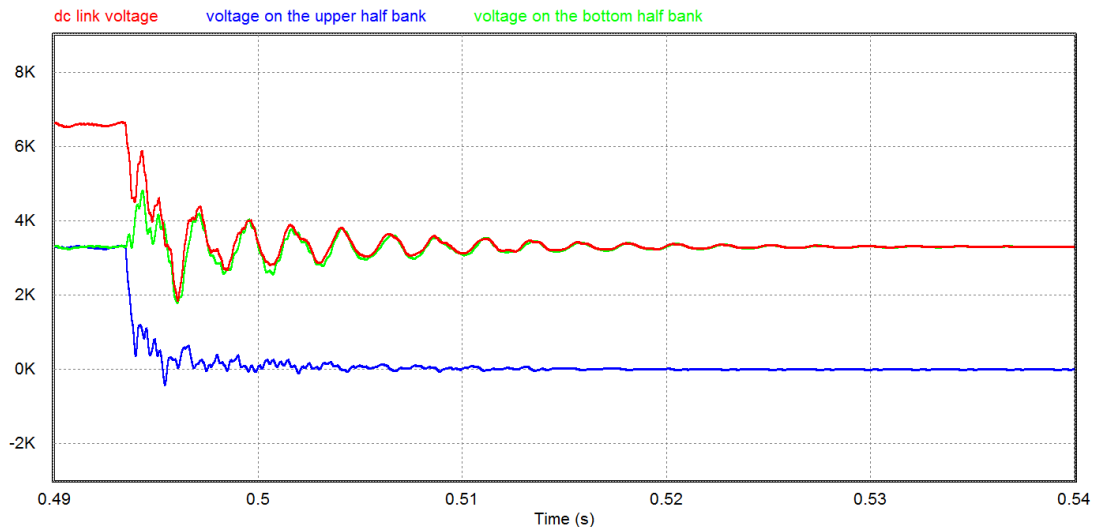


Figure 5-52 Voltages trend on the capacitor bank during the fault

The current trend on the faulty leg is reported in fig. 5-53, in fig. 5-54 is shown the value of I^2t during the fault.

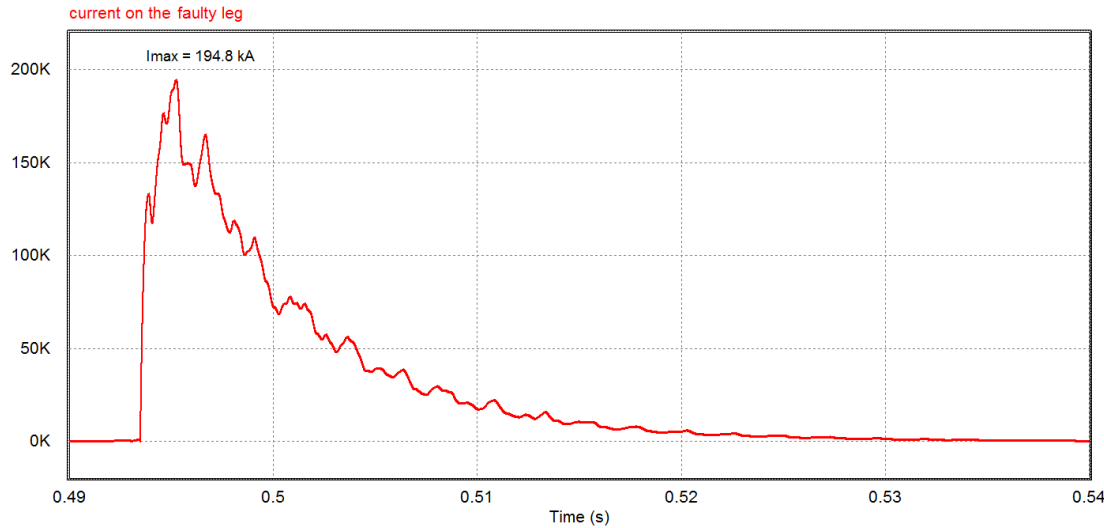


Figure 5-53 Current on the faulty leg, in the overall circuit without protections

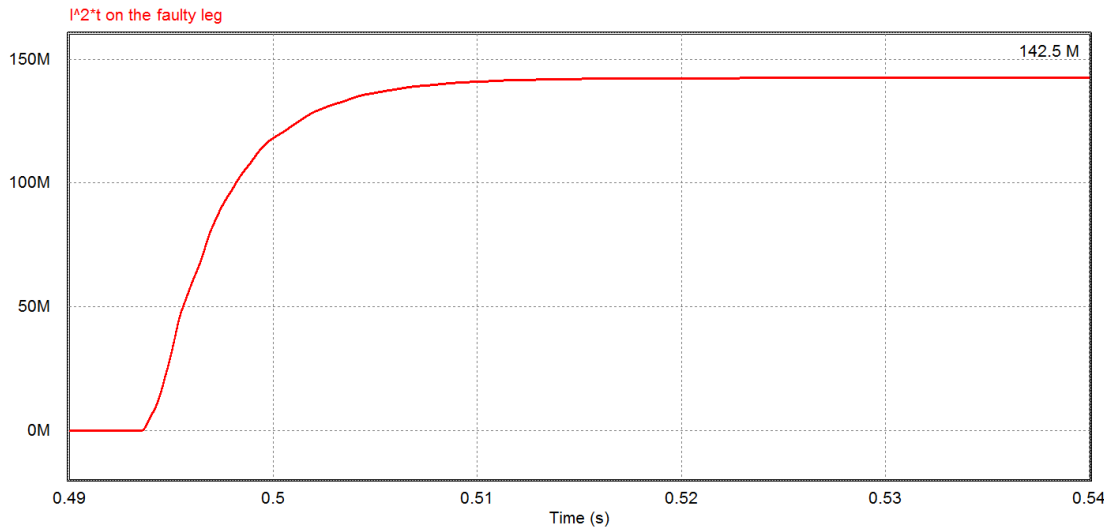


Figure 5-54 I^2t on the faulty leg, in the overall circuit without protections

In fig. 5-55 and 5-56 the current on the freewheeling diodes of the other two legs and the related I^2t trends are represented.

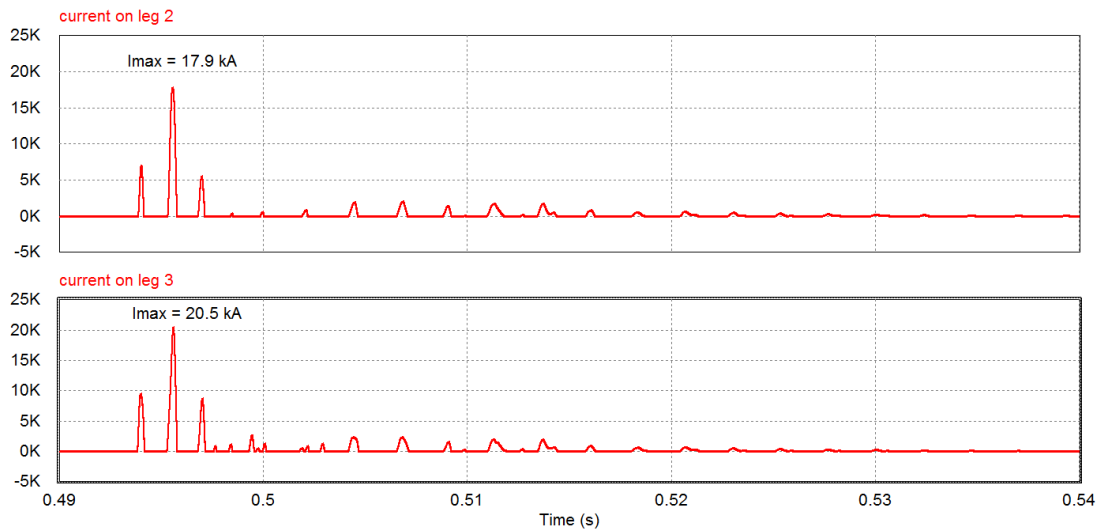


Figure 5-55 Current on the freewheeling diodes of the healthy legs, in the overall circuit without protections

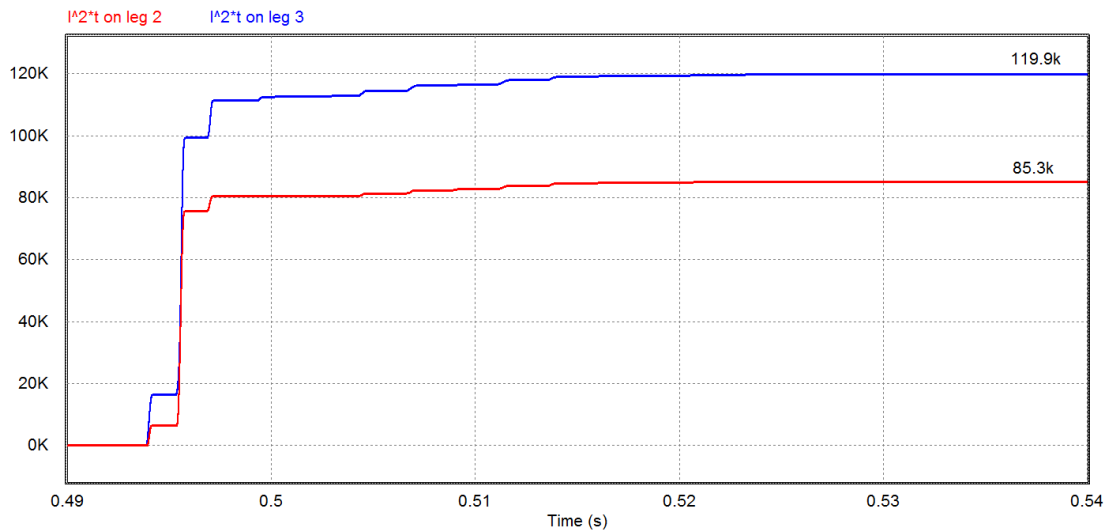


Figure 5-56 I^2t on the freewheeling diodes of the healthy leg, in the overall circuit without protections

The ac/dc converter is switched off $100\mu s$ after the time of the fault, but it continues to provide power until the current nullifies. This period of time when the ac/dc converter is contributing to the fault is very short, therefore its energy contribution can be neglected; obviously only if the fault is properly detected and the alpha controller of the thyristor bridge is disabled.

The same analysis is done simulating the presence of fuses and the same values are shown in fig. from 5-57 to 5-60.

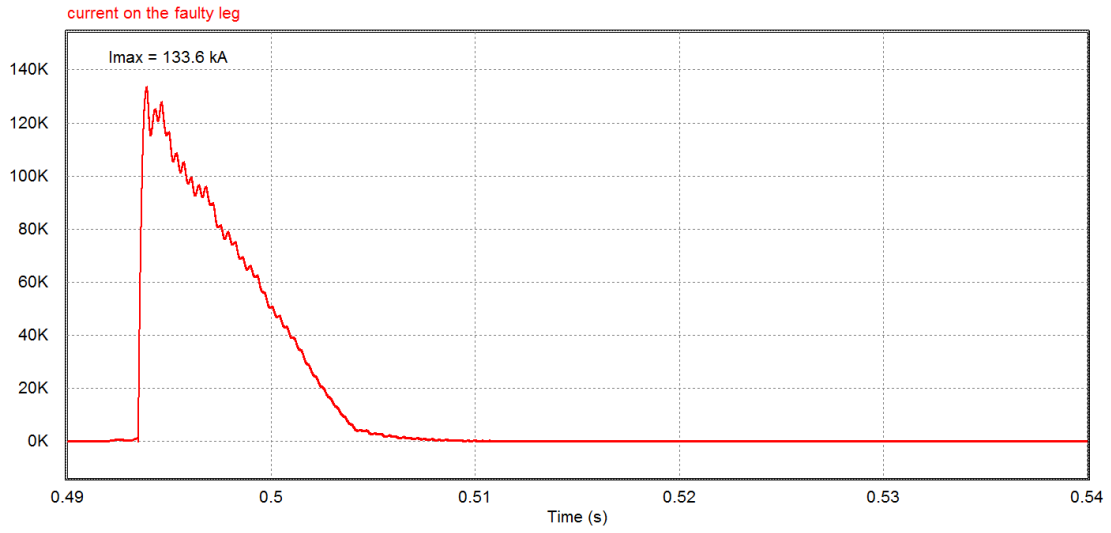


Figure 5-57 Current on the faulty leg, in the overall circuit using fuses

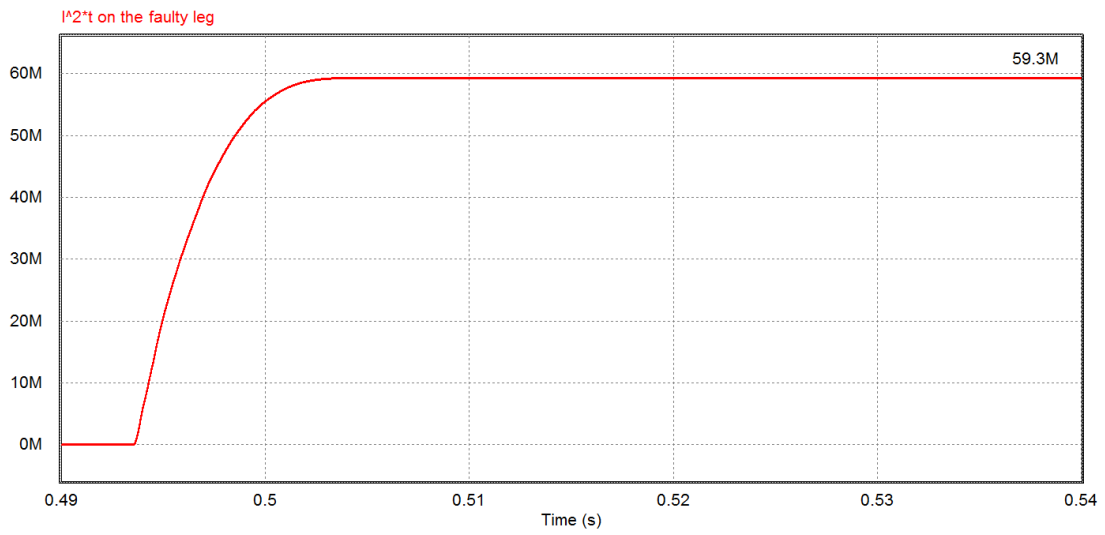


Figure 5-58 I^2t on the faulty leg, in the overall circuit using fuses

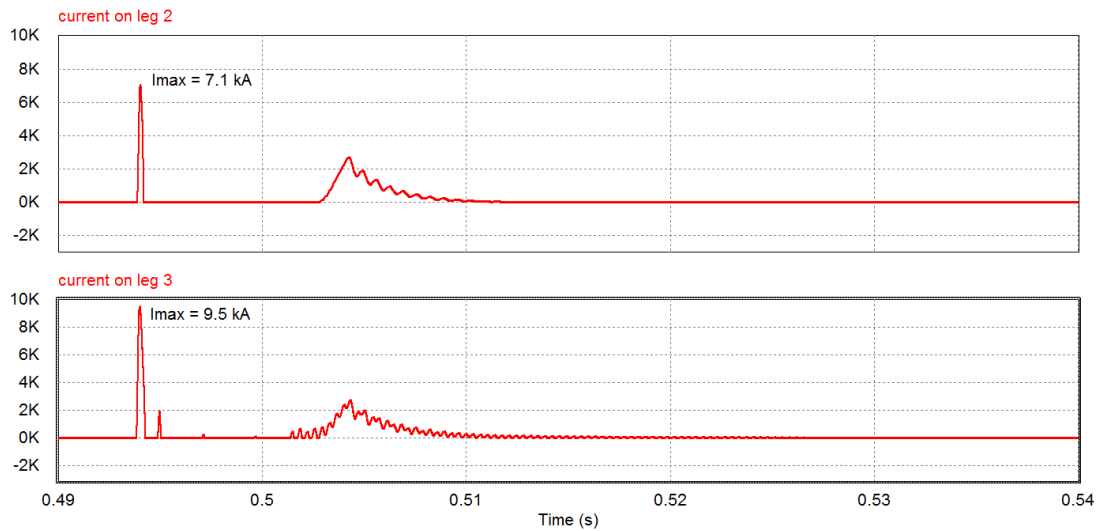


Figure 5-59 Current on the freewheeling diodes of the healthy legs, in the overall circuit using fuses

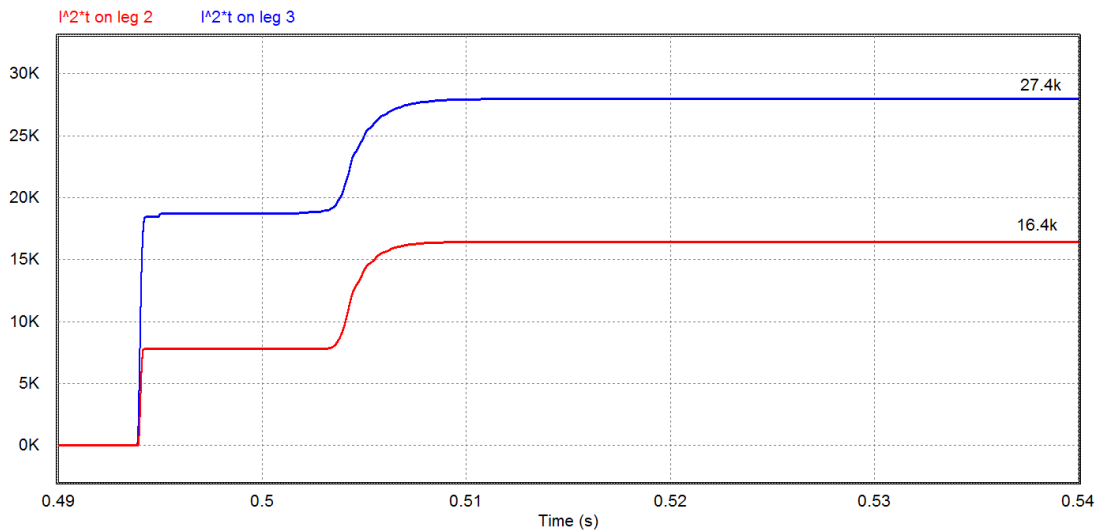


Figure 5-60 I^2t on the freewheeling diodes of the healthy legs, in the overall circuit using fuses

As we expect, the behaviour is basically the same than in the case of simplified model. This confirm that the energy coming from the ac/dc converter is negligible in the determination of the electrical stresses.

The comparison of electrical stresses between the case without protection and the case with the fuses is shown in table 5-9 (notice that the values are very similar to the values of table 5-5).

Table 5-9 Stress parameters comparison between the case with fuses and the case without the fuses in the overall circuit, with $0.1m\Omega$ as resistance of faulty IGCT

	Without fuses	Using fuses
Current peak on the damaged leg	192.5 kA	131.9 kA
I^2t on the damaged leg	139.1 MA ² s	59.2 MA ² s
Current peak on the freewheeling diodes	20.3 kA	9.5 kA
I^2t on the freewheeling diodes	116.9 kA ² s	27.4 kA ² s

5.5 Conclusions on the results of the simulations

In previous paragraphs the results of simulation of the system have been obtained for both the two protection systems considered, having noticed that the simplified circuit provides a good simulation of the fault and of stress parameters on the components.

The primary purpose of the protection system is to avoid the propagation of the fault to the other healthy modules.

Therefore the healthy components in the faulty module can be damaged during the fault, but they have to sustain the dissipated energy without explosions that can damage the nearby modules.

Moreover the diodes of the healthy modules must withstand the current flowing in them when the phenomenon of inversion of the current occurs.

While the current peak sustainable by diodes and IGCTs is well known and provided by the producers (annexes 1 and 2), the energy that these components can withstand without exploding is not known a priori. The producer of the IGCTs, ABB, has provided a presumed limit value for the explosion of $200\text{MA}^2\text{s}$. However, this is just an indicative estimation. The actual limit depends on the application, i.e. on how the components will be installed in the modules, for example on the packaging of components and on the clamping mechanical forces of the stacks composing the modules. Moreover, the limit value for the diodes is not known and probably it is quite lower. For these reasons, a precautionary much lower value has been chosen as limit of I^2t for the faulty module: the threshold of $60\text{-}80\text{MA}^2\text{s}$ should not be overcome.

The protection systems considered to avoid the fault propagation must guarantee that:

- The faulty module does not explode
- The diodes on the healthy modules are not damaged by the current peaks

In table 5-10 the stress parameters obtained from simulations with the protections system based on crowbar and fuses are summarized (taken from tables 5-5 and 5-8) , comparing them with the limits of components (from tables 3-6 and 3-7).

Table 5-10 Stress parameters with crowbar and fuses as protection systems and limits of components

	with crowbar	with fuses	Limits
Current peak on the faulty module	174.7 kA	133.2 kA	22kA diodes/26kA IGCT
I^2t on the faulty module	99.6 MA^2s	59.1 MA^2s	200 MA^2s 60-80 MA^2s for precautionary margin
Current peak on the freewheeling diodes	10.4 kA	9.8 kA	22kA

The first row of table 5-10 shows that probably the healthy components of the faulty modules would be damaged during the fault by the high current peak, with both the protection systems. However this is admitted. In fact after this a serious fault, the faulty modules will be entirely replaced.

The second row of the table shows that using the crowbar as protection, the I^2t on the faulty leg overcomes the limits, while using the protection based on fuses the I^2t is kept under the threshold.

Finally, from the third row of the table: both the protection systems keep the current peaks on the diodes of the healthy modules much below the limit.

Resuming all the results obtained, the preferable protection systems is the one based on fuses because:

- The crowbar used in industrial system would not sustain the energy dissipated on the typical Inconel bars and a new type of crowbar should be designed ad hoc for this application (see paragraph 5.3.6)
- The crowbar is less effective than the fuses in the protection from the explosion of the faulty modules
- The crowbar would need space next to the dc link to install the cabinet holding the device
- Fuses are a passive protection system, while the crowbar depends on the thyristors activation

The protection system based on fuses is effective in the protection of healthy modules.

Being this type of fuse developed ad hoc for the currents and voltages of this system, it must be tested before the installation

6 Conclusions

In this thesis I have critically analysed in various conditions different protections from internal fault in the inverters of the AGPS-CS, finally selecting a protection based on fuses.

To reach this conclusion I have modelled the AGPS from the layout of the system, with more detail for the circuit interested by the fault, calculating the stray parameters from the known or assumed geometries of the connections. I have implemented the simulation model in PSIM tool and I have simulated the fault starting from the regime condition. From simulations I have considered the current behaviour in IGCTs and diodes making up the inverters to evaluate the electrical stress they are subjected: current peaks and let-through energy (related to I^2t).

I have simulated the fault both without protections and with the protections based on crowbar and fuses. From simulations, I have observed the phenomena of the inversion of the current on the healthy modules.

Being not know the resistance of the faulty IGCT, I have done simulations with different values of resistance to determine the influence of this parameter on the electrical stresses.

The protection based on crowbar has been rejected because of the not sustainable energy deposited on the Inconel bars composing the crowbar, because of its lower effectiveness in the protection of faulty modules from the explosion of components and because of the space it needs for the installation.

The protection based on fuses has been preferred and the effective protection has been verified by simulating the fault in all the inverters.

Future analysis should be the simulations of the internal fault in an inverter occurring at lower voltages on the dc link than the nominal value, to verify the effectiveness of the protection in all the operational conditions required to the system.

Subsequently, before the installation of the system, these fuses must be tested to verify if their intervention occurs as foreseen in the simulations, because they have been designed ad hoc for this system.

7 Acknowledgments

I would like to thank Eng. Loris Zanotto for his support and the patience with which he has always helped me anytime I needed.

I would also like to thank Prof. Paolo Bettini for having given me the opportunity to continue working on the fusion field also in the Master thesis.

Finally I want to thank my parents for having always supported me.

References

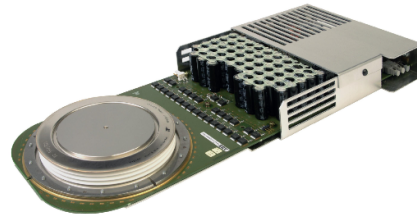
- [1] Alberto Ferro, *Study of the power supply system for the acceleration grids of the ITER neutral beam injector*, PHD thesis, 2011
- [2] D. Marcuzzi, P. Agostinetti, M. Dalla Palma, F. Degli Agostini, M. Pavei, A. Rizzolo, M. Tollin, L. Trevisan “Detail design of the beam source for the SPIDER experiment”, *Fusion engineering and design*, 2010, n. 85, pp. 1792-1797
- [3] <http://www.nidec-asi.com/>
- [4] <http://new.abb.com/semiconductors>
- [5] <https://www.infineon.com/>
- [6] Jose Rodriguez, Steffen Bernet, Peter K. Steimer, Ignatio E. Lizama, “A Survey on Neutral-Point-Clamped Inverters”, *IEEE Transactions on industrial electronics*, vol 57, n.7, July 2010
- [7] <https://powersimtech.com>
- [8] Private communication from NIDEC
- [9] Frederick W. Grover, *Inductance calculations*, 2004, pp.35-36
- [10] Ned Mohan, Tore M. Underland, William P. Robbins, *Elettronica di Potenza*, 2005, pp. 153-157
- [11] P. Tenti, *Conversione static dell’energia elettrica*, 1996, pp. 43-45
- [12] http://www.siba-fuses.com/front_content.php#

ANNEX 1

V_{DRM}	=	6500 V	Asymmetric Integrated Gate- Commutated Thyristor 5SHY 42L6500
I_{TGQM}	=	3800 A	
I_{TSM}	=	26×10^3 A	
$V_{(T0)}$	=	1.88 V	
r_T	=	0.56 m Ω	
V_{DC}	=	4000 V	

Doc. No. 5SYA1245-03 Dec. 12

- High snubberless turn-off rating
- High electromagnetic immunity
- Simple control interface with status feedback
- AC or DC supply voltage
- Option for series connection (contact factory)



Blocking

Maximum rated values ¹⁾

Parameter	Symbol	Conditions	min	typ	max	Unit
Rep. peak off-state voltage	V_{DRM}	Gate Unit energized			6500	V
Permanent DC voltage for 100 FIT failure rate of GCT	V_{DC}	Ambient cosmic radiation at sea level in open air. Gate Unit energized			4000	V
Reverse voltage	V_{RRM}				17	V

Characteristic values

Parameter	Symbol	Conditions	min	typ	max	Unit
Rep. peak off-state current	I_{DRM}	$V_D = V_{DRM}$, Gate Unit energized			50	mA

Mechanical data (see Fig. 11, 12)

Maximum rated values ¹⁾

Parameter	Symbol	Conditions	min	typ	max	Unit
Mounting force	F_m		36	40	44	kN

Characteristic values

Parameter	Symbol	Conditions	min	typ	max	Unit
Pole-piece diameter	D_p	± 0.1 mm		85		mm
Housing thickness	H	clamped	25.5		26.0	mm
		unclamped				
Weight	m				2.9	kg
Surface creepage distance	D_s	Anode to Gate	33			mm
Air strike distance	D_a	Anode to Gate	10			mm
Length	l	± 1.0 mm		439		mm
Height	h	± 1.0 mm		41		mm
Width IGCT	w	± 1.0 mm		173		mm

¹⁾ Maximum rated values indicate limits beyond which damage to the device may occur

ABB Switzerland Ltd, Semiconductors reserves the right to change specifications without notice.



GCT Data**On-state** (see Fig. 3, 4, 5, 6, 14)*Maximum rated values ¹⁾*



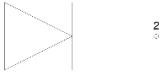
Parameter	Symbol	Conditions	min	typ	max	Unit
Max. average on-state current	$I_{T(AV)M}$	Half sine wave, $T_C = 85\text{ °C}$, Double side cooled			1290	A
Max. RMS on-state current	$I_{T(RMS)}$				2030	A
Max. peak non-repetitive surge on-state current	I_{TSM}	$t_p = 3\text{ ms}$, $T_j = 125\text{ °C}$, sine half wave, $V_D = V_R = 0\text{ V}$, after surge			40×10^3	A
Limiting load integral	I^2t				2.4×10^6	A^2s
Max. peak non-repetitive surge on-state current	I_{TSM}	$t_p = 10\text{ ms}$, $T_j = 125\text{ °C}$, sine half wave, $V_D = V_R = 0\text{ V}$, after surge			26×10^3	A
Limiting load integral	I^2t				3.38×10^6	A^2s
Max. peak non-repetitive surge on-state current	I_{TSM}	$t_p = 30\text{ ms}$, $T_j = 125\text{ °C}$, sine half wave, $V_D = V_R = 0\text{ V}$, after surge			17×10^3	A
Limiting load integral	I^2t				4.34×10^6	A^2s
Stray inductance between GCT and antiparallel diode	L_D	Only relevant for applications with antiparallel diode to the IGCT			300	nH
Critical rate of rise of on-state current	$di_T/dt_{(cr)}$	For higher di_T/dt and current lower than 100 A an external retrigger puls is required.			200	A/ μs

Characteristic values

Parameter	Symbol	Conditions	min	typ	max	Unit
On-state voltage	V_T	$I_T = 3800\text{ A}$, $T_j = 125\text{ °C}$		3.7	4.0	V
Threshold voltage	$V_{(T0)}$	$T_j = 125\text{ °C}$		1.80	1.88	V
Slope resistance	r_T	$I_T = 1000...3800\text{ A}$		0.50	0.56	$m\Omega$

ABB Switzerland Ltd, Semiconductors reserves the right to change specifications without notice.

ANNEX 2

	Technische Information / technical information	 Infineon Technologies Bipolar GmbH & Co. KG																								
Schnelle beschaltungslose Diode Fast Hard Drive Diode	D1131SH																									
<p>Key Parameters</p> <table border="0"> <tr><td>V_{RRM}</td><td>6500 V</td></tr> <tr><td>I_{FAVM}</td><td>1100 A ($T_C=85\text{ }^\circ\text{C}$)</td></tr> <tr><td>$I_{FSM}$</td><td>22000 A</td></tr> <tr><td>V_{TO}</td><td>2,19 V</td></tr> <tr><td>r_T</td><td>1,364 mΩ</td></tr> <tr><td>R_{thJC}</td><td>7,5 K/kW</td></tr> <tr><td>Clamping Force</td><td>36 ... 52 kN</td></tr> <tr><td>Max. Diameter</td><td>121 mm</td></tr> <tr><td>Contact Diameter</td><td>86 mm</td></tr> <tr><td>Height</td><td>26 mm</td></tr> </table>			V_{RRM}	6500 V	I_{FAVM}	1100 A ($T_C=85\text{ }^\circ\text{C}$)	I_{FSM}	22000 A	V_{TO}	2,19 V	r_T	1,364 m Ω	R_{thJC}	7,5 K/kW	Clamping Force	36 ... 52 kN	Max. Diameter	121 mm	Contact Diameter	86 mm	Height	26 mm				
V_{RRM}	6500 V																									
I_{FAVM}	1100 A ($T_C=85\text{ }^\circ\text{C}$)																									
I_{FSM}	22000 A																									
V_{TO}	2,19 V																									
r_T	1,364 m Ω																									
R_{thJC}	7,5 K/kW																									
Clamping Force	36 ... 52 kN																									
Max. Diameter	121 mm																									
Contact Diameter	86 mm																									
Height	26 mm																									
 <p>Infineon Φ type designation</p>																										
<p>For type designation please refer to actual short form catalog http://www.ifbip.com/catalog</p>																										
<p>Merkmale</p> <ul style="list-style-type: none"> • Volle Sperrfähigkeit 50/60Hz über einen weiten Temperaturbereich • Hohe DC Sperrstabilität • Hohe Stoßstrombelastbarkeit • Hoher Gehäusebruchstrom • Sanftes Ausschaltverhalten bei hohen Stromsteilheiten 		<p>Features</p> <ul style="list-style-type: none"> • Full blocking capability 50/60Hz over a wide temperature range • High DC blocking stability • High surge current capability • High case non-rupture current • Soft turn-off behavior at high turn-off di/dt 																								
<p>Typische Anwendungen</p> <ul style="list-style-type: none"> • Mittelspannungsumrichter • Freilaufdiode für IGCT - Applikationen • Freilaufdiode für IGBT - Applikationen • Pulsed Power - Applikationen 		<p>Typical Applications</p> <ul style="list-style-type: none"> • Medium voltage converters • Freewheeling Diode for IGCT - applications • Freewheeling Diode for IGBT - applications • Pulsed power applications 																								
	<table border="1"> <thead> <tr> <th>content of customer DMX code</th> <th>DMX code digit</th> <th>DMX code digit quantity</th> </tr> </thead> <tbody> <tr><td>serial number</td><td>1..7</td><td>7</td></tr> <tr><td>SP material number</td><td>8..16</td><td>9</td></tr> <tr><td>datecode (production day)</td><td>17..18</td><td>2</td></tr> <tr><td>datecode (production year)</td><td>19..20</td><td>2</td></tr> <tr><td>datecode (production month)</td><td>21..22</td><td>2</td></tr> <tr><td>vT class (optional)</td><td>23..26</td><td>4</td></tr> <tr><td>QR class (optional)</td><td>27..30</td><td>4</td></tr> </tbody> </table>		content of customer DMX code	DMX code digit	DMX code digit quantity	serial number	1..7	7	SP material number	8..16	9	datecode (production day)	17..18	2	datecode (production year)	19..20	2	datecode (production month)	21..22	2	vT class (optional)	23..26	4	QR class (optional)	27..30	4
content of customer DMX code	DMX code digit	DMX code digit quantity																								
serial number	1..7	7																								
SP material number	8..16	9																								
datecode (production day)	17..18	2																								
datecode (production year)	19..20	2																								
datecode (production month)	21..22	2																								
vT class (optional)	23..26	4																								
QR class (optional)	27..30	4																								
		 <p>www.ifbip.com support@infineon-bip.com</p>																								
Date of Publication: 2014-06-01	Revision: 8.0	Seite/page 1/11																								



Technische Information /
technical information



Schnelle beschaltungslose Diode
Fast Hard Drive Diode

D1131SH

Infineon Technologies Bipolar
GmbH & Co. KG

Elektrische Eigenschaften / Electrical properties
Höchstzulässige Werte / Maximum rated values

Periodische Rückwärts-Spitzenspannung repetitive peak reverse voltage	$T_{vj} = 0^{\circ}\text{C} \dots T_{vj\text{max}}$	V_{RRM}	6500	V
Durchlaßstrom-Grenzeffektivwert maximum RMS on-state current	$T_c = 85^{\circ}\text{C}$	I_{FRMSM}	1730	A
Dauergrenzstrom average on-state current	$T_c = 85^{\circ}\text{C}, f = 50\text{Hz}$	I_{FAVM}	1100	A
Stoßstrom-Grenzwert surge current	$T_{vj} = 25^{\circ}\text{C}, t_p = 10\text{ms}$	I_{FSM}		
Grenzlastintegral I^2t -value	$T_{vj} = 25^{\circ}\text{C}, t_p = 10\text{ms}$	I^2t		
Max. Ausschaltverluste max. turn-off losses	$T_{vj} = T_{vj\text{max}}$ $I_{FM} = 2500\text{A}, V_{CL} = 2800\text{V}$ clamp circuit $L_S \leq 0,25\mu\text{H}$ $R_{CL} = 68\Omega, C_{CL} = 3\mu\text{F}$ $D_{CL} = 34\text{DSH65}$	P_{RO}	5	MW

Charakteristische Werte / Characteristic values

Gleichspannung continuous direct reverse voltage	failure rate $\lambda < 100$	$V_{R(D)}$	estimate value	3200	V
Durchlaßspannung on-state voltage	$T_{vj} = T_{vj\text{max}}, i_F = 2500\text{A}$	V_F	typ. max.	5,2 5,6	V
Schleusenspannung threshold voltage	$T_{vj} = T_{vj\text{max}}$	$V_{(TO)}$	typ. max.	1,98 2,19	V
Ersatzwiderstand slope resistance	$T_{vj} = T_{vj\text{max}}$	r_T	typ. max.	1,288 1,364	mΩ
Durchlaßkennlinie on-state characteristic	$200\text{A} \leq i_F \leq 3000\text{A}$ $V_F = A + B \cdot i_F + C \cdot \ln(i_F + 1) + D \cdot \sqrt{i_F}$	$T_{vj} = T_{vj\text{max}}$	typ. max.	A 0,702 B 0,000211 C -0,0784 D 0,0917 A 0,7 B 0,000279 C -0,044 D 0,0913	
Spitzenwert der Durchlassverzögerungsspannung peak value of forward recovery voltage	$T_{vj} = T_{vj\text{max}}, di_F/dt = 5000\text{A}/\mu\text{s}$ $I_{FM} = 4000\text{A}$	V_{FRM}	typ.	360	V
Sperrstrom reverse current	$T_{vj} = T_{vj\text{max}}, V_R = V_{RRM}$	i_R	max.	150	mA
Sperrverzögerungsladung recovered charge	$T_{vj} = T_{vj\text{max}}$ $I_{FM} = 2500\text{A}, V_{CL} = 2800\text{V},$	Q_r	max.	3500	mAs
Rückstromspitze peak reverse recovery current	$-di/dt = 1000\text{A}/\mu\text{s}$ clamp circuit $L_S \leq 0,25\mu\text{H},$	I_{RM}	max.	1300	A
Ausschaltverlust Energie turn-off energy	$R_{CL} = 68\Omega, C_{CL} = 3\mu\text{F},$ $D_{CL} = 34\text{DSH65},$	W_{RO}	max.	8	Ws
Abklingsanftheit reverse recovery softness factor	$T_{vj} = T_{vj\text{max}}$ $I_{FM} = 2500\text{A}, V_R = 2800\text{V},$ $-di_{rr}/dt_{(i=0)} = 1000\text{A}/\mu\text{s}, \Delta t_{tr} = 200\text{ns}$	F_{RRS}	typ.	1,6	

prepared by: TM	date of publication: 2014-06-01
approved by: JP	revision: 8.0